

https://dspace.org/

Investigating ICA for EEG electrode optimization for a sensorimotor BCI

Feller, Shani

2020
https://hdl.handle.net/10539/31108

Downloaded from a DSpace repository. https://dspace.org/

Investigating ICA for EEG electrode optimization for a sensorimotor BCI

Shani Feller

Johannesburg, 2020

A dissertation submitted to the Faculty of Engineering and the Built Environment, University of Witwatersrand, Johannesburg, in fulfilment of the requirements for the degree of Master of Science in Engineering.

Declaration

I declare that this dissertation is my own unaided work. It is submitted to the degree of Master of Science in Engineering to the University of the Witwatersrand, Johannesburg. It has not been submitted before for any degree or examination to any other University.



.....

(Signature of Candidate)

……1st…… day of ……September…… year ……2020…….

Abstract

A robotic/orthotic hand that is controlled by an electroencephalograph (EEG)-based brain computer interface (BCI) which can perform wrist extension (WE) and wrist flexion (WF), can benefit motor impaired individuals to perform everyday activities. Numerous EEG electrodes are typically needed for the spatial resolution required for this task. However, this makes the system expensive, time-consuming to set up and uncomfortable for the user. This research explores the development of a new electrode reduction method that produces an optimised and reduced EEG electrode set, when differentiating between WE and WF movements.

A 128-electrode, EEG database consisting of recordings from 5 subjects was used in this study. The method utilises independent component analysis (ICA) and features related to event-related desynchronization and resynchronization (ERD/ERS) modulations, to produce a reduced electrode set. The method was applied to two movement type investigations: 1) right-hand and left-hand movements and 2) unilateral WE and WE movements. The effectiveness of the method was tested by evaluating the amount of motor-control information that was retained during the electrode reduction. This was done by combining the analysis of three tests: 1) classification accuracy. 2) visual comparison of the inter-trial variance plots of ERD/ERS. 3) comparing the amount of variance retained across all electrodes sets.

The results suggest that the optimal channel configuration for both investigations was a 16-electrode configuration. The 16-electrode configuration obtained a classification accuracy of 70.51 % and 61.61 % for investigation 1 and investigation 2 respectively which is a loss of classification accuracy of 12.01 % and 11.16 % respectively, when compared to using the full electrode set. This research illustrates the potential in using ICA as a primary technique for electrode reduction and suggests that non-motor related electrodes may have an important role in recording motor-related cortical activity.

Dedication

To Liviu, Terry, Gal and Romy Feller and Alessandro Barbosa. Thank you for your continuous love, support and encouragement throughout this process.

Acknowledgements

I would like to thank my supervisor, Mr Abdul-Khaaliq Mohamed, for all his guidance and advice that I have received throughout this study. It is greatly appreciated

I would also like to acknowledge the financial assistance received by the SITA Air Transport Community Foundation, over the course of this research.

Lastly, I would like to thank my family and friends, for their continuous love, support and encouragement throughout this research.

Table of Contents

Declaration ..... **i**

Abstract ..... **ii**

Dedication ..... **iii**

Acknowledgements ..... **iv**

Table of Contents ..... **v**

List of Figures ..... **ix**

List of Tables ..... **xix**

Glossary of Terms and Abbreviations ..... **xxi**

Chapter 1 - Introduction **1**

1.1 Introduction to the Problem 1

1.2 Control of a bionic hand 1

1.3 EEG as a Solution 3

1.4 Research Gap 3

1.5 Research Question 5

1.6 Procedure to Answer the RQ 5

1.6.1 Investigation 1: RH and LH movements 5

1.6.2 Investigation 2: WE and WF movements 6

1.6.3 Breakdown of the RQ 6

1.7 Organisation of Research 8

Chapter 2 - Background **9**

2.1 Wrist Movements 9

2.2 BCI 10

2.3 EEG 11

2.4 ICA and its Application with EEG 12
2.5 Neuroanatomy 15
2.6 Neural Brain Signals 17
2.7 Sensorimotor Rhythms 18
2.8 Chapter Summary 20
Chapter 3 - Literature Review 21
3.1 Exploring Movement Tasks in BCI 21
3.2 EEG Channel Reduction for BCI Applications 23
3.3 ICA in EEG Channel Reduction 28
3.4 Features Used in Movement Tasks 29
3.5 Chapter Summary 33
Chapter 4 - Data Preparation 34
4.1 EEG Database Description 34
4.2 EEG Electrode Placement 35
4.3 Pre-processing 37
4.4 Data arrangement 38
4.5 Limitations of Dataset 39
4.6 Chapter Summary 40
Chapter 5 - Method 41
5.1 ICA and Manual Selection of ICs 42
5.2 Feature Extraction 43
5.3 Feature Selection 44
5.4 Best Performing ICs (Baseline) 46
5.5 Channel Selection 48
5.6 Chapter Summary 52
Chapter 6 – Testing Procedure 53

6.1 Classification 54
6.1.1 Accuracy Calculation 55
6.2 Retention of Motor Control Information 56
6.2.1 IC Visual Inspection 56
6.2.2 Variance Retained 58
6.3 Chapter Summary 59
Chapter 7 - Results 60
7.1 Investigation 1: RH vs LH 60
7.1.1 Reduced Channel Sets 60
7.1.2 Classification Accuracy 62
7.1.3 IC Visual Analysis 63
7.1.4 Variance Retained 65
7.2 Investigation 2: WE vs WF 66
7.2.1 Reduced Channel Sets 66
7.2.2 Classification Accuracy 70
7.2.3 IC Visual Analysis 71
7.2.4 Variance Retained 76
7.3 Chapter Summary 77
Chapter 8 – Discussion 78
8.1 Investigation 1 & 2 Analysis 79
8.1.1 Investigation 1 Summary 81
8.1.2 Investigation 2 Summary 83
8.2 Answering the RQ 84
8.3 Reduced Channel Sets 84
8.4 Significance of Results 86
8.5 Critique of the Method 86

8.5.1 Limitations of the Database 86

8.5.2 Limitations of Manually Selecting ICs 87

8.5.3 Limitations of the Measurement Techniques 88

8.6 Future Work 89

8.7 Chapter Summary 90

Chapter 9 – Conclusion 91

References 93

Appendix A – Ethical Clearance Certificate 105

Appendix B – Scalp Plots and ITV Plots of Best-Performing-ICs-Baseline 106

B.1 Investigation 1 106

B.1.1. Scalp Plots 106

B.1.2. ITV Plots 107

B.2 Investigation 2 108

B.2.1. Scalp Plots 108

Appendix C – Electrode Location of Reduced Channel Sets 116

C.1 Investigation 1 116

C.2 Investigation 2 118

Appendix D – ITV Plots of Best-Performing-ICs-Reduced 122

D.1 Investigation 1 122

D.2 Investigation 2 124

List of Figures

Figure 1.1: Broad methodology overview. The research is divided into two investigations. The method is applied to each investigation. Four reduced channel sets are produced for each test subject, for each investigation. The reduced channel sets are then assessed by comparing results from part A and B. The results from part A and B of each investigation will be compared and used in order to fully answer the RQ. 7

Figure 2.1: Illustration of WF and WE movements. a) WF and b) WE 9

Figure 2.2: BCI overview 10

Figure 2.3: Graphical description of volume conduction. 13

Figure 2.4: Illustration of Brodmann's areas, adapted from [58] 16

Figure 2.5: Motor homunoculous illustrating the topographical mapping of the M1 to the control of specific body parts, adapted from [58]. Both WE and WF movements are controlled by the wrist portion of the homunoculous which is highlighted in yellow. 16

Figure 2.6: Typical ERD/ERS waveform 19

Figure 3.1: Motor homunoculous illustrating the topographical mapping of the M1 to the control of specific body parts, adapted from [58]. a) shows the mapping of upper limb, lower-limb and tongue movements to the motor cortex. b) shows the mapping of wrist and finger movements to the motor cortex. c) shows the mapping of different wrist movements (about the same joint) to the motor cortex. 23

Figure 3.2: Reduced electrode sets for Cecotti et al., [60] and Speier et al., [17] respectfully 24

Figure 3.3: Reduced electrode sets for Lahiri et al., [31],[30] 26

Figure 3.4: Spatially uniform electrode distributions for Schwarz et al., [57] 27

Figure 3.5 A general overview of a typical evolutional algorithm. 29

Figure 4.1: Time sequence and instructions for a single trial, from Mohamed et al. [4] 35

Figure 4.2: GSN electrode placement of the 128-electrode set. 36

Figure 4.3: Diagram illustrating the dataset arrangement. At this point the data was arranged in a 3D array: [channels × time × trials]. In investigation 1, one dataset was created per subject consisting of both RH and LH real movements. In investigation 2, two datasets were created per person (when applicable), one for RH that contains WE and WF and the other for LH that contains WE and WF movements. 39

Figure 5.1: Method overview. The method is applied to both investigations. The method takes in clean data that was processed in Chapter 4. The method ranks the channels according to a calculated score, which is then used to form reduced channel configurations. This method provides three types of information used for testing in Chapter 6. 41

Figure 5.2: Example of a selected IC based on the visual inspection of the scalp and ITV plot, from subject 2, investigation 1. a) shows the IC scalp plot. b) shows the average ITV graph and the ERD/ERS pattern. The dashed line indicates when movement starts. 42

Figure 5.3: FE method overview. Total number of features per IC = 28 x 7 = 196 features per IC. 44

Figure 5.4: Description of the feature set. The features were stored in a 2D array: [trials × features]. Each feature set contains the features describing its class. The number of features extracted depends on the number of visually-selected-ICs. 44

Figure 5.5: Reduced feature set based on the selected features. The features were stored in a 2D array: [trials × features]. Each feature set contains the selected features describing a class. 45

Figure 5.6: Graphical explanation of an IC scoring method from subject 2, investigation 1. In this example, a total of 50 features were selected; each feature had a BD value associated with it. The BD value of each feature related to a single IC was summed to provide each IC with an IC score. 48

Figure 5.7: Graphical explanation of the channel scoring method from subject 2, investigation 1. a) shows the distribution of IC 20 across all 128 channels. b) shows the distribution of IC 77 across all 128 channels. 49

Figure 5.8: The electrode placement of the top three ranked channels and their associated CS, for subject 2 investigation 1 52

Figure 6.1: Testing procedure overview. Results from three subsections in this procedure are compared. 1. The baseline classification accuracy (A-1) is compared to the classification accuracy of the reduced sets (B 1). 2. Visual inspection of the best-performing-ICs-baseline (A-2) is compared to the best-performing-ICs-reduced (B-2). 3. The variance contained in the original channel set (A-3) is compared to the variance contained in the reduced channel sets (B-3). 53

Figure 6.2: Graphical representation of the datasets used for classification. 70 % of the trials were used to train the SVM, while the remaining 30 % were used to test the SVM. The data was stored in 2D arrays: [trials × features]. Each dataset contains the selected features and its associated class label. Outliers were removed from the dataset and the trials were then randomized. 55

Figure 6.3: An example of an ITV plot with typical ERD/ERS characteristics. 58

Figure 6.4: Graphical illustration of the method used to calculate the correlation between PC 1 of the original dataset and PC 2 of the reduced channel dataset. 59

Figure 7.1: Subject 2's reduced-channel configurations obtained for investigation 1. The location of the electrodes corresponding to the selected channels is presented. a) 24-channel configuration, b) 16-channel configuration, c) 8-channel configuration, d) 3-channnel configuration. 62

Figure 7.2: Classification accuracies obtained for the differentiation between LH and RH movement using the original 128-channel dataset and the reduced channel dataset. Classification accuracies for subjects 2, 3, 5 and the average classification accuracy across all subjects are presented. 63

Figure 7.3: ITV plots of best-performing-ICs-reduced for subject 2. The ITV plots are ordered according to the IC score. a) 128-channels. b) 24-channels. c) 16-channels. d) 8-channels. e) 3-channels. The ITV plots underlined in red illustrate similar ERD/ERS characteristics. 64

Figure 7.4: ITV plots of best-performing-ICs-reduced for subject 3. The ITV plots are ordered according to the IC score. a) 128-channels. b) 24-channels. c) 16-channels. d) 8-channels. e) 3-channels. The ITV plots underlined in red illustrate similar ERD/ERS characteristics. 64

Figure 7.5: ITV plots of best-performing-ICs-reduced for subject 5. The ITV plots are ordered according to the IC score. a) 128-channels. b) 24-channels. c) 16-channels. d) 8-channels. e) 3-channels. The ITV plots underlined in red illustrate similar ERD/ERS characteristics. 65

Figure 7.6: Subject 2's RH reduced channel configurations obtained for investigation 2. The location of the electrodes corresponding to the selected channels is presented. a) 24-channel configuration, b) 16-channel configuration, c) 8-channel configuration, d) 3-channel configuration. 70

Figure 7.7: Classification accuracies obtained for the differentiation between WE and WF movement using the original 128-channel dataset and the reduced channel dataset. Classification accuracies for each subject's RH and LH datasets (when available) and the average classification accuracy across all datasets are presented. 71

Figure 7.8: ITV plots of best-performing-ICs-reduced for subject 1 RH. The ITV plots are ordered according to the IC score. a) 128-channels. b) 24-channels. c) 16-channels. d) 8-channels. e) 3-channels. The ITV plots which are underlined in red illustrate similar ERD/ERS characteristics 72

Figure 7.9: ITV plots of best-performing-ICs-reduced for subject 2 LH. The ITV plots are ordered according to the IC score. a) 128-channels. b) 24-channels. c) 16-channels. d) 8-channels. e) 3-channels. The ITV plots which are underlined in red illustrate similar ERD/ERS characteristics 73

Figure 7.10: ITV plots of best-performing-ICs-reduced for subject 2 RH. The ITV plots are ordered according to the IC score) 128-channels. b) 24-channels. c) 16-channels. d) 8-channels. e) 3-channels. The ITV plots which are underlined in red illustrate similar ERD/ERS characteristics 73

Figure 7.11: ITV plots of best-performing-ICs-reduced subject 3 LH. The ITV plots are ordered according to the IC score) 128-channels. b) 24-channels. c) 16-channels. d) 8-channels. e) 3-channels. The ITV plots which are underlined in red illustrate similar ERD/ERS characteristics. 74

Figure 7.12: ITV plots of best-performing-ICs-reduced subject 3 RH. The ITV plots are ordered according to the IC score) 128-channels. b) 24-channels. c) 16-channels. d) 8-channels. e) 3-channels. The ITV plots which are underlined in red illustrate similar ERD/ERS characteristics. 74

Figure 7.13: ITV plots of best-performing-ICs-reduced subject 4 LH. The ITV plots are ordered according to the IC score) 128-channels. b) 24-channels. c) 16-channels. d) 8-channels. e) 3-channels. The ITV plots which are underlined in red illustrate similar ERD/ERS characteristics 75

Figure 7.14: ITV plots of best-performing-ICs-reduced subject 5 LH. The ITV plots are ordered according to the IC score) 128-channels. b) 24-channels. c) 16-channels. d) 8-channels. e) 3-channels. The ITV plots which are underlined in red illustrate similar ERD/ERS characteristics 75

Figure 7.15: ITV plots of best-performing-ICs-reduced subject 5 RH. The ITV plots are ordered according to the IC score) 128-channels. b) 24-channels. c) 16-channels. d) 8-channels. e) 3-channels. The ITV plots which are underlined in red illustrate similar ERD/ERS characteristics 76

Figure 8.1: Discussion chapter overview. Conclusions from the analysis of investigation 1 and investigation 2 are used to determine the effectiveness of the method, and in turn answer the RQ. 78

Figure A.1: Ethical clearance certificate. 105

Figure B.2: Scalp plots of all best-performing-ICs-baseline for subject 2's dataset. 106

Figure B.3: Scalp plots of all best-performing-ICs-baseline for subject 3's dataset. 106

Figure B.4: Scalp plots of all best-performing-ICs-baseline for subject 5's dataset. 106

Figure B.5: ITV ERD/ERS patterns (averaged over all trials) of best-performing-ICs-baseline for subject 2. 107

Figure B.6: ITV ERD/ERS patterns (averaged over all trials) of best-performing-ICs-baseline for subject 3. 107

Figure B.7: ITV ERD/ERS patterns (averaged over all trials) of best-performing-ICs-baseline for subject 5. 107

Figure B.8: Scalp plots of all best-performing-ICs-baseline for subject 1 RH's dataset. 108

Figure B.9: Scalp plots of all best-performing-ICs-baseline for subject 2 LH's dataset. 108

Figure B.10: Scalp plots of all best-performing-ICs-baseline for subject 2 RH's dataset. 109

Figure B.11: Scalp plots of all best-performing-ICs-baseline for subject 3 LH's dataset. 109

Figure B.12: Scalp plots of all best-performing-ICs-baseline for subject 3 RH's dataset. 110

Figure B.13: Scalp plots of all best-performing-ICs-baseline for subject 4 LH's dataset. 110

Figure B.14: Scalp plots of all best-performing-ICs-baseline for subject 5 LH's dataset. 111

Figure B.15: Scalp plots of all best-performing-ICs-baseline for subject 5 RH's dataset. 111

Figure B.16: ITV ERD/ERS patterns (averaged over all trials) of best-performing-ICs-baseline for subject 1 RH. 112

Figure B.17: ITV ERD/ERS patterns (averaged over all trials) of best-performing-ICs-baseline for subject 2 LH. 112

Figure B.18: ITV ERD/ERS patterns (averaged over all trials) of best-performing-ICs-baseline for subject 2 RH. 113

Figure B.19: ITV ERD/ERS patterns (averaged over all trials) of best-performing-ICs-baseline for subject 3 LH. 113

Figure B.20: ITV ERD/ERS patterns (averaged over all trials) of best-performing-ICs-baseline for subject 3 RH. 114

Figure B.21: ITV ERD/ERS patterns (averaged over all trials) of best-performing-ICs-baseline for subject 4 LH. 114

Figure B.22: ITV ERD/ERS patterns (averaged over all trials) of best-performing-ICs-baseline for subject 5 LH. 115

Figure B.23: ITV ERD/ERS patterns (averaged over all trials) of best-performing-ICs-baseline for subject 5 RH. 115

Figure C.24: Subject 2's reduced channel configurations obtained for investigation 1. The location of the electrodes corresponding to the selected channels is presented. a) 24-channel configuration, b) 16-channel configuration, c) 8-channel configuration, d) 3-channel configuration. 116

Figure C.25: Subject 3's reduced channel configurations obtained for investigation 1. The location of the electrodes corresponding to the selected channels is presented – a) 24-channel configuration, b) 16-channel configuration, c) 8-channel configuration, d) 3-channel configuration 117

Figure C.26: Subject 5's reduced channel configurations obtained for investigation 1. The location of the electrodes corresponding to the selected channels is presented – a) 24-channel configuration, b) 16-channel configuration, c) 8-channel configuration, d) 3-channel configuration 117

Figure C.27: Subject 1's RH reduced channel configurations obtained for investigation 2. The location of the electrodes corresponding to the selected channels is presented. a) 24-channel configuration, b) 16-channel configuration, c) 8-channel configuration, d) 3-channel configuration. 118

Figure C.28: Subject 2's LH reduced channel configurations obtained for investigation 2. The location of the electrodes corresponding to the selected channels is presented. a) 24-channel configuration, b) 16-channel configuration, c) 8-channel configuration, d) 3-channel configuration. 118

Figure C.29: Subject 2's RH reduced channel configurations obtained for investigation 2. The location of the electrodes corresponding to the selected channels is presented. a) 24-channel configuration, b) 16-channel configuration, c) 8-channel configuration, d) 3-channel configuration. 119

Figure C.30: Subject 3's LH reduced channel configurations obtained for investigation 2. The location of the electrodes corresponding to the selected channels is presented. a) 24-channel configuration, b) 16-channel configuration, c) 8-channel configuration, d) 3-channel configuration. 119

Figure C.31: Subject 3's RH reduced channel configurations obtained for investigation 2. The location of the electrodes corresponding to the selected channels is presented. a) 24-channel configuration, b) 16-channel configuration, c) 8-channel configuration, d) 3-channel configuration. 120

Figure C.32: Subject 4's LH reduced channel configurations obtained for investigation 2. The location of the electrodes corresponding to the selected channels is presented. a) 24-channel configuration, b) 16-channel configuration, c) 8-channel configuration, d) 3-channel configuration. 120

Figure C.33: Subject 5's LH reduced channel configurations obtained for investigation 2. The location of the electrodes corresponding to the selected channels is presented. a) 24-channel configuration, b) 16-channel configuration, c) 8-channel configuration, d) 3-channel configuration. 121

Figure C.34: Subject 5's RH reduced channel configurations obtained for investigation 2. The location of the electrodes corresponding to the selected channels is presented. a) 24-channel configuration, b) 16-channel configuration, c) 8-channel configuration, d) 3-channel configuration. 121

Figure D.35: ITV ERD/ERS patterns (averaged over all trials) of best-performing-ICs-reduced for subject 2's dataset. a) 24-channel configuration. b) 16-channel configuration. c) 8-channel configuration. d) 3-channel configuration. 122

Figure D.36: ITV ERD/ERS patterns (averaged over all trials) of best-performing-ICs-reduced for subject 3's dataset. a) 24-channel configuration. b) 16-channel configuration. c) 8-channel configuration. d) 3-channel configuration. 123

Figure D.37: ITV ERD/ERS patterns (averaged over all trials) of best-performing-ICs-reduced for subject 5's dataset. a) 24-channel configuration. b) 16-channel configuration. c) 8-channel configuration. d) 3-channel configuration. 123

Figure D.38: ITV ERD/ERS patterns (averaged over all trials) of best-performing-ICs-reduced for subject 1 RH's dataset. a) 24-channel configuration. b) 16-channel configuration. c) 8-channel configuration. d) 3-channel configuration. 124

Figure D.39: ITV ERD/ERS patterns (averaged over all trials) of best-performing-ICs-reduced for subject 2 LH's dataset. a) 24-channel configuration. b) 16-channel configuration. c) 8-channel configuration. d) 3-channel configuration. 124

Figure D.40: ITV ERD/ERS patterns (averaged over all trials) of best-performing-ICs-reduced for subject 2 RH's dataset. a) 24-channel configuration. b) 16-channel configuration. c) 8-channel configuration. d) 3-channel configuration. 125

Figure D.41: ITV ERD/ERS patterns (averaged over all trials) of best-performing-ICs-reduced for subject 3 LH's dataset. a) 24-channel configuration. b) 16-channel configuration. c) 8-channel configuration. d) 3-channel configuration. 125

Figure D.42: ITV ERD/ERS patterns (averaged over all trials) of best-performing-ICs-reduced for subject 3 RH's dataset. a) 24-channel configuration. b) 16-channel configuration. c) 8-channel configuration. d) 3-channel configuration. 126

Figure D.43: ITV ERD/ERS patterns (averaged over all trials) of best-performing-ICs-reduced for subject 4 LH's dataset. a) 24-channel configuration. b) 16-channel configuration. c) 8-channel configuration. d) 3-channel configuration. 126

Figure D.44: ITV ERD/ERS patterns (averaged over all trials) of best-performing-ICs-reduced for subject 5 LH's dataset. a) 24-channel configuration. b) 16-channel configuration. c) 8-channel configuration. d) 3-channel configuration. 127

Figure D.45: ITV ERD/ERS patterns (averaged over all trials) of best-performing-ICs-reduced for subject 5 RH's dataset. a) 24-channel configuration. b) 16-channel configuration. c) 8-channel configuration. d) 3-channel configuration. 127

List of Tables

Table 2.1: Lobes of the brain and their functions 15

Table 2.2: EEG signal frequency band description 18

Table 3.1: A summary of different features used in different movement tasks' studies 31

Table 4.1: Approximate correspondence between electrode placement of the GSN System and the International 10-10 System [75] 36

Table 4.2: Summary of the number of channels and trials removed for each subject 38

Table 4.3: Number of datasets per test subject per investigation 39

Table 5.1: Number of visually-selected-ICs isolated for both investigations 43

Table 5.2: Optimal number of selected features used for the baseline classification for both investigations 46

Table 5.3: Number of best-performing-ICs-baseline that contributed features for baseline classification for both investigations 47

Table 5.4: Graphical explanation of the channel scoring system taken from subject 2, investigation 1. It illustrates how the CS was calculated 50

Table 5.5: Graphical explanation of the channel scoring system taken from subject 2, investigation 1. It illustrates the ranking of the channels. The top three ranked channels are highlighted in yellow. 51

Table 6.1: Number of best-performing-ICs-reduced that contributed features for reduced channel classification for both investigations 57

Table 7.1: 24 top-ranked channels and their corresponding CS for subject 2, 3 and 5 for investigation 1 61

Table 7.2: The loss of classification accuracy calculated between the baseline classification and the reduced channel sets. This is presented for subjects 2, 3, 5 and is averaged across all subjects. 63

Table 7.3 : The correlation between the variance contained in the 128-channel dataset and each reduced channel's dataset. These results are presented for subjects 2, 3, 5 and are averaged across all subjects. 65

Table 7.4: 24 top-ranked channels and their corresponding CS for subject 1's RH dataset, subject 2's LH dataset and subject 2's RH dataset for investigation 2 67

Table 7.5: 24 top-ranked channels and their corresponding CS for subject 3's LH dataset, subject 3's RH dataset and subject 4's LH dataset for investigation 2 68

Table 7.6: 24 top-ranked channels and their corresponding CS for subject 5's LH and RH datasets, for investigation 2 69

Table 7.7: The loss of classification accuracy calculated between the baseline classification and the reduced channel sets. This is presented for each subject's RH and LH channel sets (when available) and is averaged across all the datasets 71

Table 7.8: The correlation between the variance contained in the 128-channel dataset and each reduced channel's dataset. These results are presented for each subject's RH and LH channel sets (when available) and are averaged across all the datasets. 76

Table 8.1: Graphical overview of all the results obtained for the three metrics: classification accuracy, ITV plots and a measure of variance. 81

Glossary of Terms and Abbreviations

Abbreviation/Term	Description
AAR	Adaptive auto-regressive
ADL	Activity of daily living
Alpha frequency band	Frequency band of EEG signal occurring between 8 Hz and 12 Hz
Anterior	Referring to the front of the body
Baseline classification	Classification using the original 128-electrode dataset
BC	Bhattacharyya's coefficient
BCI	Brain computer interface
BD	Bhattacharyya's distance
Best-performing-ICs-baseline	The ICs which contributed features for the baseline classification
Best-performing-ICs-reduced	the ICs which contributed features for the classification of the reduced channel's datasets
Beta frequency band	Frequency band of EEG signal occurring between 12 Hz and 30 Hz
Bionic	Prosthetic or orthotic robotic hand
Channel	Digitized recorded EEG signal
Contralateral	Associated to or affecting the opposite side of the body
CS	Channel score
CSP	Common spatial patern
Delta frequency band	Frequency band of EEG signal occurring below 4 Hz
ECoG	Electrocorticogram
EEG	Electroencephalograph
Electrode	Physical sensor which is used to record the EEG signal
EMG	Electromyogram
EOG	Electrooculogram
ERD	Event-related desynchronization
ERS	Event-related resynchronization
FE	Feature extraction
FFT	Fast Fourier transform
FMRI	Functional magnetic resonance imaging
FS	Feature selection
Gamma frequency band	Frequency band of EEG signal occurring between 30 Hz and 100 Hz
GSN	Geodesic sensor net
IC	Independent component
IC Score	Score given to an IC based on the BD values of the related features
ICA	Independent component analysis
Ipsilateral	Associated to or affecting the same side of the body

ITV	Inter-trial variance, method to calculate non-phase locked components of ERD and ERS modulations
LH	Left hand
M1	Primary motor cortex
MFE	Mass finger extension
MFF	Mass finger flexion
MI	Motor imagery
Mu frequency band	Frequency band of motor-related EEG signal occurring between 8 Hz and 12 Hz
P300	Evoked potentials
PC	Principal components
PCA	Principal component analysis
PMA	Premotor area/cortex
Posterior	Referring to the back of the body
RH	Right hand
RQ	Research question
SCP	Slow cortical potential
SMA	Supplementary motor area/cortex
SMR	Sensorimotor rhythm
SNR	Signal-to-noise ratio
SVM	Support vector machine
Theta frequency band	Frequency band of EEG signal occurring between 4 Hz and 8 Hz
TRP	Tripod pinch
Unilateral	Associated to or affecting only one side of the body
Visually-selected-IC-baseline	ICs that were visually selected
VEP	Visually evoked potential
WE	Wrist extension, can be described as raising the back of the hand towards the posterior part of the forearm
WF	Wrist flexion, can be described as bending the palm towards the anterior part of the forearm

Chapter 1 - Introduction

1.1 Introduction to the Problem

Upper limb motor impaired individuals such as upper limb amputees, victims of strokes and spinal cord injuries as well as other individuals with neurological issues, struggle to perform simple, daily activities that require the basic functioning of their hands [1]–[3]. Not being able to hold objects prevents them from performing simple daily activities. This affects their ability to eat, drink, write and get dressed by themselves.

Basic hand movements that aid in the normal functioning of a hand include: wrist extension (WE), wrist flexion (WF), tripod pinch (TRP), mass finger extension (MFE) and mass finger flexion (MFF) [4]. Out of these important hand movements, WE and WF are vital as they allow for the overall movement of the hand, which enables the execution of hand gestures [5]. WE and WF movements provide the hand with stability and support for performing fine and gross motor hand skills [5]–[7]. The movement of the wrist is important for the execution of daily activities that require controlled hand movements such as grasping a cup or cutting food with a knife [8]. As a result, without the use of wrist movements, these impaired individuals are unable to perform simple tasks that most of the population perform with ease. Therefore, a prosthetic or orthotic robotic (will be referred to as a bionic hand from here onwards) that can perform both WE and WF movements will aid in returning some means of functionality back to the user.

1.2 Control of a bionic hand

Electromyogram (EMG), electrocorticogram (ECoG) and electroencephalograph (EEG) are common methods used to record electrophysiological signals [2], [9]. These electrophysiological signals can be translated into command signals which can be used to control a bionic hand [2].

An EMG-based bionic hand uses signals received from upper limb muscle activation (such as muscles of the arm or forearm) as command signals to control the bionic hand [10]. This solution is not suitable for individuals whose upper body is fully paralysed, such as stroke victims and individuals with spinal cord injuries [10]. Additionally, upper limb amputation can occur at any point (at any level in the arm or forearm), thus finding enough muscle activation to control the device may be difficult [10].

A brain computer interface (BCI) can be used to solve this problem. A BCI system measures and records the electrical activities of the brain and then translates this information into meaningful information and command signals that can control a bionic hand [11]. The electrical activity of the brain can be recorded through invasive (ECoG) and noninvasive (EEG) measurement devices [2], [9].

ECoG records neural brain signals from electrodes implanted directly into the brain [2]. This technique requires surgery, which is expensive and yields major health concerns, such as a risk of infection and a risk of brain damage [2]. However, the signals recorded have a good signal-to-noise (SNR) ratio [2]. The signals recorded using non-invasive methods such as an EEG device have a low SNR, since the signals are attenuated as they pass through the brain (see Section 2.3) [12]. However, using an EEG device is preferable as there are fewer risks associated with it, as the neural brain signals are recorded using electrodes placed on the surface of the scalp [1]. This technique is also less expensive and more practical to use [13]. Due to these advantages, EEG devices are commonly used in conjunction with a BCI system to control an external device [2], such as a bionic hand.

The EEG signal is recorded by measuring the voltage difference between two physical electrodes [14]. This recorded voltage difference forms an EEG channel [14]. From here onwards, a channel will refer to the digitized recorded EEG signal, while an electrode will refer to the physical sensor which is used to record the EEG signal.

1.3 EEG as a Solution

An EEG BCI system can be used to control a bionic hand (that can perform WE and WF movements). As mentioned, EEG signals are the measured and recorded electrical activity of the brain. User intention can be inferred through the analysis and interpretation of the EEG signals [13]. For example, the user thinks about moving their hand to grasp a glass or hold a pen. This intention is recorded by the EEG device and is embedded in the EEG signals. The BCI system then interprets the EEG signals and translates the motor intention into control information. This control information can then be used to bring about an action from an external device, such as the movement of a bionic hand.

However, current BCI systems have a major disadvantage, due to the complexities of EEG (see Section 2.3) many EEG electrodes (ranging up to 256 electrodes) are required for high spatial resolution [15], [16]. This is especially important for the discrimination of unilateral wrist movement, as the brain regions responsible for these types of movements are close together (see Section 0) resulting in the necessity of the additional information. But using many electrodes is expensive, time consuming to set up – as the placement of each electrode is unique to the individual (as it is based according to their skull measurements) and it is rather uncomfortable for the user [17], [18].

Therefore, designing a BCI system that uses a minimal number of electrodes and still performs its required function is required. A BCI system with a reduced number of electrodes that can accurately differentiate between the neural brain signals responsible for WE and WF movements will aid in the development of a practical bionic hand that can return basic functionality back to the user.

1.4 Research Gap

EEG studies focusing on the discrimination between unilateral WE and WF are limited in comparison to other movement types (refer to Section 3.1). No reliable EEG channel reduction studies for WE and WF movement have been published.

Therefore, a study showing channel reduction for an EEG-based BCI interpreting WE and WF is novel.

Extracting relevant neural information pertaining to WE and WF is extremely difficult as these movements are generated by spatially close regions of the brain [19], [20] (see Section 0). This makes differentiation between these movements very difficult [19], [20].

Current channel reduction methods do not provide insight into the specific type of control information that is retained during the reduction process. A channel reduction method that focuses on retaining maximal motor control information may assist in producing a reduced channel set that has adequate motor control information, so that differentiation between WE and WF movements can occur.

Event-related desynchronization (ERD) and event-related resynchronization (ERS) modulations of EEG signals, is an electrophysiological phenomenon that occurs when motor activity such as WE and WF is executed [13], [21], [22]. ERD/ERS signal modulations exhibit a distinct shape and pattern that is well researched and easily detected [4], [13], [15], [22], [23]. Therefore, characteristics describing this pattern can be used to isolate motor control information.

Independent component analysis (ICA) can help with this. The EEG signal is the electrical representation of a combination of the numerous neural process occurring simultaneously in the human brain at a given moment. However, only information relating to WE and WF is needed. This is where ICA and ERD/ERS characteristics comes into play. ICA has been successfully used in the differentiation of wrist movements [24]. ICA breaks down signals into its independent components (ICs) or independent sources [24]. Therefore, it can be used to decompose the EEG signal into its ICs each representing an internal cortical source of information (such as those responsible for wrist movement control) [24].

It is theorized that the ICs related to WE and WF motor control can be isolated using ERD/ERS characteristics, and the rest of the irrelevant information from the full scalp EEG dataset can be discarded. It is also theorized that the retained ICs

can be mapped back to a few channels responsible for capturing majority of the WE and WF motor-related information. It is then hypothesized that the retained ICs can be used to produce a reduced set of EEG channels/electrodes. The use of ICA to perform channel reduction is a novel application. The purpose of this research is to test the above hypothesis.

1.5 Research Question

The aim of this research is to answer the following research question (RQ):

To what extent can ICA be used to find an optimized and reduced EEG channel set (from a 128-channel dataset) when discriminating between WE and WF movements?

1.6 Procedure to Answer the RQ

In order to answer the RQ, a novel EEG channel reduction method based on ICA and ERD/ERS characteristics was designed. The method aimed to produce a reduced channel set that retains maximal motor control information, so that the differentiation between different movement types is possible. This research focused on testing the effectiveness of this method.

The method was evaluated through the examination of two movement types. Thus, the research was divided into two investigations:

1) discriminating between right hand (RH) and left hand (LH) movements and
2) discriminating between WE and WE movements.

1.6.1 Investigation 1: RH and LH movements

This investigation tested the method's ability to retain motor control information related to RH and LH movements during channel reduction. Five real movement types: WE, WF, TPR, MFE and MFF are used for this investigation. The differentiation between the neural signals responsible for the generation of RH and LH groups of these real movement types is explored in this investigation.

Differentiating between RH and LH movements is considered an easier task, since the brain regions responsible for the generation of these movements are spatially apart [25] (refer to Section 0). The differentiation between RH and LH movements is also well researched (refer to Section 3.1), therefore the results obtained can be compared to the literature. Results consistent with literature, would suggest that the method is able to produce a reduced electrode set that retains motor control information. Hence this investigation was done first.

1.6.2 Investigation 2: WE and WF movements

This investigation tests the method's ability to retain motor control information related to WE and WF movement during channel reduction. Real WE and WF movements are used in this investigation. The differentiation between the neural signals responsible for the generation of WE and WF movements is explored in this investigation. The differentiation between WE and WF movements is relatively more difficult, since movements about the same wrist are generated by spatially close brain regions [19], [20] (see Section 0).

1.6.3 Breakdown of the RQ

The effectiveness and performance of the method is tested by measuring how well the reduced channel sets can differentiate between the investigated movement type, in comparison to the complete (128-channel) dataset. As a result, each investigation is divided into two main parts, part A and part B, which are detailed below. The results from part A and part B of each investigation will be compared and used to fully answer the RQ. This breakdown is shown in Figure 1.1.

Part A:

- A-1: This subsection investigates how well each movement type can be differentiated when using the original 128-channel dataset. A baseline classification accuracy is obtained as a result.
- A-2: This subsection investigates the baseline classification accuracy obtained on a deeper level, by examining the ICs used in the baseline classification and visually examining the ERD/ERS pattern that they produce.

- A-3: This subsection also investigates the baseline classification accuracy obtained on a deeper level, by examining the amount of variance contained within the original (128-channel) dataset.

Part B:

- B-1: This subsection investigates how well each movement type can be differentiated when using the reduced channel sets produced by the novel ICA based method. A classification accuracy is obtained as a result.
- B-2: This subsection investigates the classification accuracies obtained on a deeper level, by examining the ICs used for the classification and visually examining the ERD/ERS pattern that they produce.
- B-3: This subsection also investigates the classification accuracies obtained on a deeper level, by examining the amount of variance contained within each reduced channel's datasets.

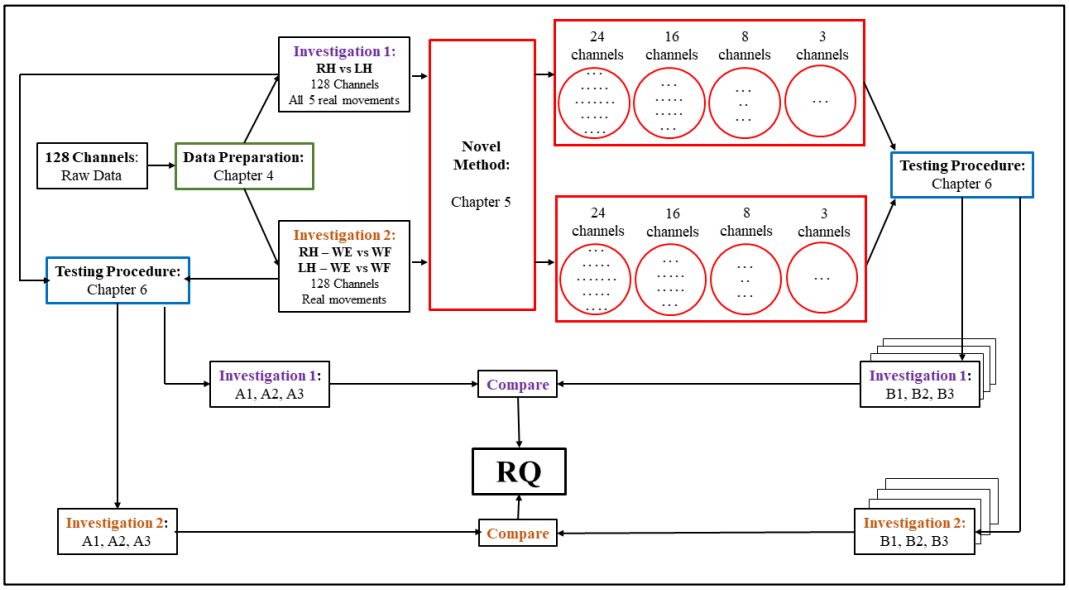


Figure 1.1: Broad methodology overview. The research is divided into two investigations. The method is applied to each investigation. Four reduced channel sets are produced for each test subject, for each investigation. The reduced channel sets are then assessed by comparing results from part A and B. The results from part A and B of each investigation will be compared and used in order to fully answer the RQ.

1.7 Organisation of Research

The rest of the research is structured in the following manner. Chapter 2 provides the necessary theory required in order to investigate this problem. Relevant literature pertaining to the research is explained in Chapter 3 . The method is divided into three sections: data preparation, core channel reduction method and testing procedure, as illustrated in Figure 1.1. Chapter 4 discusses the data preparation section. It details the steps taken to pre-process and arrange the data into the desired format. Chapter 5 describes the designed channel reduction method. This takes in clean data and reduces the original 128-channel dataset into reduced channel configurations comprising of the top 24, 16, 8 and 3 rated channels. Chapter 6 discusses the testing procedures that were implemented in order to measure the performance of the reduced channel sets and thus the effectiveness of the designed channel reduction method. Chapter 7 presents the results obtained, while the discussion of the results is found in Chapter 8 . Chapter 9 then summaries and concludes the study.

Chapter 2 - Background

This chapter provides the necessary theory of several concepts referred to throughout the research. This background will help with the contextualization of the study. The importance of wrist movements for daily activities will be discussed followed by background to BCI systems and EEG devices. ICA and its application with EEG are then explored. Some basic neuroanatomy is then presented followed by information on the different types of neural brain signals. Finally, sensorimotor rhythms are discussed.

2.1 Wrist Movements

The wrist joint can move in three different planes: pronation/supination, flexion/extension and ulnar/radial deviation [5]–[7]. WF can be described as bending the palm down towards the anterior part of the forearm, while WE can be described as raising the back of hand towards the posterior part of the forearm. This is graphically explained in Figure 2.1. The total range of motion for both WF and WE is typically 65-75° [6], [26].

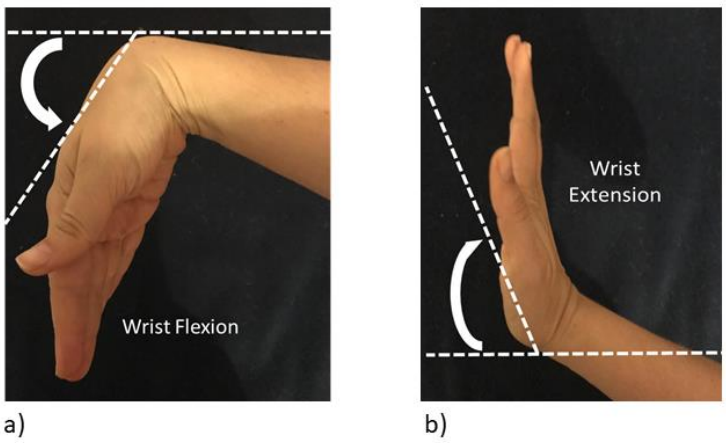


Figure 2.1: Illustration of WF and WE movements. a) WF and b) WE

Movements about the wrist joint are vital in ensuring the proper functioning of the entire hand [5]. The wrist joint allows for the formation of fundamental hand movements such as making a composite grip as well as thumb opposition [5]. Being

able to make a full composite grip is important as it allows a person to grasp an object. Thus, activities of daily living (ADLs) such as writing (holding a pen), eating (holding utensils), drinking (grasping a glass) and dressing becomes possible [8]. Furthermore, WE and WF affects finger mobility, thus aiding in the development of fine finger motor skills such as writing [6], [7]. WE and WF also provides a person with the ability to perform different hand gestures, thus aiding in communication with others.

2.2 BCI

A BCI system assists in returning some motor functionality back to motor impaired individuals [2], [11]. This functionality is often through the control of an external device such as a bionic hand [11], a wheelchair [11] or a virtual keyboard [3]. The BCI system records the electrical activity of the brain, extracts the desired electrophysiological signals as features and then translates them in order to interpret the user's intent [13]. The electrophysiological brain signals are then used as the control signal for the actuation of an external device [2]. Figure 2.2 shows an overview of the main sections of a BCI system. BCIs are categorized according to the electrophysiological signal that it interprets [2]. The different types of neural brain signals are described in Section 2.6. A sensorimotor BCI is used to interpret neural motor outputs [13] such as WE and WF movements.

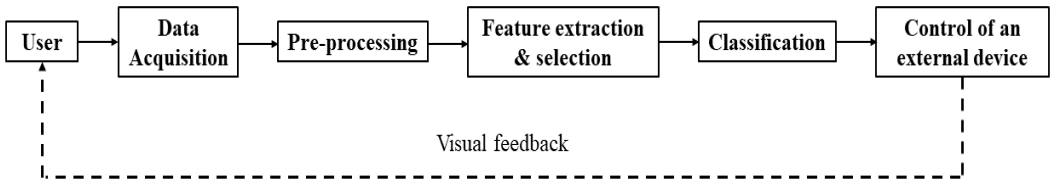


Figure 2.2: BCI overview

A sensorimotor BCI uses the modulations of the sensorimotor rhythms (SMRs) to control the BCI [13]. SMR modulations occurs during motor activity as well as during motor imagery (MI) activity, refer to Section 2.7 for more details [13], [27], [28]. MI is the mental imagination of movement without any motor execution occurring [9], [29]–[31]. MI related SMR modulations occur both in healthy and in

motor impaired individuals [27], [28]. Studies suggest that individuals can learn to control these SMR modulations [13], [27]. As a result, the control of these SMR modulations can allow motor impaired individuals to control an external device such as a bionic hand [27].

BCI results can be analyzed either on a single-trial or a multi-trial basis. Single-trial analysis focuses on the neural brain signal patterns found in each trial separately. This type of analysis is appropriate for BCI studies as it can lead to processing of data in real-time [32]. However, this technique can be problematic due to the large amount of inter-trial variability found in EEG as well as the significant background noise contained in the EEG signal, thus making it is difficult to extract the neural patterns of interest [33], [34]. Therefore, multi-trial analysis can be used to extract an overall neural signal pattern, by averaging across all the trials, so that the SNR increase and the neural brain pattern of interest is emphasized [33], [35]. One can then make inferences from the extracted neural brain pattern.

2.3 EEG

Typically, BCI systems use an EEG device to measure and record the electrical activity of the brain, as it is non-invasive, safe, relatively inexpensive, portable and has a high temporal resolution (approximately 0.05s) [13]. However, EEG has a low spatial resolution [15], [16]; therefore numerous electrodes across the surface of the scalp are used to record this electrical activity. The drawbacks of using many electrodes are discussed in Section 1.3.

This electrical activity is generated by neural processes occurring simultaneously in the brain at a given moment [36]. These neural processes originate from cortical sources from all over the brain. As the electrical activity propagates from the cortical source, towards the electrodes, it moves through various layers of tissue (brain, cerebral spinal fluid, skull and scalp) [37]. Each tissue layer has a different electrical property associated with it [16]. As a result, the electrical activity of the brain becomes mixed and spatially distorted as it moves through these different tissue layers [16]. This is phenomena known as volume conduction. As a result, many electrodes record the electrical activity generated by a single cortical

source [38]. The amount of cortical activity produced during an activity and the way in which it spreads throughout the brain is unique to an individual [39]. As a result, EEG signals have a large inter-subject variability associated with them.

EEG signals are sensitive to undesired noise, which results in the formation of signal artifacts [40]. The origin of these artifacts can be physiological or non-physiological [41]. Examples of physiological artifacts are electrooculogram (EOG) artifacts which are generated by eye movements and eye blinks and EMG artifacts which are generated by muscle activity such as face, tongue and neck movements [41], while examples of non-physiological artifacts are line noise interference, movement of electrodes and interreference from surrounding equipment [40], [41].

The standard electrode placement for EEG is based on the International 10-20 System [13] and its derivations. This system relies on two points of reference, the nasion and the inion [13]. Electrodes are then placed at 10 % or 20 % intervals [13] away from each other depending on the number of electrodes required. As a result, the electrode setup is based according to the individual's measurements and thus is unique to the individual. This makes the initial setup time consuming.

2.4 ICA and its Application with EEG

Each EEG channel contains a mixture of signals which originate from numerous neural processes from spatially separate cortical regions. This is graphically shown in Figure 2.**3**. Therefore, it is necessary to unmix these signals in order to extract information from specific cortical areas, such as the motor cortices. Spatial filters are typically used to unmix the EEG signal, by decomposing the EEG signal into many components which represent the different cortical sources [42]. Thus, spatial filters are often used to remove signal artifacts as well increase the spatial resolution of the signal [42]. Common spatial filtering techniques are ICA, common spatial pattern (CSP), principal component analysis (PCA) and beamformer [42]–[44].

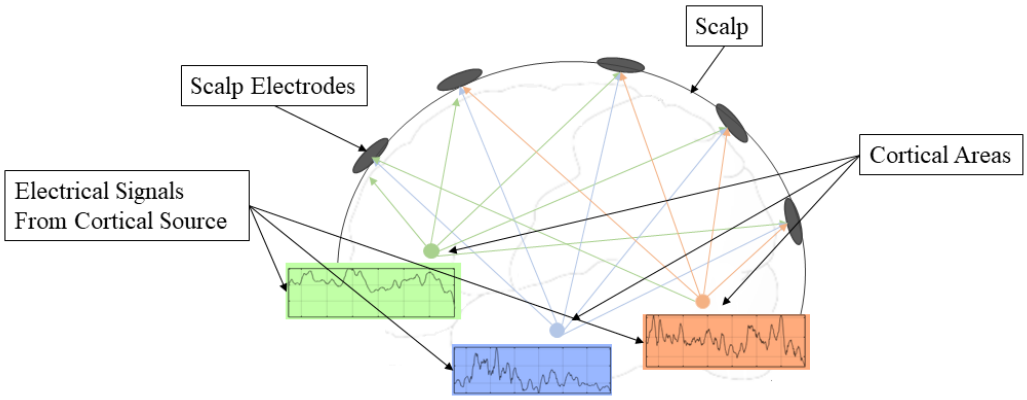


Figure 2.3: Graphical description of volume conduction.

ICA is a blind source separation technique which attempts to decomposes the EEG signal into numerous independent sources, or ICs [45]. Each IC estimates an internal cortical source of information. As a result, ICA has widely been used in EEG research as a spatial filter by aiding in the removal of noise and muscle artifacts [21], [39], [45]–[52]. It is also used as a source localising tool, which aids in the extraction of optimal features for classification, by identifying the cortical sources related to a certain cognitive task [46], [47], [52].

When using ICA, it is assumed that:

1. The number of ICs or sources is less than the number of EEG electrodes/channels [53].
2. Volume conduction (EEG signal mixing) occurs almost instantaneously and that the summation of the various sources (cortical and artifact) is linear [53], [54]. Therefore, ICA can be used to reverse the volume conduction and linear summation of sources (cortical and artifact) recorded at the electrodes on the scalp [54].
3. The EEG electrodes [53] and the sources (both cortical and artifact) remain spatially fixed over time [54]. As a result, the various sources project to the EEG channels with a fixed weighting [54].
4. The cortical sources are statistically independent and have a non-Gaussian distribution [53], [54]. However, this assumption is not completely physiologically true as many cortical sources do not function independently from each other [53], [54].

All these assumptions do not always remain true, yet ICA is still commonly used in EEG research for artifact removal and cortical source localisation [21], [39], [45]–[52]. It can also improve classification in BCI applications [15]. Therefore, ICA can be used to decompose the EEG signal into many ICs, so that the ICs related to motor control information can be identified and isolated.

ICA aims to identify the various cortical sources by determining the ideal mixing matrix (*A*) [46]. The mixing matrix estimates the way in which the source activity (*S*) is projected to each electrode's recorded signals (*X*). The *Infomax* algorithm is often used to calculate the mixing matrix by minimizing the mutual information between the estimated cortical sources [21], [46], [47]. The source activity (*S*) can then be estimated by multiplying the EEG signals (*X*) obtained from the channels with the unmixing matrix (*W*) [46]. The unmixing matrix is the inverse of the mixing matrix. This is shown in Equation 2.1, Equation 2.2 and Equation 2.3 [55]–[57].

$$X = A \times S \tag{2.1}$$

$$W = A^{-1} \tag{2.2}$$

$$S = W \times X \tag{2.3}$$

The mixing matrix (*A*) shows the projection of each IC to every channel in the dataset [54]. Each projection has a relative weighting associated with it [54]. A channel associated with a large weighting indicates the importance of the electrode in recording the cortical activity of that source, while a small weighting indicates that that channel plays a minor role in the recording. As a result, this projection and relative weighting can be used to identify which electrodes are important for the recording of cortical activity from certain cortical sources. ICA can therefore be used to identify which electrodes are important for the recording of cortical activity related to the motor cortex and to WE and WF movements.

2.5 Neuroanatomy

The human brain is divided into three main sections: the cerebrum, the cerebellum and the brain stem [58]. The cerebrum is the largest part and controls important bodily functions [58]. The cerebrum is dived into four lobes which are described in Table 2.1 and shown in Figure 2.4. The outer layer of the cerebrum is known as the cerebral cortex, which is divided into 50 distinct areas called Brodmann's areas [58]. This representation allows for easy differentiation between the different cortical regions. This is illustrated in Figure 2.4.

Table 2.1: Lobes of the brain and their functions

Brain Region	**Function**
Frontal Lobe	Language, reasoning, and motor skills [58].
Parietal Lobe	Deals with memory and sensory signals such as: pain, pressure, touch [58].
Occipital Lobe	Interprets signals received from the eyes [58].
Temporal Lobe	Processes auditory signals and deals with memory [58].

The motor cortex is the main region of the brain which is responsible for motor control. It is located in the posterior region of the frontal lobe [58]. The motor cortex is divided into three regions: the primary motor cortex (M1), the premotor area (PMA) and the supplementary motor area (SMA) [58]. The M1 is responsible for the control of motor activity in the body [58]. The PMA and SMA work together to interpret the signals produced by the M1 [58].

M1 is located at Brodmann's cortical area 4 [58], while the PMA and SMA lie anterior to M1 at Brodmann's cortical area 6 [58]. These regions are shown in Figure 2.4. Information from these three Brodmann areas is of main concern for sensorimotor BCIs, while most of the information from the other 47 Brodmann areas is usually discarded [59].

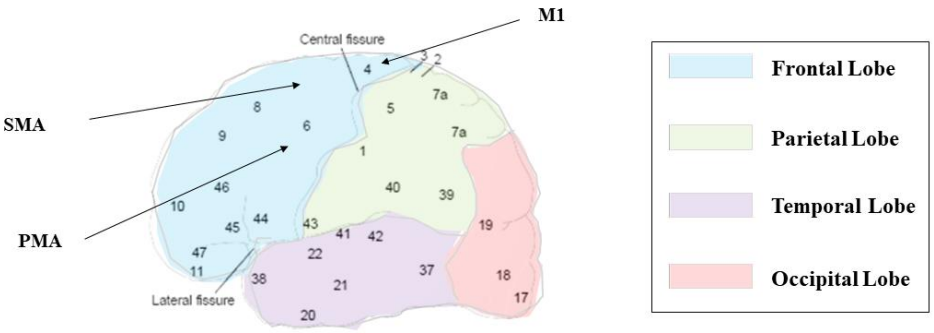


Figure 2.4: Illustration of Brodmann's areas, adapted from [58]

The M1 is spatially arranged according to the control that it provides to specific areas of the body [58]. This approximate mapping of the M1, is shown by the motor homunculus [58] in Figure 2.5. The control of certain areas of the body requires more cortical information than others, for example fine motor skills of the hand require a great amount of cortical activity [58]. Thus, a large portion of the M1 is assigned for the control of the hand, as seen in Figure 2.5.

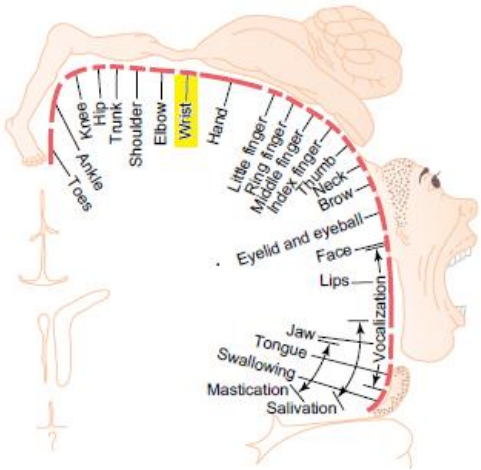


Figure 2.5: Motor homunoculous illustrating the topographical mapping of the M1 to the control of specific body parts, adapted from [58]. Both WE and WF movements are controlled by the wrist portion of the homunoculous which is highlighted in yellow.

Due to the contralateral control of the brain, RH and LH movements elicit the activation of the contralateral hemisphere of the motor cortex [58]. Thus, these signals are generated by spatially distant cortical sources. However, unilateral wrist movements such as WE and WF elicit the activation of the same hemisphere of the motor cortex (since both movements are movements about the same joint).

Additionally, the signals responsible for WE and WF movements are generated by the same cortical regions, as shown in Figure 2.5.

2.6 Neural Brain Signals

Electrophysiological brain signals can be divided into four different groups based on their activity patterns. These signals can serve as the control signal for a BCI system. The main control signals are: visually evoked potential (VEP), P300 evoked potentials (P300), slow cortical potentials (SCP) and SMRs [2], [13]. The generation of each signal has a different physiological phenomenon associated with it.

VEPs are modulations of the EEG signal occurring in the visual cortex due to a visual stimulus [13], while the P300 signal is associated with positive peaks in the EEG signal after receiving a sporadic stimulus [13]. SCP are associated with slow voltage changes in the EEG signal due to varying quantities of neuronal activity [13]. SMR are modulations in the rhythmic activity recorded over the sensorimotor cortex, which correspond to the execution of a motor task [13].

The control signals can also be categorized according to six frequency bands [55]. Each frequency band has different physiological event associated with it and irregularities can indicate possible pathologies [14]. The different frequency bands are known as the delta, theta, alpha, beta and gamma frequency bands [14], [55] and are described further in Table 2.2.

Newer research shows that the gamma frequency band plays a role in M1, however features from this frequency band are not as established in literature as ERD/ERS features from the mu and beta frequency bands. Refer to Section 2.7 for further details.

Table 2.2: EEG signal frequency band description

Frequency band	Frequency Range	Related with:
Delta	Below 4 Hz	Deep sleep [55], [60].
Theta	4-8 Hz	Drowsiness and meditation [55], [60].
Alpha	8-12 Hz	Relaxation. This rhythm is generated by the occipital region of the brain [13], [55], [60], [23].
Mu	8-12 Hz	Movement. This rhythm is generated by the sensorimotor cortex [61].
Beta	12-30 Hz	Mental activity, attention and alertness [55], [60].
Gamma	30-100 Hz	Cognitive and motor tasks [13], [55], [60].

2.7 Sensorimotor Rhythms

SMR are neural rhythmic activity which are recorded over the sensorimotor cortex of the brain [13]. They are found in the mu (8-12 Hz) and beta (12-30 Hz) frequency bands [13]. At rest the SMR are synchronized [4], [13]. In preparation for movement, desynchronization of the rhythmic activity occurs in the contralateral hemisphere [4], [13], [15], [22], [23]. This is associated with a decrease in the amplitude of the mu and beta rhythms and occurs approximately two seconds before movement onset [13]. This phenomena is known as ERD [4], [13], [15], [22], [23]. Once movement has been completed, the SMR resynchronizes in both hemispheres and the amplitudes of the mu and beta rhythms increase [4], [13], [22], [23]. This is known as ERS [4], [13], [22]. The ERD/ERS modulations exhibit a distinct shape and pattern that can be detected. An ideal ERD/ERS pattern is illustrated in Figure 2.6.

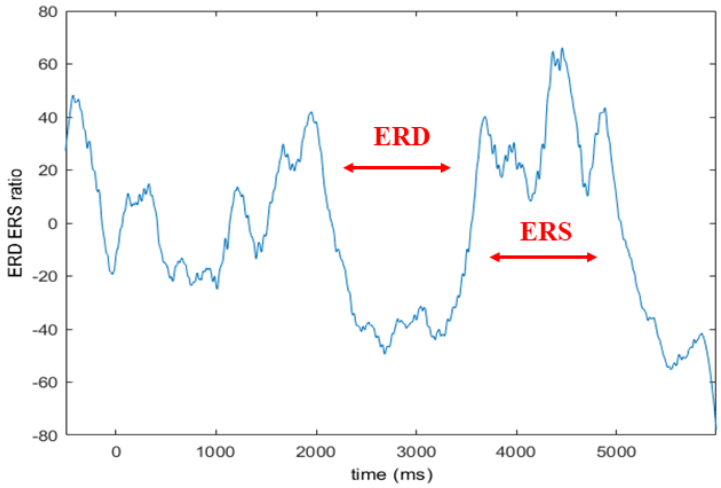


Figure 2.6: Typical ERD/ERS waveform

EEG signals contain both phase-locked and non-phase-locked components [62]. EEG phase-locked components can be revealed by averaging across all the trials [62]. This classical method is known as the additive averaging method and is often used to calculate event-related potentials [62]. This method magnifies the phase-locked component and attenuates the non-phase-locked components of the EEG signal [62].

ERD and ERS modulations are both time-locked and non-phase-locked [2], [62], [63]. Time-locked implies that the electrophysiological response occurs at approximately the same time after the onset of the stimulus for every trial, while non-phase-locked implies that the electrophysiological response occurs at different phase angles after the onset of the stimulus for every trial [62], [63]. Thus, using the traditional, additive average method would diminish the non-phase-locked components [62], [63]. A different method known as the inter-trial variance (ITV) method can be used to extract these non-phase-locked components [62], [63]. The ITV method computes the changes in power of a bandpass filtered EEG signal [62]. This is shown in Equation 2.4. In this equation, N is the number of all the trials used, i and j refer to the trial number and sample number respectively. $x_{f(i,j)}$ is the bandpass filtered signal of a given trial and $\bar{x}_{f(i,j)}$ is the mean of the bandpass filtered signal across all the trials [62].

ERD and ERS is then expressed as a change in power with respect to the reference interval [63]. This is shown in Equation 2.5, where *R* is the average of $ITV_{(j)}$ across the reference interval [63]. This change in power is either a decrease or an increase which represents either an ERD or an ERS respectively [63].

$$ITV_{(j)} = \frac{1}{N-1}\sum_{i=1}^{N}(x_{f(i,j)} - \bar{x}_{f(i,j)})^2 \quad 2.4$$

$$ERD_{(j)} = \frac{R - ITV_{(j)}}{R} \times 100\% \quad 2.5$$

2.8 Chapter Summary

This chapter detailed several concepts which are important for the contextualization of this study. Basic information on wrist movements, BCI systems, EEG, ICA, neuroanatomy, neural brain signals and SMRs was presented.

Chapter 3 - Literature Review

This chapter discusses the relevant literature related to BCI movement tasks and explores channel-set optimization and reduction for BCI applications. The gap in the current research area is highlighted by examining the different movement tasks used in BCI systems, describing the various channel-set reductions for different types of BCIs and exploring the role of ICA in current channel reduction techniques. The various features used to differentiate between different movement tasks is then discussed.

3.1 Exploring Movement Tasks in BCI

Numerous EEG studies have explored the classification of LH and RH imaginary and executed movements, with varying degrees of accuracy, 64 % to 99 % [44], [48], [55], [64], [65]. The neural regions responsible for the generation of RH and LH movements are spatially distant (see Section 0), thus discrimination between these movements can be achieved by taking advantage of this distance. However, the differentiation of these movements is a binary-class classification, which will limit the complexity and control of a BCI system such as the control of a bionic hand, causing it to be less dexterous [66].

Following the studies of RH vs. LH neural discrimination, EEG research led to the discrimination of additional limb movements whose activations elicit spatially distant brain regions. Typical limb movements include a combination of upper limb, lower-limb and tongue movements [19], [22], [39], [65], [66]. These movements are topographically mapped to distinct regions of the M1. This is illustrated in Figure 3.1a. These regions are spatially apart allowing one to differentiate between them as done with RH vs LH movements. In a similar manner, Caracillo and Castro [65] investigated the classification of RH, LH and arm movements. Furthermore, the classification between shoulder, elbow and finger movements [19], [22], [66] and the differentiation of RH, LH, tongue and right foot movements [39] have been thoroughly documented. These studies provide an increase in the number of classes and control signals available [22]. However, the

increase in the number of classes does not directly translate to better bionic hand control as only certain movement types are useful in the control of a bionic hand (see Section 1.1), such as those that will assist ADLs (see Section 2.1).

In order to further increase the number of control dimensions available to the BCI system, there has been recent research into discriminating EEG signals responsible for different hand and finger movements as this will increases the number of classes available to the BCI system for bionic hand control. The hand movements investigated include: full finger flexion and extension [67]; the palmar grasp, the pincer grasp and the lateral grasp [68]; clockwise and anticlockwise wrist movement (which comprises supination and pronation movements) [67]. Wrist and finger movements have been differentiated in [4], while the binary classification between ten pairs of executed finger movements on the same hand have been explored in [69]. However, these studies contended with an additional challenge: the brain region responsible for the activation of hand and finger movements are spatially close. This can be seen in Figure 3.1b.

The differentiation of different types of unilateral wrist movements (flexion, extension, supination, pronation) of the same wrist have also been thoroughly explored [15], [20], [21], [24], [49], [70]–[72]. Sepulveda et al., [73] investigated the class separability of four different wrist movements (WE, WF, radial and ulnar deviation of the wrist). Different movements about the same wrist joint are generated by the same region of the brain, illustrated in Figure 3.1c. As a result, the signals produced for the movement of the same limb are similar, making it difficult to determine which signal is responsible for which movement [20], [21], [74]. Despite the difficulty surrounding the differentiation of these movement types, Vuckovic and Sepulveda [20] were able to achieve a classification accuracy of 82 % when differentiating between WE and WF. Other classification accuracies for unilateral hand movements range from 61 % [72] to 69 % [71].

Despite the importance of wrist movements (mainly WE and WF) mentioned in Section 1.1 and Section 2.1, research regarding the differentiation of the neural brain signals responsible for these movement types is limited. Thus, it is worthwhile

to further explore the differentiation of these movements and to expand this research field.

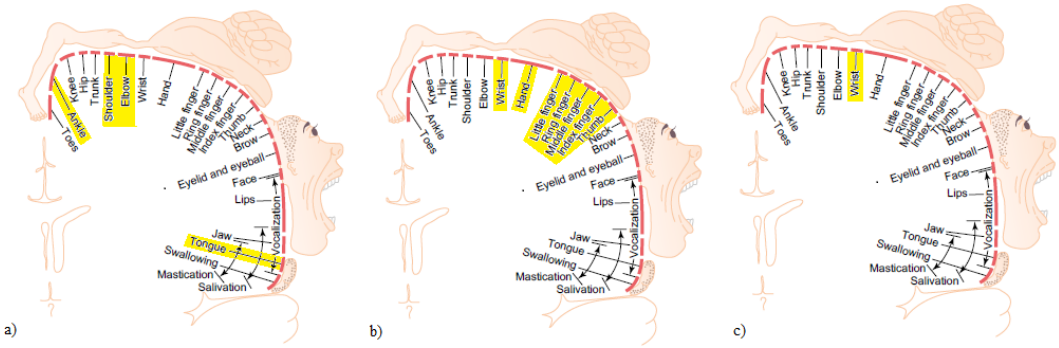


Figure 3.1: Motor homunoculous illustrating the topographical mapping of the M1 to the control of specific body parts, adapted from [58]. a) shows the mapping of upper limb, lower-limb and tongue movements to the motor cortex. b) shows the mapping of wrist and finger movements to the motor cortex. c) shows the mapping of different wrist movements (about the same joint) to the motor cortex.

3.2 EEG Channel Reduction for BCI Applications

A main concern with current BCI systems is the number of EEG electrodes required for the system to operate efficiently. This is elaborated further in Section 1.3. As a result, there is a trade-off between increasing the number of electrodes required for greater spatial resolution and decreasing the electrode usage for the practicality of everyday use. In this sub-section, channel reduction and optimization will be briefly examined for all BCI types (refer to Section 2.6 for background on the different types of BCIs): P300 BCIs [17], [18], [75], steady-state VEP (SSVEP) BCIs [76], sensorimotor BCIs [44], [46], [51], [77], [78], as well as hybrid BCI combinations [43], [79], but the focus will be on sensorimotor BCIs.

For a P300 speller BCI, Cecotti et al. [75] reduced a 32-channel set with a classification accuracy of 95.83 % down to eight channels with a classification accuracy of 94.92 %, using a Bayesian linear discriminant analysis classifier. The reduced channel set was reduced by using a backwards selection technique, which removed the least significant channel using a backward elimination technique in an iterative process. For a P300 speller BCI, Speier et al. [17] were able to reduce the

32-channel set with a classification accuracy of 86.88 % to four channels with a classification accuracy of 89.69 %, using a naïve Bayes classifier. The reduced channel set was reduced by using a Gibbs sampling method. The final set of electrodes for both Cecotti et al., [75] and Speier et al., [17] are illustrated in Figure 3.**2**a and Figure 3.2b respectively.

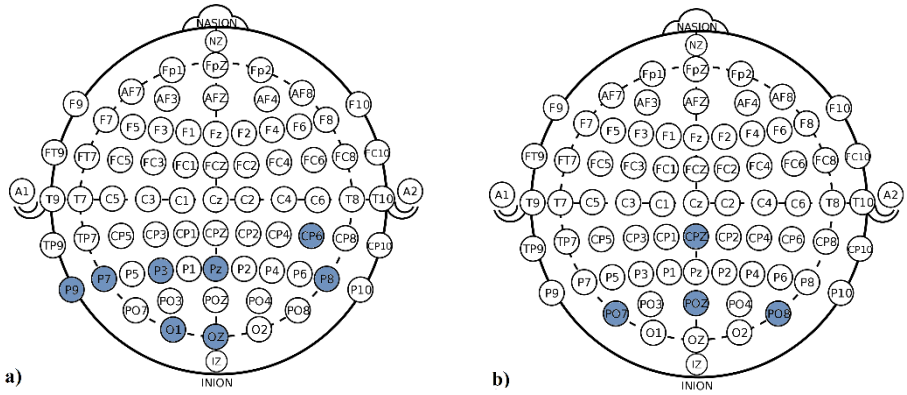


Figure 3.2: Reduced electrode sets for Cecotti et al., [60] and Speier et al., [17] respectfully

Ko et al., [43] designed a hybrid BCI system that uses both MI (RH vs LH) and steady-state VEP (SSVEP) as the input signals. The number of channels used was reduced from a set of 32 channels to three channels (C3, C4, Cz), using the common CSP algorithm for the detection of ERD/ERS patterns and a support vector machine (SVM) classifier [43]. The three electrode hybrid system obtained an accuracy of 95 % when differentiating between RH and LH movements, in comparison with 99 % when using the 32-channel set [43]. The hybrid BCI system was able to achieve these results as the system had additional information, i.e. input from two brain activity patterns. It should be noted that the three electrodes/channels selected are considered to be optimal for MI studies as they are related to movement and motor control [59]; Cz, C3 and C4 are the main electrodes associated with the M1 [59]. This study shows that significant channel reduction is possible if additional information is available. However, when only one brain activity pattern (e.g. MI) is used as the input signal, it is unlikely that such results will be obtained. Furthermore, differentiating between WE and WF (unilateral movements of the same joint) is more challenging than the MI explored by Ko et al. [62]. This implies

that the final reduced number of channels required for discriminating between WF and WE may be more than in the above-mentioned studies (e.g. 16 channels).

Lahiri et al. [46],[47] optimized an initial channel set consisting of 19 channels for the discrimination between a variety of different limb movements. The resultant reduced channel sets are illustrated in Figure 3.3. The channel set was reduced to five channels (Figure 3.3a) and four channels (Figure 3.3b) when differentiating between LH and RH executed and imaginary movements. When distinguishing between left- and right-legged executed and imaginary movements, the channel set was reduced to six channels (Figure 3.3c) and three channels (Figure 3.3d). While differentiating between finger and tongue movements a channel set of five channels (Figure 3.3e) was obtained. The reduced channel set shown in Figure 3.3a illustrates that not all channel chosen reflect the desired physiological cortical process. Electrodes P3 and P4 are not typically associated with motor activity but are linked with strong visual alpha waves. This study demonstrate that it is possible to significantly reduce the number of electrodes required for sensorimotor BCI systems while maintaining accuracy of MI discrimination, but it is unknown whether the underlying neural information obtained is reflective of movement control or of different control signals. The EEG signals provided from channels P3 and P4 could be linked to the visual clues in the experiment, or be associated with motor related cortical activity that has been spread through the brain (see Section 2.3). Using anatomically appropriate knowledge in the reduction method is ideal for ensuring that only relevant channels related to movement control are chosen. ICA will provide the means to select anatomically relevant channels, using motor related features such as ERD/ERS. Thus, providing clarity on the type of information that the control signal is reflective of.

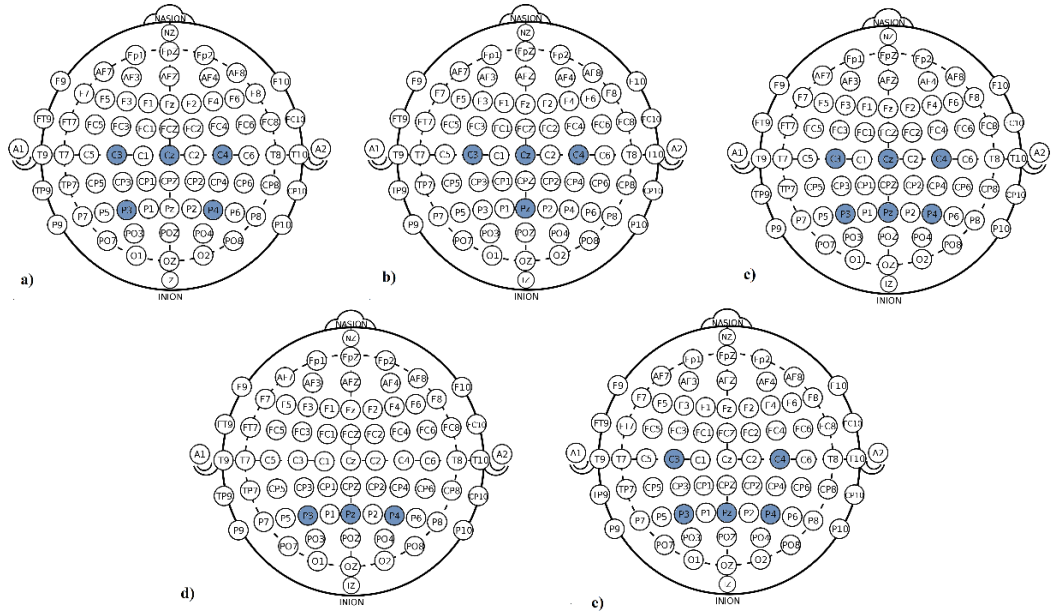


Figure 3.3: Reduced electrode sets for Lahiri et al., [31],[30]

Schwarz et al. [68] experimented with using a variety of spatially uniform distributions of channel sets when differentiating between three different executed unilateral grasp movements: palmar grasp, pincer grasp and lateral grasp. Unlike the methods previously mentioned, this approach does not use the EEG data to drive the choice of the reduced set of channels. Instead, it explores the classification results obtained when using a reduced number of channels from a few pre-defined layouts. The pre-defined layouts may exclude some important EEG channels and may also include some non-crucial EEG channels. The various pre-defined layouts are illustrated in Figure 3.4. A standard 61 channel layout resulted in an average classification accuracy (across subjects) of 66.9 %, while a standard 25, 15 and 5 channel layouts obtained classification accuracies of 64.2 %, 59.8 % and 54 % respectively when using a shrinkage based linear discriminant analysis classifier. This study shows the possibility of applying electrode reduction techniques to an EEG dataset consisting of unilateral hand movements. It also illustrates the possibility of using preselected electrode configurations as a form of channel reduction for unilateral hand movement discrimination. However, this must be done with caution since it can bring in other non-motor cortical information (as with Lahiri et al., [46],[47]).

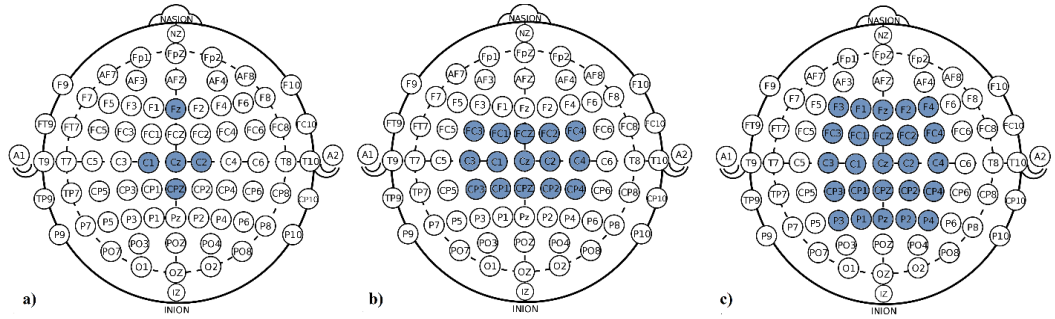


Figure 3.4: Spatially uniform electrode distributions for Schwarz et al., [57]

In order to determine the class separability of four different wrist movements (WE, WF, radial and ulnar deviation of the wrist) Sepulveda et al. [73] found the combination of the best channels and features from a total of 28 channels and 93 features. In this research the greatest class separation was achieved when a channel from the temporal region (T7) was chosen, but the temporal region is responsible for higher-order processing of sensory inputs such as auditory and visual stimuli [58]. These results surprisingly suggest that non-motor related electrodes may be responsible for recording motor activity. However, a few issues concerning the validity of this study have been identified. Channels were removed prematurely, which could affect the validity of the study, only channels located on the left hemisphere of the brain were considered. Furthermore, there is no mention that the data underwent artifact removal or spatial filtering – both stages are vital in ensuring that accurate results are achieved. Despite the questionable methods, this study has provided a foundation which can be expanded upon. The problems found in the study can be resolved and extended in new research. This study shows that the discrimination of unilateral wrist movements (such as WE and WF) in a reduced channel set is worthwhile exploring.

The number of electrode reduction studies for BCI systems are few. Of these electrode reduction studies, some are done for non-motor BCI systems such as: P300 speller and SSVEP. Of the few studies implemented for sensorimotor BCI systems, only two involve unilateral hand movements. In many of the studies discussed above, channels associated with non-motor cortical information were selected. This suggests that non-motor related electrodes may play a role in recording motor activity and movement intent. This indicates a need to obtain some

insights into the specific type of control information that is retained during the channel reduction process.

3.3 ICA in EEG Channel Reduction

Numerous channel reduction studies have been explored in Section 3.2. In these studies, ICA is not frequently used in the channel reduction process. However, when ICA is used, it is applied only as an artifact removal technique or as a source localization tool [46], [47], [51], [52]. Typical optimization techniques such as backward elimination [75], Gibbs sampling method [17] and evolutionary methods [46], [47], [52] are commonly used for channel reduction.

Lahiri et al. [46], [47] and Datta et al. [52] both use ICA in their channel reduction methods, but only in the capacity of source localization. The EEG signals and the corresponding ICs produced were transformed into common EEG features which described each class. The features commonly used in sensorimotor BCIs are explored in the next subsection. Once the features pertaining to each class is produced, an evolutionary algorithm such as a self-adaptive firefly algorithm [46], [47] or an artificial bee colony with adaptive scale factor algorithm [52] is applied in order to obtain the reduced channel set. These evolutionary algorithms imitate the characteristic behaviours of insects in order to select the optimal channels by optimizing three objectives. The first objective aims to maximize the correlation between the features selected before and after channel selection [46], [47], [52], the second aims to minimize the mutual information between the features selected from the chosen channels [46], [47], [52], while the last objective is to maximize the ratio of difference between the chosen features for two tasks [46], [47]. These objectives ensure that sufficient cortical information has been retained and redundant information has been removed, while ensuring that the features chosen, provide sufficient class separation for the two tasks. These evolutionary algorithms omit the addition of anatomical knowledge to influence the channel selection. A general overview of a typical evolutionary algorithm is shown in Figure 3.5.

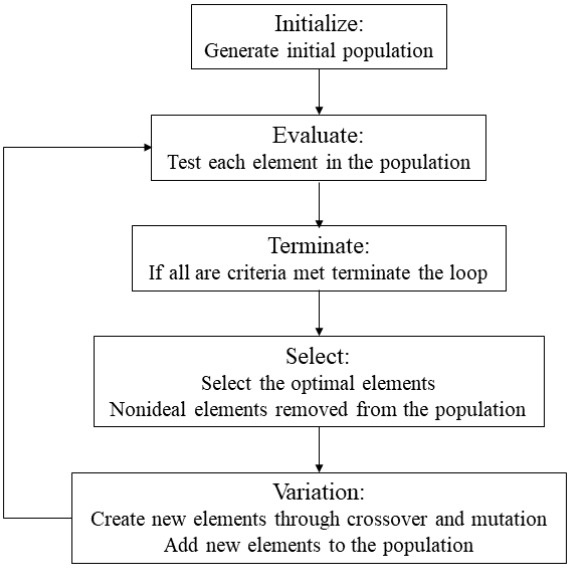


Figure 3.5 A general overview of a typical evolutional algorithm.

ICA has never been used as the primary method for channel reduction. In the research described in [46], [47], [52], the various authors did not focus on identifying and isolating specific (motor-related) cortical sources during the channel reduction process. Therefore, instead of using an evolutionary method, as described in [46], [47], [52], it is hypothesized that using ICA in conjunction with physiological and anatomical knowledge and insight can be used to select the optimal channels. It should be possible to use ICA as the primary technique for channel reduction.

3.4 Features Used in Movement Tasks

In order to differentiate between the brain signals responsible for WE and WF movements, relevant motor-related features used in EEG-based sensorimotor BCIs must be investigated. This sub-section explores the different motor-related features that have been applied to EEG BCI studies, involving common BCI motor tasks, unilateral hand movements and more specifically, WE and WF. It aims to justify the choice of using features based on ERD/ERS in the method. Table 3.1 provides a summary of the different types of features used in different movement tasks' studies.

ERD/ERS of the mu and beta frequency bands are commonly used as features in the differentiation of common limb movements (e.g. RH, LH, shoulder and tongue movements) [19], [22], [39]. ERD/ERS has also been used in conjunction with SSVEP features for a MI SSVEP hybrid BCI system in the classification RH and LH movements [43], [79].

Other features used (less commonly) for these types of movement classifications are adaptive auto-regressive (AAR) parameters, Hjorth parameters, power spectral density (PSD), discrete wavelet transform (DWT) [46], [47], [52], movement related cortical potential (MRCP) [80], [81] and time-domain features such as the standard deviation, the mean and the median of the cleaned EEG channel [48]. Additionally, the detection of the ERD and MRCP patterns have been used together in order to detect the onset of upper limb movements [81], [82]. Combining features from both MRCP and SMR can increase the classification accuracy of the BCI system [81].

Different types of features have been explored for the differentiation of different unilateral hand movements. ERD/ERS has been used as a feature when discriminating between fast and slow WE and wrist rotation movements [83], as well as when differentiating between unilateral wrist movements (WE and WF) and finger movements (MFE, MFF, TRP) [4]. The rebound rate of MRCP has been used in conjunction with the power contained in the mu and beta frequency bands as features, when discriminating between fast and slow wrist movement (extension and rotation) on the same limb [83].

Features based on rhythmic activity outside the mu and beta frequency bands have also been used. Different features found in the delta, theta, alpha, beta and gamma frequency band have been used in the binary classification of wrist movement (WE, WF, supination and pronation) [20]. In a similar study conducted by Vuckovic and Sepulveda [71], approximately 200 features distributed across the various EEG frequency bands were extracted to discriminate between WE and WF EEG signals. Approximately 50 % of these features were found in the delta band, 30 % in the gamma band, while the remaining 20 % were spread between the theta, alpha and beta frequency bands.The PSD of the gamma frequency band and Hjorth

parameters have been used for the classification of forearm and wrist, flexion and extension [70], while AAR parameters in conjunction with extreme energy ratio criterion have been used as features to differentiate between clockwise and anticlockwise wrist movement as well as the opening and closing of fingers [67].

Table 3.1: A summary of different features used in different movement tasks' studies

Features	**Movement Type**	**Real/MI**	**References**
ERD/ERS	RH, LH	MI	[43], [64], [79]
	RH, LH, tongue, right foot	MI, Real	[39]
	Right shoulder, right index finger flexion	Real	[19]
	Hand grasp, elbow movement	MI	[22]
	Wrist movements and finger movements.	MI, Real	[4]
ERD/ERS and MRCP	WE, WF, MFF, MFE, TRP	MI, Real	[82]
	WE, wrist rotation	MI	[83]
	Upper limb reaching movements	Real	[81]
	WE, WF, supination, pronation	MI, Real	[20]
MRCP	Palmer grasp, pincer grasp, lateral grasp	Real	[68]
Features from the delta, gamma, theta, alpha and beta frequency band	WE, WF	MI	[71]
Average power in theta, alpha and beta frequency band	RH, LH	MI, Real	[55]

PSD	RH, LH	Real	[65]
	RH, right arm	Real	[65]
Standard deviation, mean, median, power spectral entropy	RH, LH	MI	[48]
AAR parameters, Hjorth parameters, PSD, DWT	RH, LH, left leg, right leg, tongue, fingers	MI, Real	[46], [47]
	RH vs LH	Real	[52]
PSD of gamma frequency band, Hjorth parameters	Forearm and wrist, flexion and extension	MI	[70]
PSD, DWT	Right elbow, right shoulder, right fingers, left elbow, left shoulder, left fingers	MI	[66]
AAR parameters, extreme energy ratio	Wrist and finger movements	MI	[67]

From the review in this sub-section and Table 3.1, it is evident that different features have been explored in the literature, however the most commonly used motor-related features in sensorimotor BCIs are ERD/ERS of the mu and beta frequency bands (refer to Section 2.7) [84]. ERD/ERS is well researched, it's relationship with motor control is well established and the rhythmic activity has a unique waveform, making it easily identified. It has been used as a feature for wrist movement EEG classification studies. Hence the use of features based on ERD/ERS will likely allow the selection of ICs and channels holding key information related to WE and WF motor-control.

3.5 Chapter Summary

From the discussion of the relevant literature it is evident that discrimination of different movements is common in BCI research. The discrimination between unilateral WE and WF is possible but is less studied. A few channel reduction and optimization studies have been applied to sensorimotor BCIs. However, no reliable channel reduction studies for WE and WF movements have been presented.

ICA has not been used in literature as a main driver for electrode reduction, but it has been shown to be effective in isolating motor-related neural control information. Features based on ERD/ERS are well researched and have been applied to WE and WF. It is thus hypothesised that ICA coupled with ERD/ERS features and knowledge of neuroanatomy will provide a novel method for channel reduction and optimisation.

Chapter 4 - Data Preparation

This chapter describes the EEG dataset used in the study and the various steps implemented to prepare the dataset for the method.

For this study a suitable EEG database was obtained. A description of this database is provided. The EEG data was recorded using an EGI, Geodesic Sensor Net (GSN) 128 system. The placement of the EEG electrodes that formed this system is described below. Detailed steps are then provided for cleaning and processing the data according to the requirements of the method. The cleaned dataset is then arranged into various datasets, based on the two investigations in the research. Potential limitations of the datasets are described.

4.1 EEG Database Description

A suitable EEG dataset was obtained from Mohamed et al. [4]. Permission for the use of this data has been provided by Mohamed et al. [4] and ethical clearance for reuse of this data was provided by the University of the Witwatersrand. The clearance certificate can be found in Appendix A (ethic clearance certificate number: M190608).

The EEG database contains EEG recording from five male subjects. These subjects were untrained, healthy and in their early twenties. The subjects were recorded performing five different hand movements: WE, WF, FE, FF and TRP. The EEG dataset contains both real and imaginary hand movements, however, only real movements were considered for this study. Each subject performed 20 repetitions of a movement type per hand. Therefore, there are 20 trials per test subject per hand, resulting in 40 trials per movement type for each subject:

$$1 \text{ (Movement Type)} \times 2 \text{ (RH and LH)} \times 1 \text{ (Real Movement)} \times 20 \text{ (Repetitions)} = 40 \text{ trials}$$

During the data collection process, the subjects were seated, facing a computer screen with their hand and forearm resting on an armrest. The computer screen

displayed the type of movement that the subject was expected to perform as well as the instructions for that set. In the first time-interval (S1) the subjects must prepare for movement (real/imagined) onset, in the second time-interval (S2) the subjects must execute the movement for a given time. The third time-interval (S3) provides the subjects with a short rest period before the next repetition begins. In order to limit muscle artifact contamination in the recordings, the subjects were asked not to move their bodies (blink, move their eyes, swallow etc.) during S1 and S2 but rather during S3. This is illustrated in Figure 4.1.

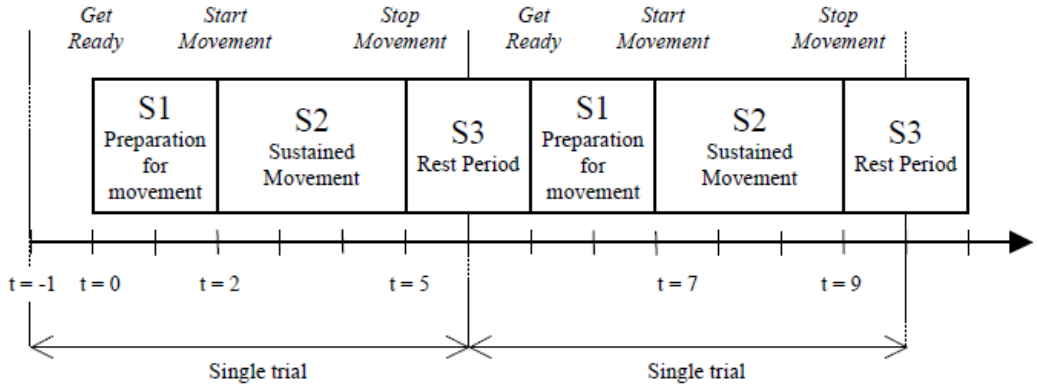


Figure 4.1: Time sequence and instructions for a single trial, from Mohamed et al. [4]

4.2 EEG Electrode Placement

The EEG data was recorded using an EGI system (system 200). The GSN 128-electrode placement system was used. Figure 4.2 shows the GSN electrode placement of the 128-electrodes. The 129th electrode was used as the reference electrode. This electrode corresponds to electrode Cz in the International 10-10 system [85]. The approximate correspondence between the electrode placements in the GSN 128 system and the International 10-10 System is listed in Table 4.1 [85].

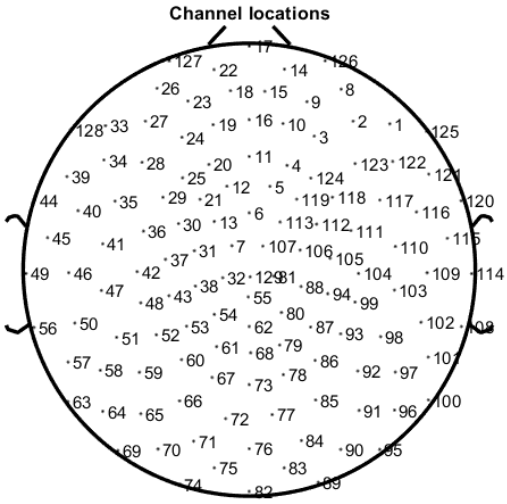


Figure 4.2: GSN electrode placement of the 128-electrode set.

Table 4.1: Approximate correspondence between electrode placement of the GSN System and the International 10-10 System [75]

GSN System	10-10 System
36	C3
104	C4
129	Cz
24	F3
124	F4
33	F7
122	F8
22	FP1
9	FP2
14	FPZ
21	FPZ
15	FPZ
11	Fz
70	O1
83	O2
52	P3
92	P4
58	T5-P7
96	T6-P8
45	T3-T7
108	T4-T8

4.3 Pre-processing

EEGLAB was used to pre-process the data [86]. The data was visually examined first, any channels or trials with excessive noise, voltage spikes or severe distortion were noted. A bandpass filter from 0.5 – 90 Hz was applied to the signal in order to limit the frequency spectrum to within the range of brain signals [13], [20], [87]. A notch filter was then used to remove the 50 Hz power line interference [4], [20].

The data was divided into 7 s trials [4], [20] according to the diagram illustrated in Figure 4.1. Each epoch began 1 s before movement preparation at time = -1 s and continued until movement was terminated at t = 6 s [4]. Thus, the data was divided into 7 s trials. To avoid low frequency drifts, the baseline value was corrected using the interval t = -1 s to t = 0 s [20].

The Automatic Artifact Removal plugin toolbox for EEGLAB was used to remove EOG and EMG artifacts from the EEG signal [88]. Removal of EOG and EMG artifacts are vital as they contaminate the EEG signal. A blind source separation-canonical correlation analysis algorithm was used to remove both EOG and EMG artifacts. The effectiveness of the artifact removal was verified by using ICA (infomax algorithm), which confirmed that the large components near the front of the head were removed. A visual inspection of the EEG signal confirmed that large voltage spikes in the signal had also been removed.

After artifact removal was conducted, the channels and trials were manually and visually inspected for any remaining large voltage spikes and severe signal distortion. Bad channels and trials were then removed. A summary of the channel and trials removed for each subject is found in Table 4.2.

Table 4.2: Summary of the number of channels and trials removed for each subject

	Number of Removed Channels		**Number of Removed Trials**	
	RH	LH	RH	LH
Subject 1	0	-	1	-
Subject 2	0	1	7	5
Subject 3	1	1	9	6
Subject 4	-	0	-	0
Subject 5	0	0	5	5

A bandpass filter from 8 – 30 Hz was then applied to the datasets in order to separate the mu and beta frequency bands from the rest of the EEG signal. This allowed for the analysis of ERD/ERS patterns which is associated with wrist movements.

4.4 Data arrangement

After pre-processing, datasets for each subject were created. The data was stored in a 3D array: [channels × time × trials] as illustrated in Figure 4.3. Imaginary movements were removed from each dataset, ensuring that only real movements were investigated. The datasets were then arranged according to the investigation that was being studied. This is explained graphically in Figure 4.3. This arrangement allowed for the same ICA mixing matrix to be calculated and applied to both movement classes in each dataset [20].

Investigation 1 (RH vs LH): One dataset was created per test subject (when applicable). This dataset contained both RH and LH real movements from all five movement types (WE, WF, MFF, MFE, TRP). A total of three datasets were created for this investigation, as described in Table 4.3. Subject 1 and 4 were excluded from this investigation, as EEG data was recorded for only one of their hand movements.

Investigation 2 (WE vs. WF): Two datasets were created per test subject (when applicable). One dataset contained only right-handed real WE and WF movements

while the other dataset contained only left-handed real, WE and WF movements. A total of eight datasets were created for this investigation, as described in Table 4.3.

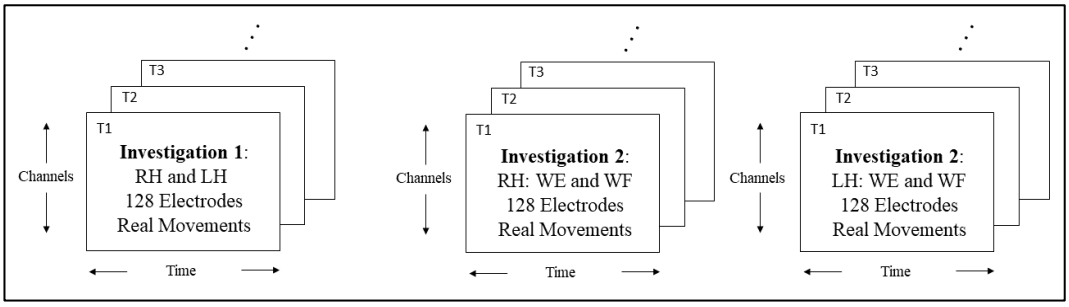


Figure 4.3: Diagram illustrating the dataset arrangement. At this point the data was arranged in a 3D array: [channels × time × trials]. In investigation 1, one dataset was created per subject consisting of both RH and LH real movements. In investigation 2, two datasets were created per person (when applicable), one for RH that contains WE and WF and the other for LH that contains WE and WF movements.

Table 4.3: Number of datasets per test subject per investigation

	Investigation 1	**Investigation 2**	
	RH & LH	RH	LH
Subject 1	-	-	1
Subject 2	1	1	1
Subject 3	1	1	1
Subject 4	-	1	-
Subject 5	1	1	1
Total	**3**	**8**	

4.5 Limitations of Dataset

The dataset, although suitable for this research, has a few limitations.

1. A limited number of subjects were recorded. This may have limited the analysis of the method, since the sample size is too small to reach any definitive conclusions regarding the validity of the method.

2. Only three out of the five subjects had data recorded for both right-handed and left-handed movements. The remaining two subjects only had data recorded from one hand. This restricted the analysis of Investigation 1, as the sample size was reduced.
3. Each movement type only had 20 repetitions recorded, resulting in a limited number of trials for the classification stage. This may have skewed the classification accuracies obtained.

4.6 Chapter Summary

This chapter described the EEG database that was obtained and used for this study. The placement of the EEG electrodes used to record the database was illustrated. The various steps implemented to prepare the data for the method were discussed. A description of the datasets created for each investigation was presented. Potential limitations regarding the dataset were then discussed. These datasets are used as the inputs for the method, which is discussed in the next chapter.

Chapter 5 - Method

This chapter presents the design and implementation of a novel channel reduction and optimisation method which is based on ICA. An overview of the method is presented in Figure 5.1. In this study, ICA allows for the selection of information related to motor control (WE and WF or RH and LH), which is identified using ERD/ERS patterns originating from the approximations of anatomically located motor control regions. Based on this motor control information, a novel ranking system provided each channel in the dataset with an objectively calculated score. This ranking system allowed the top 24, 16, 8 and 3 best-scoring channels to be selected and formed into new channel configurations. Each reduced channel configuration was then tested: details are given in Chapter 6 .

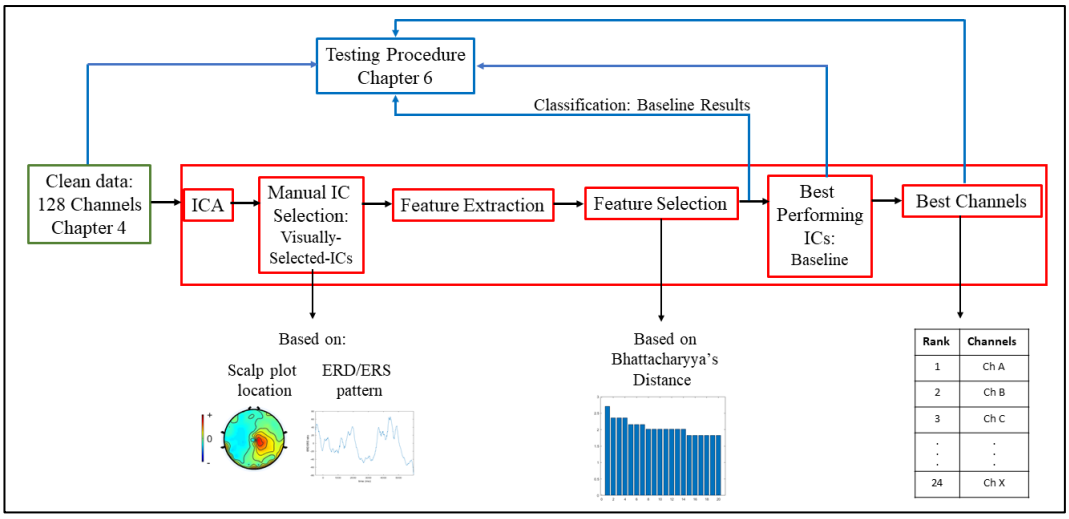


Figure 5.1: Method overview. The method is applied to both investigations. The method takes in clean data that was processed in Chapter 4. The method ranks the channels according to a calculated score, which is then used to form reduced channel configurations. This method provides three types of information used for testing in Chapter 6.

The method was applied in both investigations. The method was first applied in investigation 1 to differentiate between the neural signals responsible for RH and LH movements. The method was then applied to investigation 2, to differentiate between the neural signals responsible for WE and WF movements. Investigation 1 was carried out first, as an initial step to evaluate the method, then investigation 2.

5.1 ICA and Manual Selection of ICs

ICA (implemented using the *Infomax* algorithm) was run on each dataset described in Section 4.4. Background on ICA and its application with EEG can be found in Section 2.4. When ICA was run on each 128-electrode dataset, 128 ICs were produced. The number of ICs produced is dependent on the number of channels in the dataset.

The scalp plots and ITV graphs (see Section 2.7) for each IC were generated for visual inspection. Visual inspection was carried out in order to manually select the ICs that contributed towards movement control. For an IC to be manually selected, two criterions had to be met:

1. The scalp plots must show that the signals represented by the IC originate from the M1 region (see Section 0) of the brain or its close surroundings. An example is shown in Figure 5.2a.
2. The ITV graphs must illustrate typical ERD/ERS characteristics. An example is shown in Figure 5.2b.

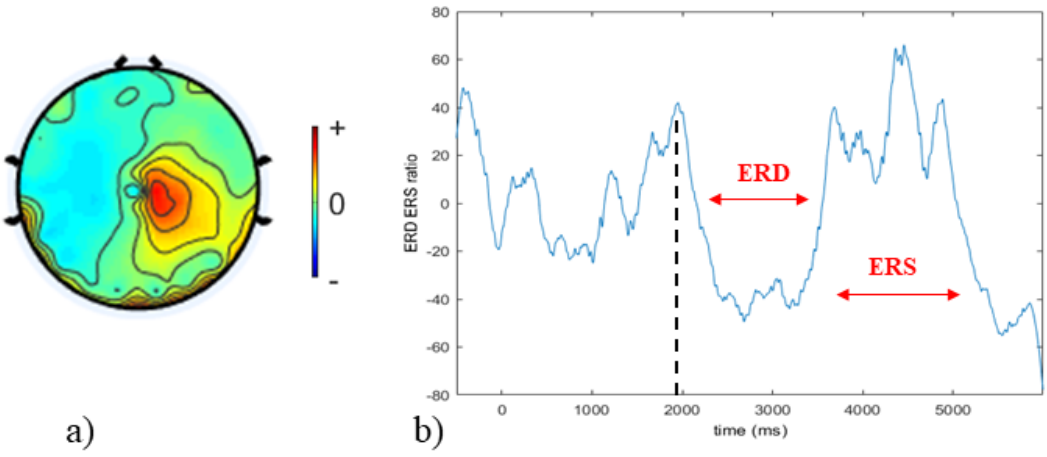


Figure 5.2: Example of a selected IC based on the visual inspection of the scalp and ITV plot, from subject 2, investigation 1. a) shows the IC scalp plot. b) shows the average ITV graph and the ERD/ERS pattern. The dashed line indicates when movement starts.

Only if both these criteria were met was the IC selected. This manual selection process was time-consuming; however, it was a vital step in attempting to isolate

movement-related signals so that non-movement-related information could be discarded. These visually and manually selected ICs are referred to as *visually-selected-ICs*. The number of *visually-selected-ICs* which were isolated for each investigation per subject is listed in Table 5.1. A new version of each dataset containing only the *visually-selected-ICs* was created.

Table 5.1: Number of visually-selected-ICs isolated for both investigations

	Investigation 1	**Investigation 2**	
	RH vs LH	WE vs WF	
		LH	RH
Subject 1	-	-	31
Subject 2	60	53	98
Subject 3	67	54	29
Subject 4	-	48	-
Subject 5	85	51	61

5.2 Feature Extraction

Features based on ERD/ERS modulations were extracted during the feature extraction (FE) stage. Features were extracted per trial per class of each dataset mentioned in Section 4.4, therefore, the features generated for each subject in both investigations differed.

In order to fully capture the desynchronization and resynchronisation of the neural rhythms, the change in power over time was calculated for the different frequencies. This was carried out for the time period: t = 1 s to t = 4 s, as this time period contains both movement preparation (S1) and movement execution (S2) segments (see Section 4.1, Figure 4.1).

In order to capture the change in power over time, a 300 ms sliding window was moved in 100 ms increments, extracting 28-time windows. For each time window, the power spectrum was calculated using a Fast Fourier transform (FFT) [2]. The frequency spectrum produced was then divided into 7 frequency bands, each

consisting of 3 Hz. The power within each of the 3 Hz frequency band was then summed to produce a feature. This is graphically explained in Figure 5.3.

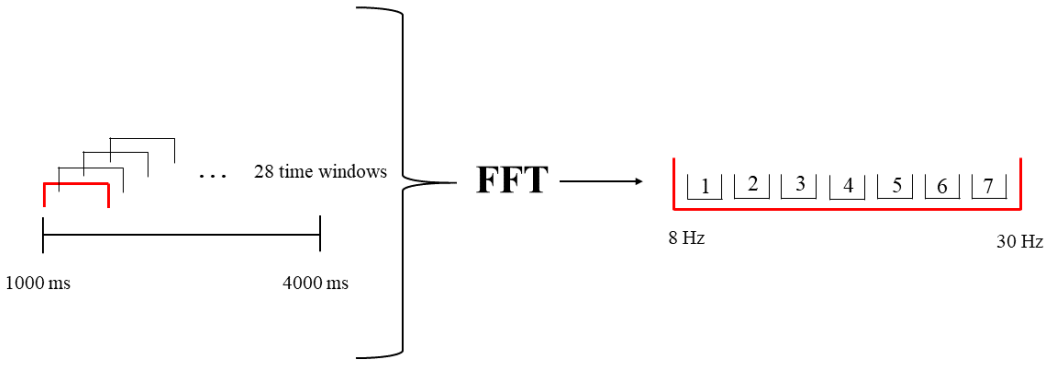


Figure 5.3: FE method overview. Total number of features per IC = 28 x 7 = 196 features per IC.

This procedure was carried out for each IC which resulted in a large feature set being generated. The number of features created per dataset = $28 \times 7 \times NumberOfIC$. For example, 11760 features were extracted from subject 2's dataset in investigation 1. A graphical representation of the dataset created is shown in Figure 5.4.

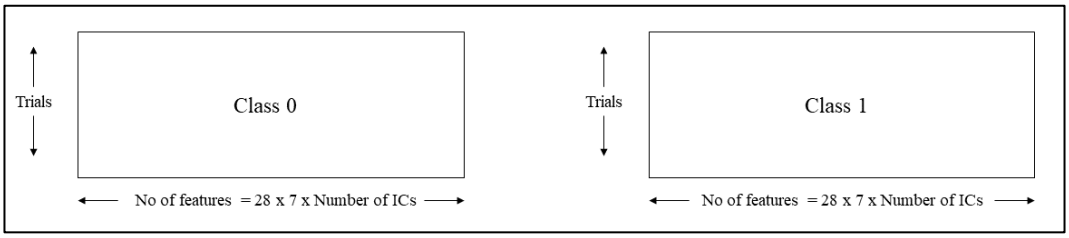


Figure 5.4: Description of the feature set. The features were stored in a 2D array: [trials × features]. Each feature set contains the features describing its class. The number of features extracted depends on the number of visually-selected-ICs.

5.3 Feature Selection

Typically, the feature selection (FS) stage is applied in order to reduce the large number of features that were extracted, so that the classification process is simplified [84]. In this study, FS is used in this capacity as well as to score the selected features, therefore the ICs from which the selected features originated can also be scored. This will be discussed in more detail in Section 5.4. Thus it was

important that significant data describing the investigated movement type was retained during FS [13]. Features which best characterized the separability of the different classes were chosen and used for classification [13]. See Section 6.1 for further details on the classification stage.

FS was achieved using the Bhattacharyya's distance (BD). The BD determines the relative relationship between two classes [39], [89], thus providing a measure of class separability [39], [89]. A larger BD value indicates that the features selected provide a greater class separation than features which have a smaller BD value [39], [89].

The BD is linked to the Bhattacharyya's coefficient (BC) through Equation 5.1 [90]. The BC calculates the amount of overlap between two classes' probability distributions, thus determining the relationship between these two classes [90]; this is shown in Equation 5.2. Variables *p* and *q* denote the probability distribution of each class.

$$BD(p,q) = -\ln\big(BC(p,q)\big) \tag{5.1}$$

$$BC(p,q) = \sum_{x \in X} \sqrt{p(x)q(x)} \tag{5.2}$$

The BD was calculated for each feature. The features were then sorted according to their BD value, so that features with the largest BD values could be selected. A reduced feature set was then formed for each class for classification. This is graphically explained in Figure 5.5. The number of features selected for each subject per dataset for both investigations is listed in Table 5.2.

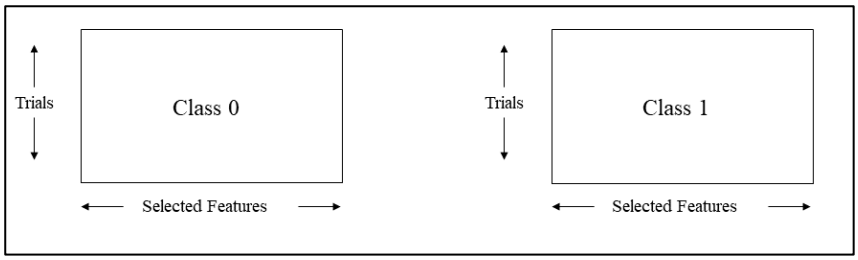


Figure 5.5: Reduced feature set based on the selected features. The features were stored in a 2D array: [trials × features]. Each feature set contains the selected features describing a class.

The optimal number of features used for baseline classification (using 128-channel data) was discovered by iteratively varying the number of features and then computing the resulting classification. The optimal number of features varied for each subject, per dataset for each investigation. This summarized in Table 5.2.

Table 5.2: Optimal number of selected features used for the baseline classification for both investigations

	Investigation 1	**Investigation 2**	
	RH vs LH	WE vs WF	
		LH	RH
Subject 1	-	-	20
Subject 2	50	50	50
Subject 3	50	50	50
Subject 4	-	20	-
Subject 5	50	50	40

5.4 Best Performing ICs (Baseline)

The *best-performing-ICs-baseline* are the ICs which contributed features that were used in the baseline classification (A-1), (see Section 1.6.3 and Section 6.1). Table 5.3 lists the number of *best-performing-ICs-baseline* that were identified for both investigations. The scalp plots and the associated ITV plots for the *best-performing-ICs-baseline* for all test subjects for both investigations are shown in Appendix B.

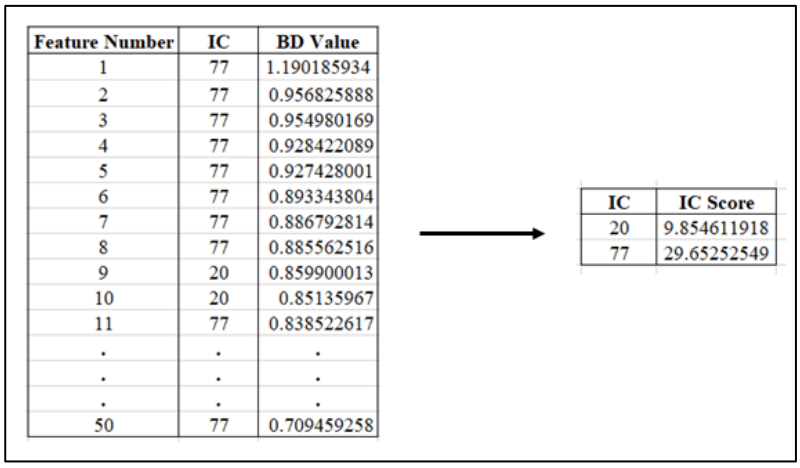
Features were extracted from all the ICs. FS used the BD to determine which features were optimal for achieving a large class separation. Each feature that was selected therefore had a BD value associated with it. Each selected feature originated from a *best-performing-ICs-baseline*. Thus, by summing all the BD values with a common IC, each *best-performing-ICs-baseline* was scored: this is referred to as an IC score. Due to inter-subject variability, the number of features selected and the number of *best-performing-ICs-baseline* from which they

originated, varied, therefore the IC score differed for each subject and each investigation. The IC score allowed each *best-performing-IC-baseline* to be ranked according to the amount of discriminatory information that it contributed.

Table 5.3: Number of best-performing-ICs-baseline that contributed features for baseline classification for both investigations

	Investigation 1	**Investigation 2**	
	RH vs LH	WE vs WF	
		LH	RH
Subject 1	-	-	23
Subject 2	2	25	38
Subject 3	1	25	2
Subject 4	-	20	-
Subject 5	3	32	26

This method is graphically explained in Figure 5.6, using an example from subject 2 investigation 1. In this example, a total of 50 features were selected during FS. From these 50 features, 13 features came from IC 20 while the remaining 37 features came from IC 77. The BD values associated with IC 20 and IC 77 were summed separately. As a result, IC 20 had an IC score of 9.85 while IC 77 had an IC score of 29.65. These scores show that IC 77 provided a larger contribution of features than IC 20.



Feature Number	IC	BD Value
1	77	1.190185934
2	77	0.956825888
3	77	0.954980169
4	77	0.928422089
5	77	0.927428001
6	77	0.893343804
7	77	0.886792814
8	77	0.885562516
9	20	0.859900013
10	20	0.85135967
11	77	0.838522617
.	.	.
.	.	.
.	.	.
50	77	0.709459258

IC	IC Score
20	9.854611918
77	29.65252549

Figure 5.6: Graphical explanation of an IC scoring method from subject 2, investigation 1. In this example, a total of 50 features were selected; each feature had a BD value associated with it. The BD value of each feature related to a single IC was summed to provide each IC with an IC score.

5.5 Channel Selection

A novel channel scoring system based off the *best-performing-ICs-baseline* was developed. Each channel consists of weighted information from multiple ICs (see Section 2.4 for more information on ICA weightings). This IC weighting was used to spread the IC score of each *best-performing-ICs-baseline* across every channel in each dataset. This provided each channel with a channel score (CS). This is explained in Equation 5.3, where *N* is the number of *best-performing-IC-baseline*, *j* and *i* denotes the IC score number and channel number respectively, while *A* refers to the mixing matrix.

$$CS_i = \sum_{j=1}^{N} A_{(i)} \times IC\ score_{(j)} \qquad 5.3$$

An example from subject 2, investigation 1 is shown in Figure 5.7, Table 5.4 and Table 5.5, in order to graphically describe this method. Figure 5.7a and Figure 5.7b show the distribution of IC 20 and IC 77 across all the 128 channels respectively. For an example, channel 5 is highlighted in both distributions. Channel 5 has a CS of 30.534 given IC 20's distribution, while channel 5 has a CS of 22.875 given IC 77's distribution. Therefore, the CS of channel 5 = CS_5 given IC 20 + CS_5 given IC 77 = 30.534 + 22.875 = 53.409.

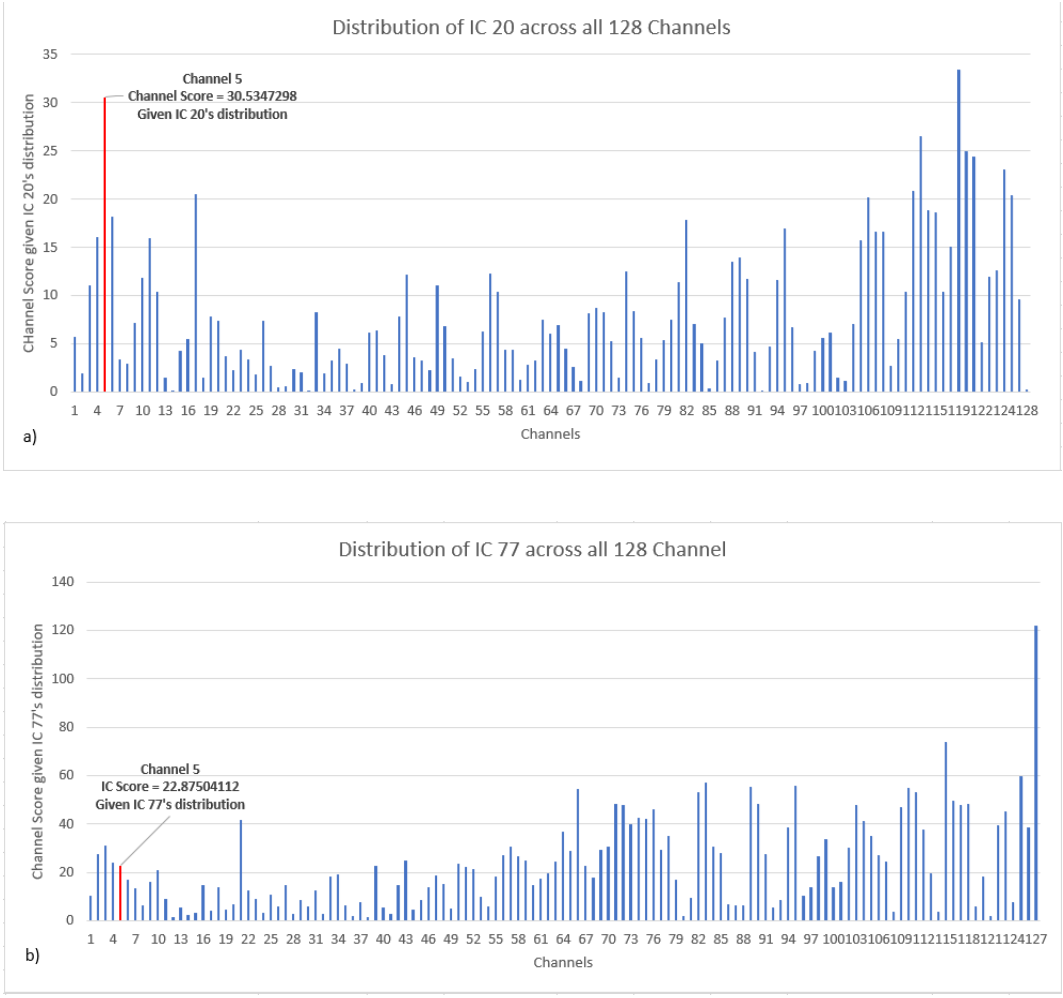


Figure 5.7: Graphical explanation of the channel scoring method from subject 2, investigation 1. a) shows the distribution of IC 20 across all 128 channels. b) shows the distribution of IC 77 across all 128 channels.

Through the implementation of this scoring system, each channel had a CS associated with it. It is assumed that channels with a greater CS contain more motor control information than channel with a smaller CS. Therefore, channels with the greatest CS were chosen to form the reduced channel configurations. This is shown in Table 5.5.

Four different channel configurations were chosen per subject, per dataset for each investigation. The four reduced channel configurations comprise of a 24-channel set, 16-channel set, 8-channel set, and 3-channel set. Figure 5.8, shows the electrode placement of the three top ranked channels and their associated CS for subject 2 investigation 1.

The number of channels (24, 16, 8 channel) chosen for the reduced channel sets, correspond to the typical number of electrodes used in standard EEG electrode sets. The 3-channel configuration is considered as a 'best case scenario' as used by Ko et al. [62].

Table 5.4: Graphical explanation of the channel scoring system taken from subject 2, investigation 1. It illustrates how the CS was calculated

Channel Number	Channel Score (CS) CSx of IC 20 + CS x of IC 77
1	16.07572919
2	29.32457528
3	41.85817948
4	40.12801675
5	53.40977093
6	34.95724183
7	16.87295021
8	9.271468722
9	23.18349514
10	32.68040786
11	24.74957113
12	11.84512396
13	6.83386033
14	2.633897723
15	7.599380445
16	20.24668125
17	24.76380473
18	15.10281469
19	12.42580755
20	14.02601844
21	45.21279514
22	14.72928566
23	13.49214778
24	6.622828757
25	.
26	.
27	.

Table 5.5: Graphical explanation of the channel scoring system taken from subject 2, investigation 1. It illustrates the ranking of the channels. The top three ranked channels are highlighted in yellow.

Channel Rank	Channel Number	Ordered CS
1	128	122.053854
2	115	92.62624726
3	119	81.67953721
4	126	80.16386137
5	95	72.78118594
6	82	70.91940902
7	89	69.18372209
8	83	63.94830323
9	111	63.54785415
10	118	62.71539783
11	110	60.4871456
12	90	60.101994
13	116	59.79636095
14	66	58.80057673
15	112	58.44950933
16	124	57.57320872
17	71	56.61799681
18	74	55.15067709
19	5	53.40977093
20	72	52.97193827
21	123	51.55982492
22	76	51.5435225
23	105	50.65358797
24	94	50.38010275
25	.	.
26	.	.
27	.	.

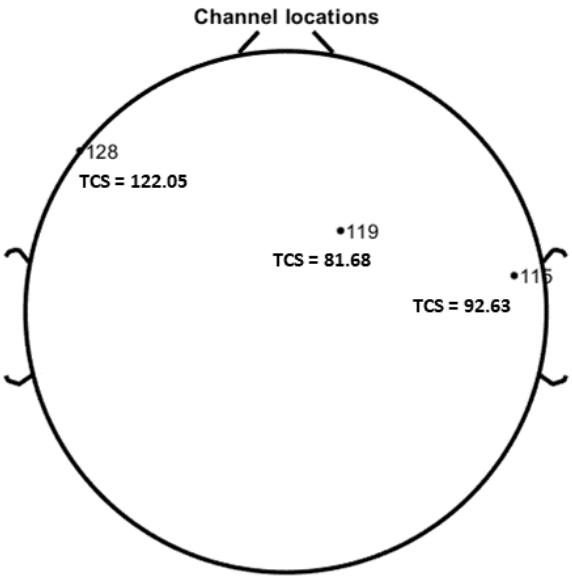


Figure 5.8: The electrode placement of the top three ranked channels and their associated CS, for subject 2 investigation 1

5.6 Chapter Summary

This chapter detailed the design of a novel channel reduction method that is aimed at retaining maximal motor control information. This method was applied to both investigations: the differentiation between RH and LH movements and the differentiation between WE and WF movements. The method uses ICA and characteristics associated with the ERD/ERS patterns to rank channels according to the motor control information that they contain and how well this information discriminated between the classes associated with each investigation on a single-trial basis. Four reduced channel configurations were produced for each test subject per dataset per investigation. These reduced channel configurations are presented in Chapter 7 . The testing of these reduced configurations, and thus, in turn, of the method, is described in the following chapter.

Chapter 6 – Testing Procedure

This chapter details the methods used to test how well each reduced channel set retains motor control information, which in turn tests the effectiveness of the method. This testing was done in three stages which are listed below and are outlined in Figure 6.1. At each stage a comparison was made between the results obtained when using the original channel set (part A) and the reduced channel sets (part B). The results from these comparisons (from both investigations) were used to assess the effectiveness of the method and thus to fully answer the RQ, as described in Section 1.6.3.

1. Measuring the classification ability of the original channel set compared to the reduced channel sets.
2. Visually examining the ERD/ERS patterns obtained from the *best-performing-ICs*.
3. Measuring the variance retained during the reduction process.

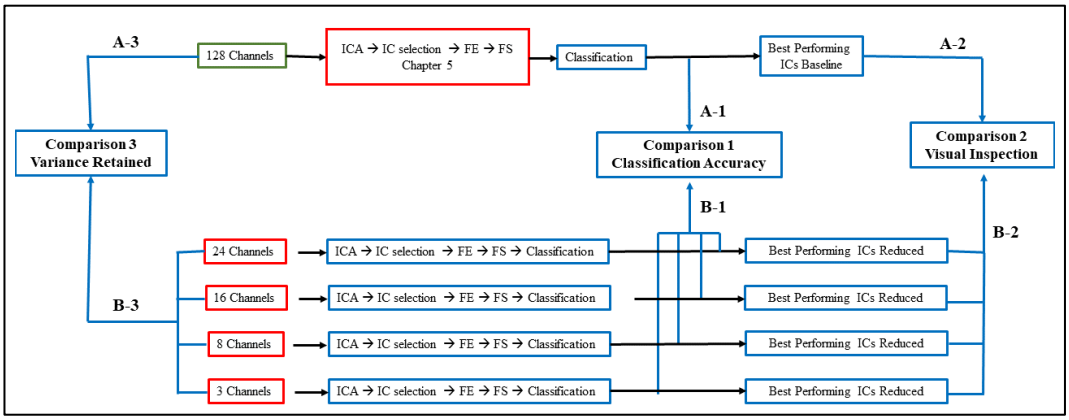


Figure 6.1: Testing procedure overview. Results from three subsections in this procedure are compared. 1. The baseline classification accuracy (A-1) is compared to the classification accuracy of the reduced sets (B 1). 2. Visual inspection of the best-performing-ICs-baseline (A-2) is compared to the best-performing-ICs-reduced (B-2). 3. The variance contained in the original channel set (A-3) is compared to the variance contained in the reduced channel sets (B-3).

The testing procedure which is outlined in Figure 6.1 was used to analyse each channel configuration (including the original 128-channel set). ICA was already

performed on the 128-channel datasets as part of Chapter 5 . ICA is also run on the reduced channel sets for each dataset. The scalp and ITV plots for each IC were generated and stored. FE and FS stages, as described in Chapter 5 , were applied to each reduced-channel dataset. Classification was used then performed on all datasets. Details on classification is presented in Section 6.1. Section 6.2 analyses the retention of motor control information in the reduced channel sets by examining the *best-performing-ICs-reduced* in Section 6.2.1 and exploring the variance contained within each channel set in Section 6.2.2. These metrics were used to analyse the classification accuracies obtained.

6.1 Classification

Classification was used to quantify the dataset's ability to differentiate between the movement types (classes) in each investigation. Classification was applied to each dataset (one original 128-channel and four reduced-channel datasets) in both investigations.

A linear SVM classifier was used to differentiate between the desired movement types (classes) in each investigation. Linear SVMs discriminate between different classes through the use of a hyperplane [2], [91]. Linear SVMs have been successful in many BCI applications [24], [44], [55], [91]. SVM classifiers are ideal since they are insensitive to overtraining [91], are simple to implement and do not require large training sets in order to achieve good results [2], [13].

Features describing the desired movement type were extracted and selected using the FE and FS stages described in Section 5.2 and Section 5.3. The number of features selected for baseline classification was discovered by iteratively increasing the number of features (from x to x number of features) and then comparing the resulting classifications to find the number of features that yielded the highest accuracy (see Section 6.1.1). The number of features selected varied for each subject per dataset for each investigation: they are listed in Table 5.2. The same number of features used for the baseline classification were then used for the classification of the reduced channel sets. This allowed for fewer variables to be considered.

Each trial in the dataset was given a class label. Outliers in the dataset were then removed so that samples that deviated from the general range would not compromise the results. Outliers were removed using MATLAB's inbuilt function *rmoutliers*, which removed elements that were more than three standard deviations away from the mean value of the dataset [92]. The trials in the dataset were randomized and the dataset was then divided into two datasets, one for training and the other for testing the SVM, with a 70 % to 30 % split respectively. These datasets are illustrated in Figure 6.2.

Classification was carried out for every channel configuration (original and reduced). This was done for all test subjects, for every dataset and for all investigations. The linear SVM classifier was implemented with the following parameters: a linear kernel function, a box constraint of 1 and a sequential minimal optimization solver. Eight-fold cross validation was conducted, and the classification accuracies obtained were averaged out. These results will assist in evaluating the performance of the reduced channel configurations.

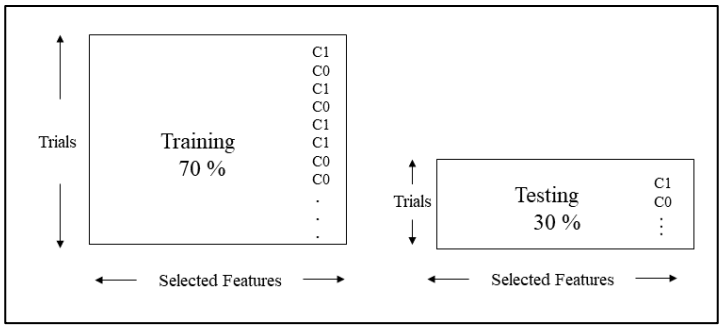


Figure 6.2: Graphical representation of the datasets used for classification. 70 % of the trials were used to train the SVM, while the remaining 30 % were used to test the SVM. The data was stored in 2D arrays: [trials × features]. Each dataset contains the selected features and its associated class label. Outliers were removed from the dataset and the trials were then randomized.

6.1.1 Accuracy Calculation

The accuracy of the classification was calculated using Equation 6.1 [91]. This equation calculates the percentage of correctly classified trials [91]. This performance measure is one of the most commonly used metrics used for the

evaluation of BCI systems [91]. This metric was commonly used in the literature detailed in Chapter 3 , thus allowing for the comparison of results.

$$Accuracy = \frac{Number\ of\ trials\ correctly\ classified}{Total\ number\ of\ trials} \quad 6.1$$

The baseline classification accuracy obtained was compared to the reduced channel sets' classification accuracy. The loss of accuracy between these two results was then calculated for each reduced channel set in both investigations. This is explained using Equation 6.2, where x is the reduced channel set size (24, 16, 8, 3).

$$\%\ Loss\ in\ Classification\ Accuracy_x = \frac{Baseline\ Accuracy - Accuracy_x}{Baseline\ Accuracy} \times 100\ \% \quad 6.2$$

6.2 Retention of Motor Control Information

The amount of motor control information retained during the reduction process was investigated using two metrics. The first metric was a visual inspection of the ITV plots produced by the *best-performing-IC-reduced*. The second metric was a measure of variance retained in each reduced channel's dataset. Both these metrics are used to better understand the classification accuracies obtained.

If the *best-performing-IC-reduced* exhibit motor related characteristics in the form of an ERD/ERS pattern, then the assumption is that motor control information was retained and used in the classification. This assumption is substantiated by calculating the correlation between the variance contained in the original 128-channel dataset and each reduced channel's dataset.

6.2.1 IC Visual Inspection

The *best-performing-IC-reduced* are the ICs which contributed features for the classification of the reduced channel sets. Table 6.1 lists the number of *best-performing-ICs-reduced* that were identified for each reduced channel's dataset in both investigations.

Table 6.1: Number of best-performing-ICs-reduced that contributed features for reduced channel classification for both investigations

	Investigation 1				**Investigation 2**							
	RH vs LH				WE vs WF				WE vs WF			
					LH				RH			
Number of channels	**24**	**16**	**8**	**3**	**24**	**16**	**8**	**3**	**24**	**16**	**8**	**3**
Subject 1	-	-	-	-	-	-	-	-	15	11	8	3
Subject 2	4	2	8	3	19	1	1	2	21	15	8	3
Subject 3	2	1	2	1	17	16	8	3	12	13	8	3
Subject 4	-	-	-	-	14	1	8	3	-	-	-	-
Subject 5	18	16	8	3	21	16	8	3	21	16	8	3

The *best-performing-IC-reduced* were then ranked according to their IC score, as explained in Section 5.4. This ranking illustrates the contribution that each IC had towards the classification. The ICs that had the largest contribution of features towards the classification were analysed, as these ICs should in theory contain more information that describes the investigated movement type. The *best-performing-IC-reduced* were analysed by visually examining the ITV plots that they produced, to see if they depicted typical ERD/ERS characteristics as seen in Figure 6.3, such as:

1. A decrease in the amplitude of the ITV graph around 2000 ms.
2. The decrease in amplitude is sustained for a significant time interval, approximately 1000-2000 ms.
3. After the decrease in amplitude, the amplitude of the ITV graph increases again.
4. The amplitude of the ITV graphs returns to approximately the original level.

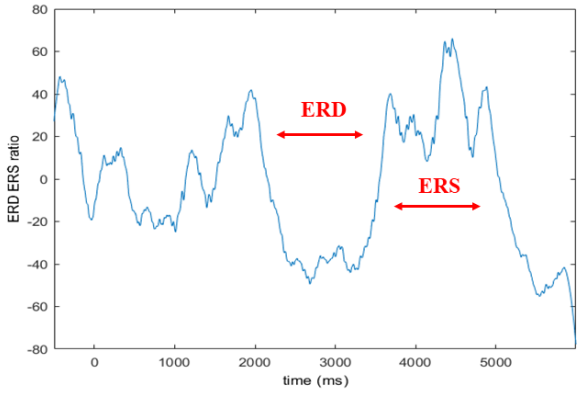


Figure 6.3: An example of an ITV plot with typical ERD/ERS characteristics.

If majority of these characteristics were present in the ITV plot, then the assumption was that motor control for that movement type had been retained in the reduced channel sets.

6.2.2 Variance Retained

The second metric used to further understand the accuracies obtained was variance. In order to measure the variance contained in each channel configuration, PCA was applied to each dataset (both the original and reduced channel datasets). PCA generated a covariance matrix whose columns represents principal components (PCs) [13]. The PCs generated describe the amount of variance that is contained in that dataset [13]. These PCs are ordered from highest to lowest variance values [13].

This process allowed for a comparison between the 128-channel dataset and the reduced channel datasets. The correlation coefficient between the first PC (maximum variance) of the original 128-channel dataset and the first PC of each reduced channel dataset was calculated using MATLAB's inbuilt function *corrcoef*. This is graphically illustrated in Figure 6.4. The *corrcoef* function calculates the correlation coefficient using Equation 6.3, where A and B is the original 128-channel dataset and the reduced channel dataset respectively, $cov(A,B)$ is the covariance between A and B, and σ_A, σ_B is the standard deviation of A and B, respectively [93].

$$p(A,B) = \frac{cov(A,B)}{\sigma_A \times \sigma_B} \qquad 6.3$$

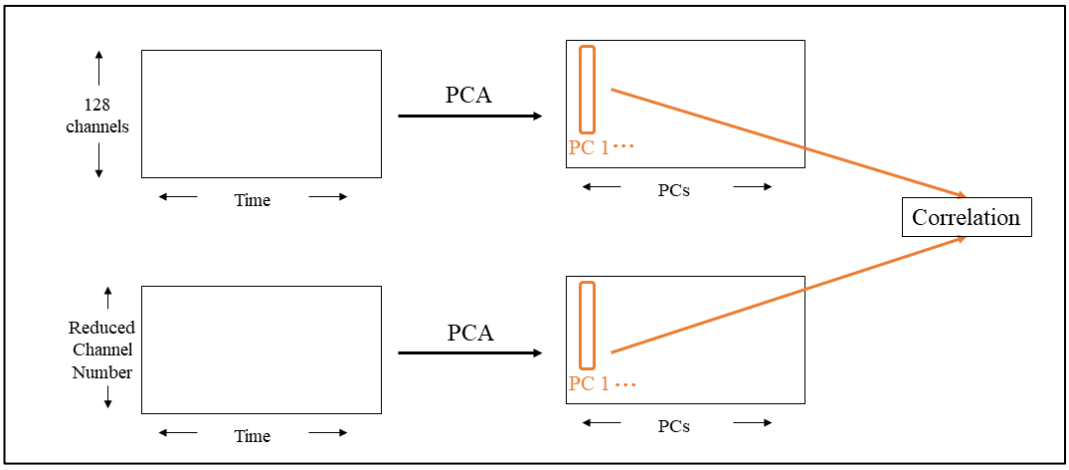


Figure 6.4: Graphical illustration of the method used to calculate the correlation between PC 1 of the original dataset and PC 2 of the reduced channel dataset.

6.3 Chapter Summary

This chapter detailed the testing procedure implemented to evaluate the method's ability to produce a reduced channel set that can differentiate between the desired movement types. Three performance measures were used for this evaluation. First, an SVM classifier was used to calculate the classification accuracies. The baseline classification accuracy (A-1) was compared to the classification accuracies of the reduced sets (B-1). These classification accuracies were then inspected by analysing the amount of motor control information that was retained. The ITV plots of the *best-performing-ICs-reduced* (B-2) were inspected to see if they contain ERD/ERS characteristics similar to that of the *best-performing-ICs-baseline* (A-2). Lastly, the amount of variance contained in the original dataset (A-3) was compared to the amount of variance contained in the reduced channel sets (B-3).

Chapter 7 - Results

This chapter presents the results obtained from both investigations after the implementation of the method and the testing procedure detailed in Chapter 5 and Chapter 6 respectively. The reduced channel configurations obtained through the implementation of the method are presented, as well as the results from the implementation of the testing procedure. The results of the testing procedure involve the analysis of:

1. The classification accuracies obtained using both the original and reduced datasets.
2. The ICs that contributed features to the classification.
3. The variance contained in the reduced datasets in comparison to the original dataset.

7.1 Investigation 1: RH vs LH

For the investigation into RH and LH movements, only data from three subjects (subjects 2, 3 and 5) were used. As explained in Section 4.4, subject 1 and subject 4 were excluded from this investigation as EEG data was recorded for only one of their hand movements.

7.1.1 Reduced Channel Sets

The top-ranked 24 channels and their corresponding CS for each subject are presented in Table 7.1. From this table, the top 16, 8 and 3 channels, which form the reduced channel sets, can be inferred. The channels selected differ for each subject, each dataset and each investigation.

The placement of the electrodes corresponding to each selected channel are illustrated in Appendix C. These figures show the reduced channel configurations produced for subjects 2, 3 and 5 respectively. For an example, the placement of the electrodes for all the reduced channel sets from subject 2, investigation 1 is presented in Figure 7.1.

Table 7.1: 24 top-ranked channels and their corresponding CS for subject 2, 3 and 5 for investigation 1

	Subject 2		**Subject 3**		**Subject 5**	
Rank	Channel	CS	Channel	CS	Channel	CS
1	128	29.70611	30	218.8595	4	59.4629
2	115	23.35335	36	153.8728	126	57.46736
3	119	21.38672	16	141.4706	9	46.06304
4	126	20.37109	29	135.0075	16	34.69833
5	95	18.37904	104	134.2659	5	30.39105
6	82	17.9623	64	121.6792	18	29.09272
7	89	17.34354	2	112.8608	15	28.19145
8	118	15.80324	14	106.2419	27	27.55255
9	111	15.77745	112	105.2816	2	27.05003
10	83	15.71044	9	103.4456	10	26.84912
11	112	15.0378	119	101.1798	50	26.31842
12	90	14.99481	92	97.87801	127	25.57563
13	116	14.85295	79	92.9561	45	25.42377
14	110	14.78281	106	88.93824	17	24.60151
15	124	14.41572	123	86.83861	106	24.23068
16	66	14.31652	118	83.37772	56	23.58025
17	5	14.27411	17	81.70218	3	23.25916
18	71	13.96643	73	81.54446	55	22.67963
19	74	13.81327	50	79.29394	34	22.66207
20	72	12.91777	94	78.4557	101	21.96259
21	123	12.90083	11	78.01783	7	20.6735
22	105	12.86003	105	77.50627	12	20.05792
23	76	12.58282	1	75.88265	120	19.75351
24	94	12.52121	28	70.30006	109	19.70846

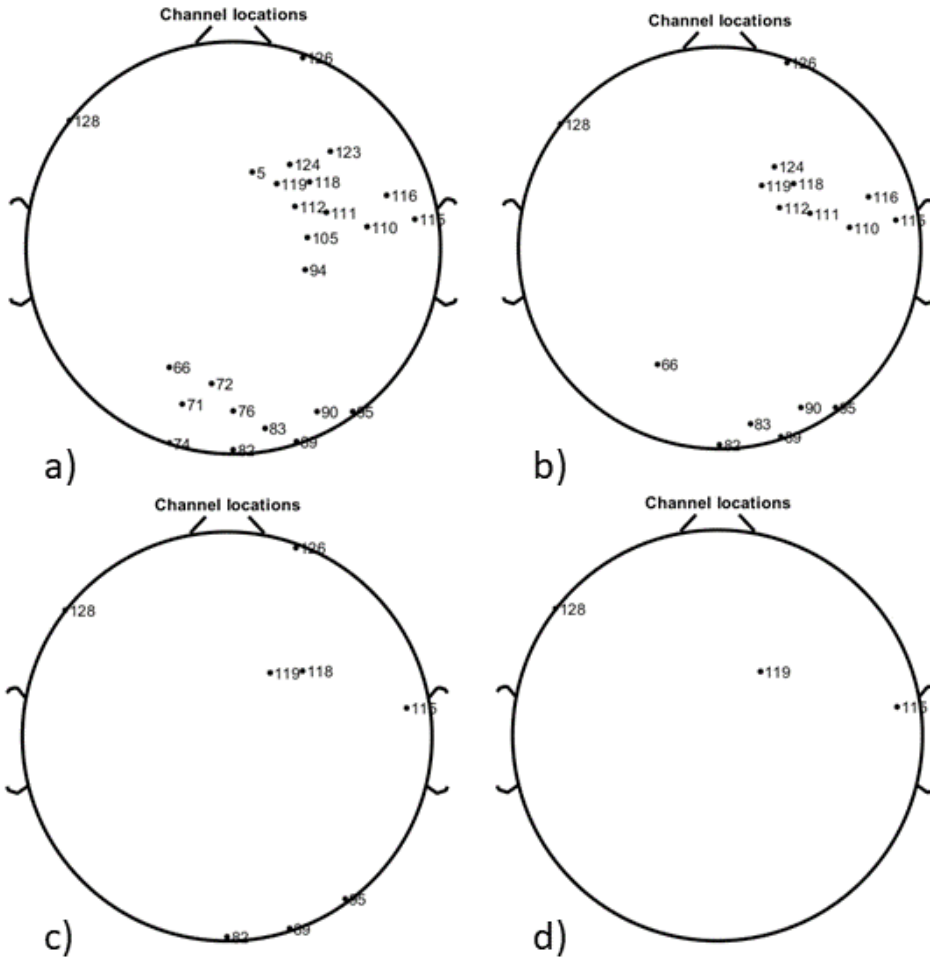
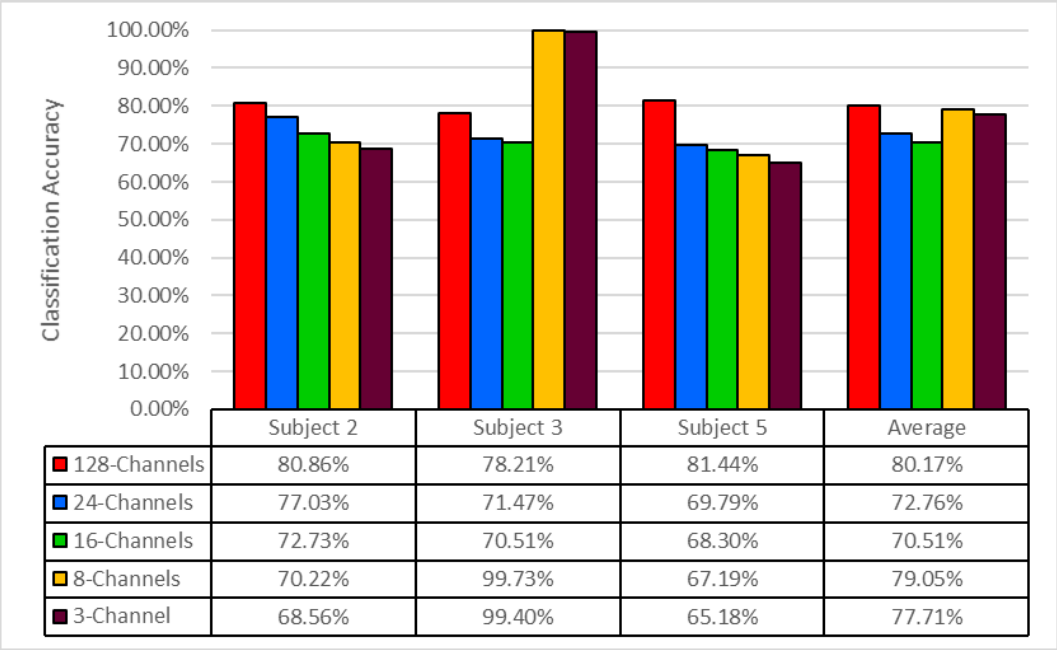


Figure 7.1: Subject 2's reduced-channel configurations obtained for investigation 1. The location of the electrodes corresponding to the selected channels is presented. a) 24-channel configuration, b) 16-channel configuration, c) 8-channel configuration, d) 3-channnel configuration.

7.1.2 Classification Accuracy

The classification accuracies obtained for the differentiation between RH and LH movements for the various channel configurations are presented in Figure 7.2. The classification accuracies are presented for each subject (subjects 2, 3 and 5) and are averaged across all the subjects. The classification accuracy obtained when using the 128-channel dataset is considered as the baseline classification accuracy.

The loss of classification accuracy between the original 128-channel dataset and each reduced channel dataset is presented in Table 7.2 for each subject (subject 2, 3 and 5) and is averaged across all the subjects.



	Subject 2	Subject 3	Subject 5	Average
128-Channels	80.86%	78.21%	81.44%	80.17%
24-Channels	77.03%	71.47%	69.79%	72.76%
16-Channels	72.73%	70.51%	68.30%	70.51%
8-Channels	70.22%	99.73%	67.19%	79.05%
3-Channel	68.56%	99.40%	65.18%	77.71%

Figure 7.2: Classification accuracies obtained for the differentiation between LH and RH movement using the original 128-channel dataset and the reduced channel dataset. Classification accuracies for subjects 2, 3, 5 and the average classification accuracy across all subjects are presented.

Table 7.2: The loss of classification accuracy calculated between the baseline classification and the reduced channel sets. This is presented for subjects 2, 3, 5 and is averaged across all subjects.

	Loss in Classification Accuracy (%)			
Number of channels	Subject 2	Subject 3	Subject 5	Average
24	4.74	8.61	14.30	9.22
16	10.06	9.84	16.13	12.01
8	13.16	-27.53	17.50	1.04
3	15.21	-27.11	19.97	2.69

7.1.3 IC Visual Analysis

The ITV plots from the *best-performing-ICs-baseline* and *best-performing-ICs-reduced* are presented for subjects 2, 3 and 5 in Figure 7.3, Figure 7.4 and Figure 7.**5** respectively. The ICs that formed the *best-performing-ICs-baseline* and *best-performing-ICs-reduced* varied between subjects, datasets and investigation. For layout purposes, only the four top-ranked IC's ITV plots from each reduced channel's datasets are presented in this section. The top four *best-performing-ICs-*

reduced are determined through the IC score. An ellipsis in the figure implies that there are additional *best-performing-ICs-baseline,* which are not presented. For a complete presentation of all the ITV plots from the *best-performing-ICs-reduced,* refer to Appendix D.

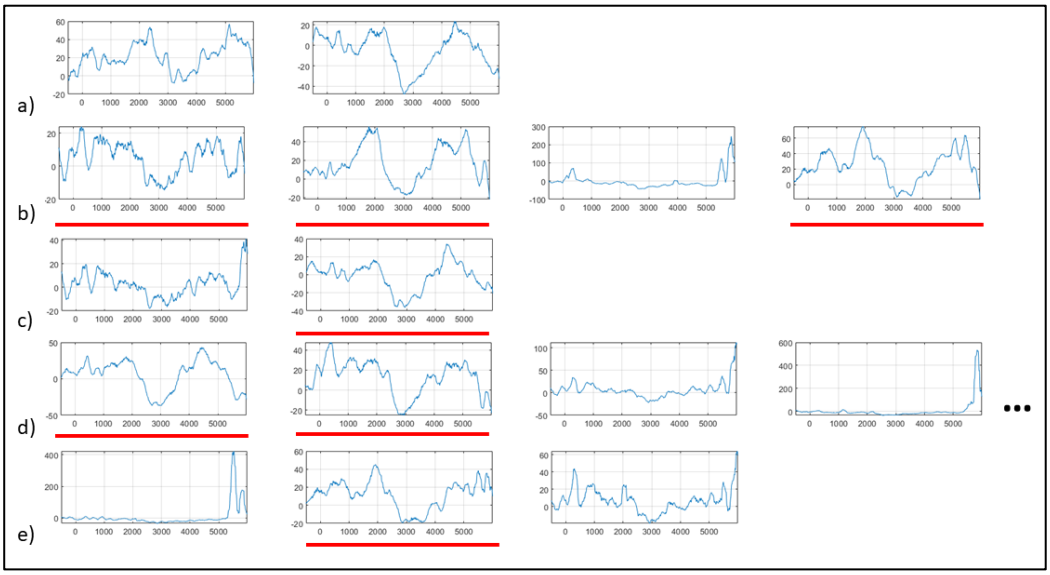


Figure 7.3: ITV plots of best-performing-ICs-reduced for subject 2. The ITV plots are ordered according to the IC score. a) 128-channels. b) 24-channels. c) 16-channels. d) 8-channels. e) 3-channels. The ITV plots underlined in red illustrate similar ERD/ERS characteristics.

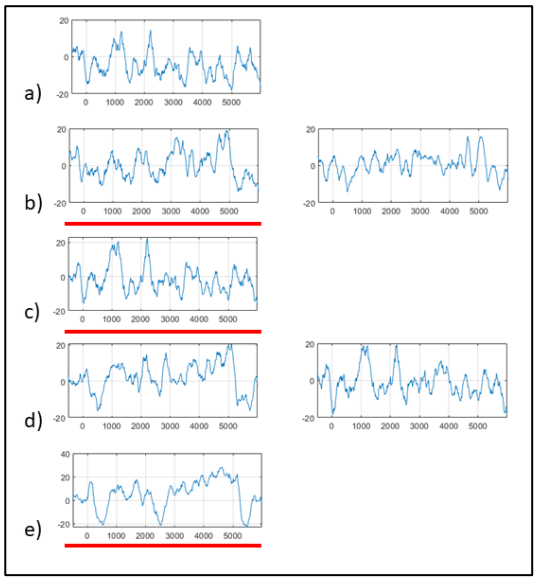


Figure 7.4: ITV plots of best-performing-ICs-reduced for subject 3. The ITV plots are ordered according to the IC score. a) 128-channels. b) 24-channels. c) 16-channels. d) 8-channels. e) 3-channels. The ITV plots underlined in red illustrate similar ERD/ERS characteristics.

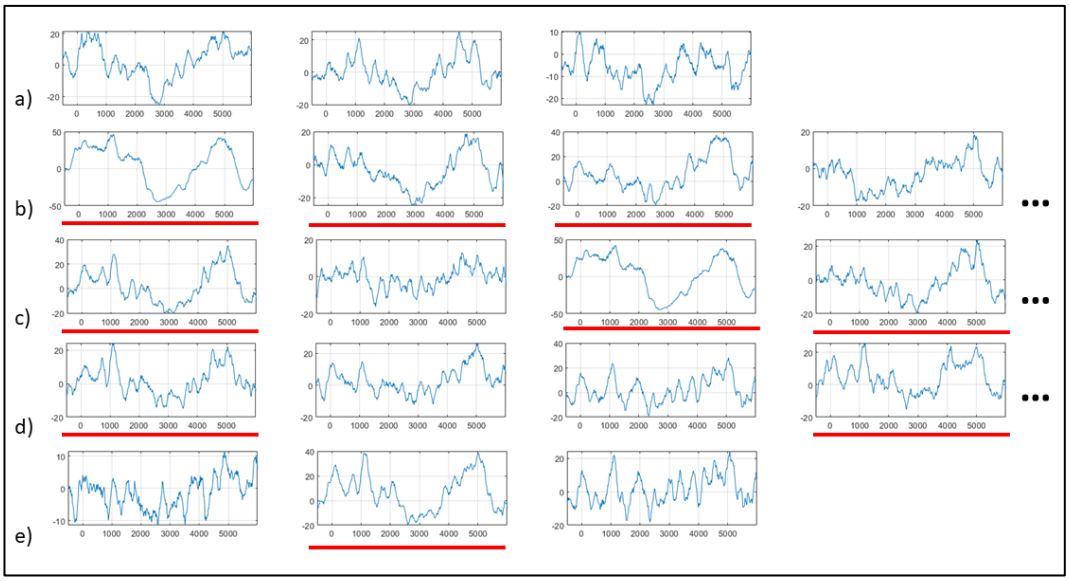


Figure 7.5: ITV plots of best-performing-ICs-reduced for subject 5. The ITV plots are ordered according to the IC score. a) 128-channels. b) 24-channels. c) 16-channels. d) 8-channels. e) 3-channels. The ITV plots underlined in red illustrate similar ERD/ERS characteristics.

7.1.4 Variance Retained

The correlation between the variance contained in the original dataset and each reduced channel dataset is presented in Table 7.3. These results are calculated for each subject and are averaged across all subjects.

Table 7.3 : The correlation between the variance contained in the 128-channel dataset and each reduced channel's dataset. These results are presented for subjects 2, 3, 5 and are averaged across all subjects.

	Correlation			
Datasets compared	Subject 2	Subject 3	Subject 5	Average
128-channel – 24-channel	0.9817	0.92516	0.6850	0.863957
128-channel – 16-channel	0.6987	0.85025	0.5610	0.703332
128-channel – 8-channel	0.6959	0.24258	0.1020	0.346835
128-channel – 3-channel	0.1537	0.25052	0.0245	0.142891

7.2 Investigation 2: WE vs WF

For the investigation into WE and WF movements, two datasets (RH and LH datasets) were used from subjects 2, 3 and 5. One data set was used from subject 1 (RH dataset) and subject 4 (LH dataset), as explained in Section 4.4,.

7.2.1 Reduced Channel Sets

The top ranked 24 channels and their corresponding CS for each subject are presented in Table 7.4, Table 7.5 and Table 7.6. From this table, the top 16, 8 and 3 channels, which form the reduced channel sets, can be inferred. The channels selected differ for each subject, per dataset and for each investigation.

The placement of the electrodes corresponding to each selected channel is illustrated in Appendix C. These figures show the reduced channel configurations produced for all the test subjects. For an example, the placement of the electrodes for all the reduced channel sets from subject 2, investigation 2, LH dataset are presented in Figure 7.6.

Table 7.4: 24 top-ranked channels and their corresponding CS for subject 1's RH dataset, subject 2's LH dataset and subject 2's RH dataset for investigation 2

	Subject 1: RH		**Subject 2: LH**		**Subject 2: RH**	
Rank	Channel	CS	Channel	CS	Channel	CS
1	83	230.7593	94	130.2441	55	185.8135
2	2	223.6432	88	118.2698	45	121.7289
3	61	130.0465	120	117.2553	128	99.32591
4	122	126.5382	87	104.1185	18	92.2506
5	68	123.3346	93	101.9289	33	90.27721
6	23	122.5705	124	100.4011	34	88.34497
7	87	122.1125	119	97.72293	13	86.44831
8	67	119.8605	106	96.08742	8	84.90177
9	70	119.6246	45	95.96956	40	81.52087
10	27	118.1188	81	95.75525	89	78.33657
11	88	114.8909	104	92.78724	56	78.00452
12	69	114.5252	80	91.36551	91	77.81844
13	62	113.7392	99	90.72686	127	75.07649
14	75	113.4448	86	89.4486	46	73.97339
15	32	112.7833	79	87.3544	126	70.79005
16	80	112.5927	105	87.11659	44	68.91966
17	63	111.5058	118	86.72998	85	68.63204
18	7	111.3829	125	86.54211	35	67.90898
19	127	109.5629	113	86.42443	96	67.63462
20	79	107.4148	115	86.00863	90	67.6283
21	74	106.7384	103	83.37062	29	66.93281
22	66	105.9233	112	81.7155	19	65.62297
23	72	105.7493	111	81.0889	32	65.6103
24	57	105.4242	17	80.47303	81	65.43805

Table 7.5: 24 top-ranked channels and their corresponding CS for subject 3's LH dataset, subject 3's RH dataset and subject 4's LH dataset for investigation 2

	Subject 3: LH		**Subject 3: RH**		**Subject 4: LH**	
Rank	Channel	CS	Channel	CS	Channel	CS
1	79	277.2759	91	1436.216	2	374.2993
2	78	208.744	84	588.2478	9	209.3164
3	86	186.1801	85	582.6281	112	188.2824
4	85	178.2524	83	483.311	8	155.4853
5	92	164.4542	102	470.4786	87	153.1986
6	41	153.4189	90	435.4139	123	134.748
7	66	151.5301	97	404.541	3	133.3287
8	19	147.7903	96	402.3476	22	132.6954
9	91	143.9806	77	361.2436	75	127.4486
10	51	135.5371	42	351.0783	19	122.0914
11	58	135.1002	89	323.4413	14	117.3222
12	25	122.6726	92	316.8115	1	116.8888
13	60	115.7084	95	288.0848	17	116.5556
14	57	114.8084	76	263.5236	23	113.787
15	117	112.8638	46	245.3803	26	112.0143
16	38	111.712	100	244.8533	114	111.7277
17	65	110.6213	101	229.7635	89	106.391
18	80	106.1732	75	224.8329	15	103.4331
19	67	106.1279	104	213.0566	126	101.0066
20	24	105.5084	82	194.8284	74	99.63605
21	59	103.5223	72	175.645	120	94.21562
22	55	101.4203	110	169.9033	119	94.13243
23	104	100.5116	40	168.6159	115	93.53204
24	84	99.93372	117	165.5478	95	91.04565

Table 7.6: 24 top-ranked channels and their corresponding CS for subject 5's LH and RH datasets, for investigation 2

	Subject 5: LH		**Subject 5: RH**	
Rank	Channel	CS	Channel	CS
1	109	73.10732	56	88.81459
2	41	71.31315	109	85.73219
3	106	70.66837	55	85.03433
4	45	70.27945	128	83.94797
5	59	70.23129	33	83.16446
6	29	70.09615	98	82.00845
7	38	69.25787	63	81.38051
8	95	67.29725	102	79.21384
9	89	66.3791	90	76.64487
10	128	66.01005	45	76.35496
11	60	65.3878	50	75.91231
12	107	64.36249	81	75.85974
13	25	62.9633	69	75.76057
14	88	62.24908	124	75.62621
15	100	62.1443	101	75.48194
16	32	61.54689	82	74.88513
17	105	61.52642	62	74.43188
18	3	61.51511	89	71.91203
19	28	61.2933	100	71.83406
20	94	61.22125	103	71.09025
21	34	61.21692	125	71.01778
22	31	60.09175	93	70.72442
23	35	59.97856	8	70.6251
24	26	59.77377	80	70.1909

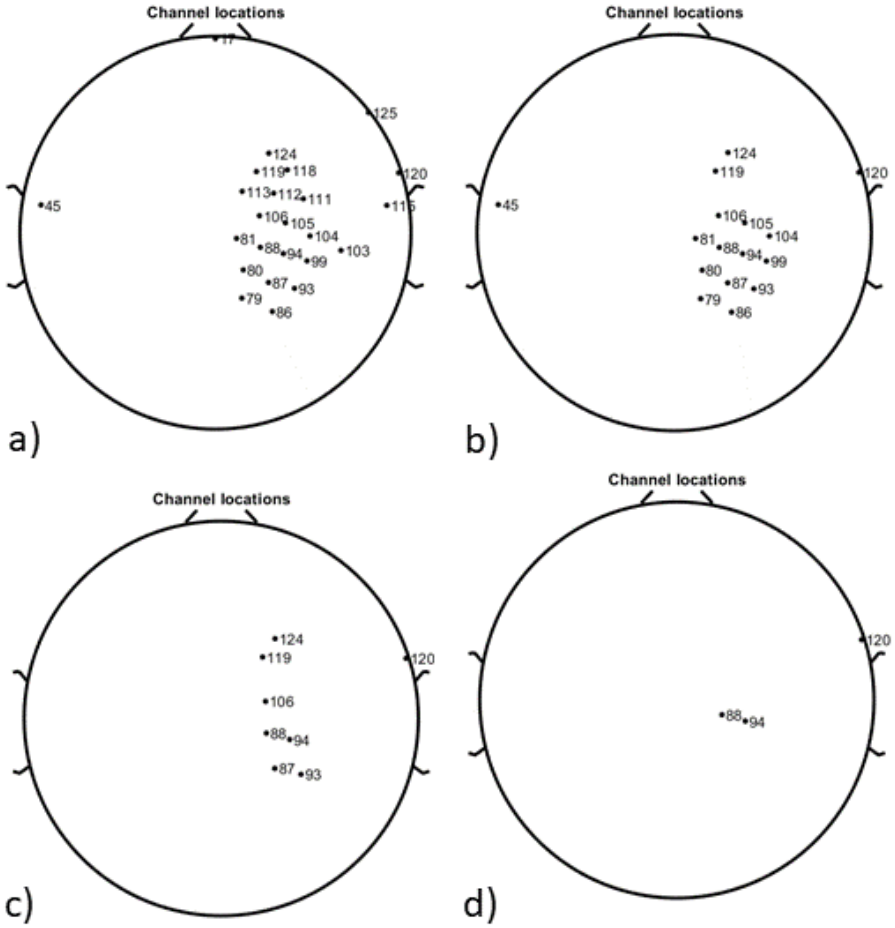
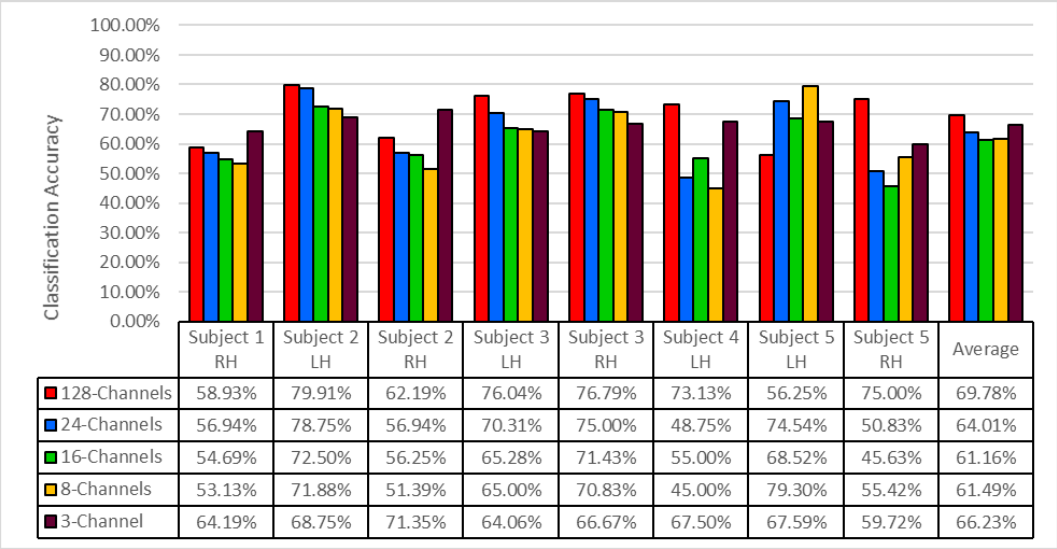


Figure 7.6: Subject 2's RH reduced channel configurations obtained for investigation 2. The location of the electrodes corresponding to the selected channels is presented. a) 24-channel configuration, b) 16-channel configuration, c) 8-channel configuration, d) 3-channel configuration.

7.2.2 Classification Accuracy

The classification accuracies obtained for the differentiation between WE and WF movements for the various channel configurations are presented in Figure 7.7. The classification accuracies are presented for each subject's RH and LH channel sets (when available) and are averaged across all the datasets. The classification accuracy obtained when using the 128-channel dataset is considered as the baseline classification accuracy.

The loss of classification accuracy between the original 128-channel dataset and each reduced channel datasets is presented in Table 7.7 for each subject's RH and LH channel sets (when available) and is averaged across all the datasets.



	Subject 1 RH	Subject 2 LH	Subject 2 RH	Subject 3 LH	Subject 3 RH	Subject 4 LH	Subject 5 LH	Subject 5 RH	Average
128-Channels	58.93%	79.91%	62.19%	76.04%	76.79%	73.13%	56.25%	75.00%	69.78%
24-Channels	56.94%	78.75%	56.94%	70.31%	75.00%	48.75%	74.54%	50.83%	64.01%
16-Channels	54.69%	72.50%	56.25%	65.28%	71.43%	55.00%	68.52%	45.63%	61.16%
8-Channels	53.13%	71.88%	51.39%	65.00%	70.83%	45.00%	79.30%	55.42%	61.49%
3-Channel	64.19%	68.75%	71.35%	64.06%	66.67%	67.50%	67.59%	59.72%	66.23%

Figure 7.7: Classification accuracies obtained for the differentiation between WE and WF movement using the original 128-channel dataset and the reduced channel dataset. Classification accuracies for each subject's RH and LH datasets (when available) and the average classification accuracy across all datasets are presented.

Table 7.7: The loss of classification accuracy calculated between the baseline classification and the reduced channel sets. This is presented for each subject's RH and LH channel sets (when available) and is averaged across all the datasets

	Loss in Classification Accuracy (%)								
Hand	**RH**				**LH**				
Subject	**1**	**2**	**3**	**5**	**2**	**3**	**4**	**5**	**Average**
24-channels	3.37	8.43	2.33	32.22	1.45	7.53	33.33	-32.51	7.02
16-channels	7.20	9.55	6.98	39.17	9.27	14.16	24.79	-21.81	11.16
8-channels	9.85	17.36	7.75	26.11	10.06	14.52	38.46	-40.97	10.39
3-channels	-8.92	-14.74	13.18	20.37	13.97	15.75	7.69	-20.16	3.39

7.2.3 IC Visual Analysis

The ITV plots from the *best-performing-ICs-baseline/reduced* are presented for each subject's RH and LH datasets (when available) in Figure 7.8 to Figure 7.15. The ICs that formed the *best-performing-ICs-baseline/reduced* varied between subjects, datasets and investigation types.

For layout purposes, only the four top-ranked IC's ITV plots from each reduced channel's datasets are presented in this section. The top four *best-performing-ICs-baseline/reduced* are determined through the IC score. An ellipsis in the figure implies that there are additional *best-performing-ICs-baseline/reduced* which are not presented. For a complete presentation of all the ITV plots from the *best-performing-ICs-baseline/reduced*, refer to Appendix D.

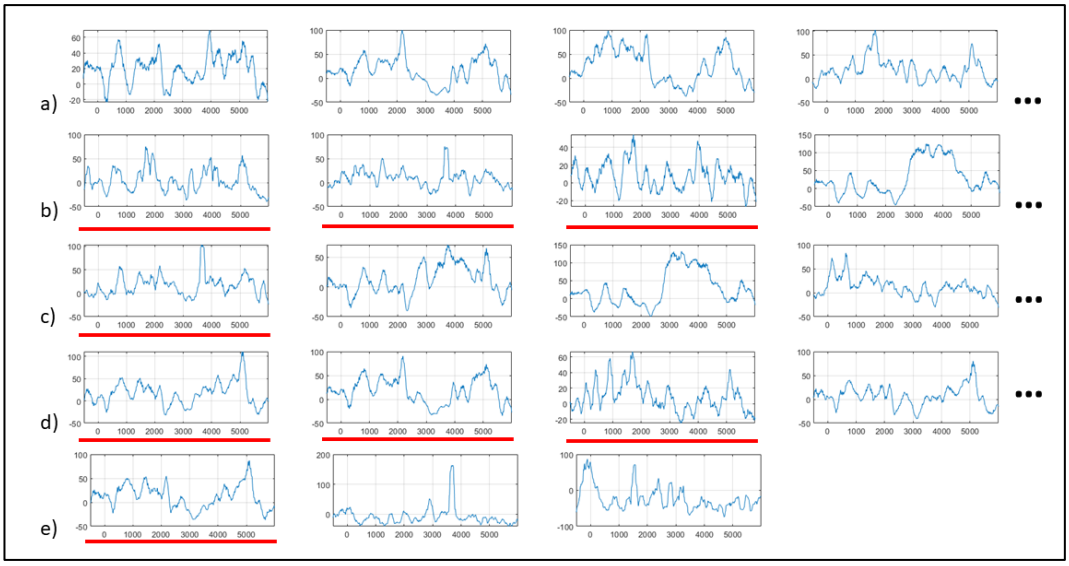


Figure 7.8: ITV plots of best-performing-ICs-reduced for subject 1 RH. The ITV plots are ordered according to the IC score. a) 128-channels. b) 24-channels. c) 16-channels. d) 8-channels. e) 3-channels. The ITV plots which are underlined in red illustrate similar ERD/ERS characteristics

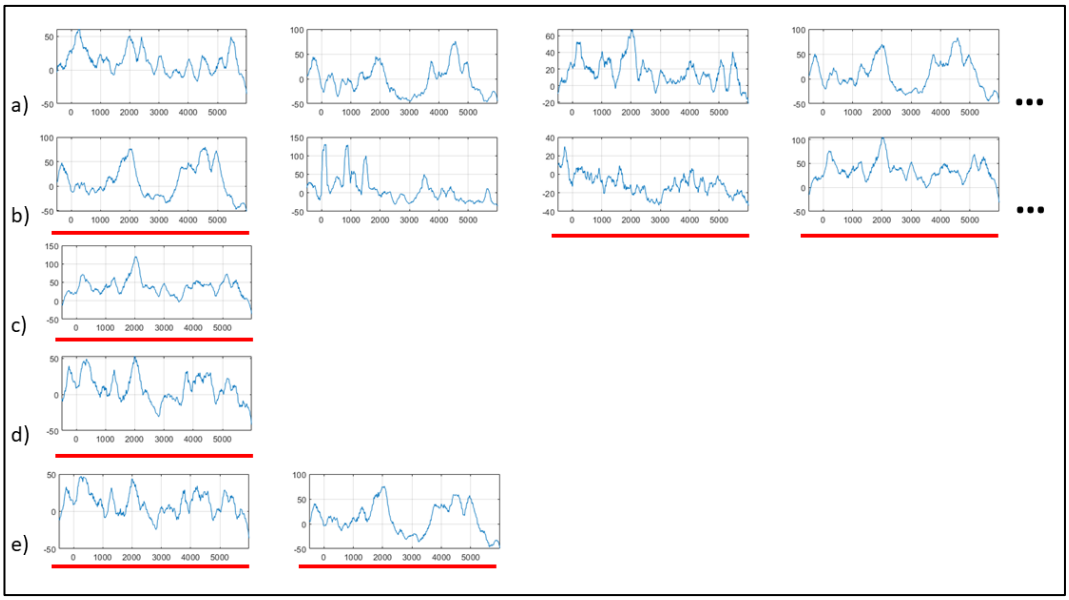


Figure 7.9: ITV plots of best-performing-ICs-reduced for subject 2 LH. The ITV plots are ordered according to the IC score. a) 128-channels. b) 24-channels. c) 16-channels. d) 8-channels. e) 3-channels. The ITV plots which are underlined in red illustrate similar ERD/ERS characteristics



Figure 7.10: ITV plots of best-performing-ICs-reduced for subject 2 RH. The ITV plots are ordered according to the IC score) 128-channels. b) 24-channels. c) 16-channels. d) 8-channels. e) 3-channels. The ITV plots which are underlined in red illustrate similar ERD/ERS characteristics

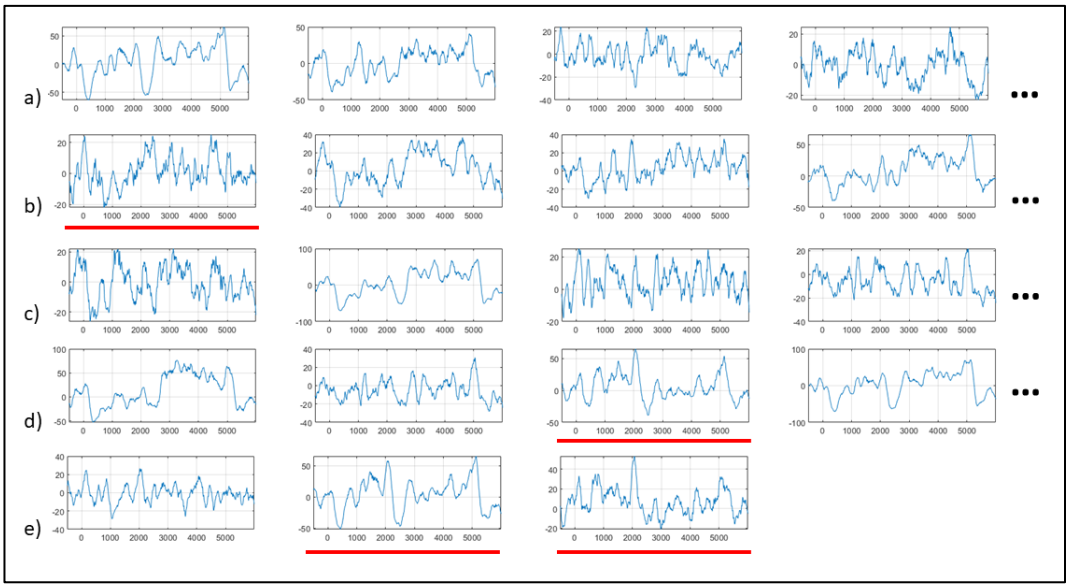


Figure 7.11: ITV plots of best-performing-ICs-reduced subject 3 LH. The ITV plots are ordered according to the IC score) 128-channels. b) 24-channels. c) 16-channels. d) 8-channels. e) 3-channels. The ITV plots which are underlined in red illustrate similar ERD/ERS characteristics.

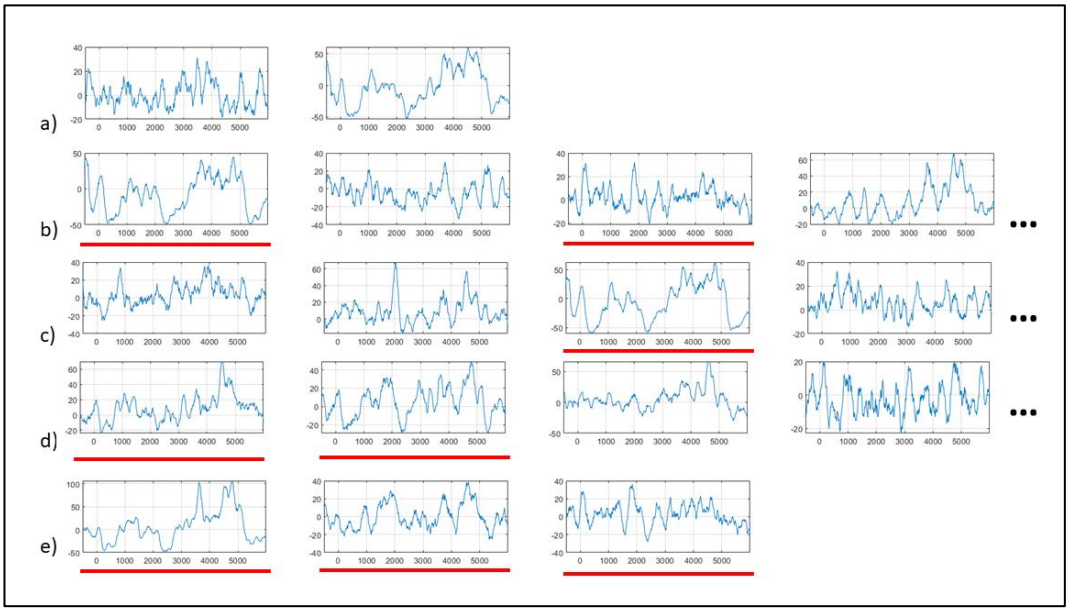


Figure 7.12: ITV plots of best-performing-ICs-reduced subject 3 RH. The ITV plots are ordered according to the IC score) 128-channels. b) 24-channels. c) 16-channels. d) 8-channels. e) 3-channels. The ITV plots which are underlined in red illustrate similar ERD/ERS characteristics.



Figure 7.13: ITV plots of best-performing-ICs-reduced subject 4 LH. The ITV plots are ordered according to the IC score) 128-channels. b) 24-channels. c) 16-channels. d) 8-channels. e) 3-channels. The ITV plots which are underlined in red illustrate similar ERD/ERS characteristics

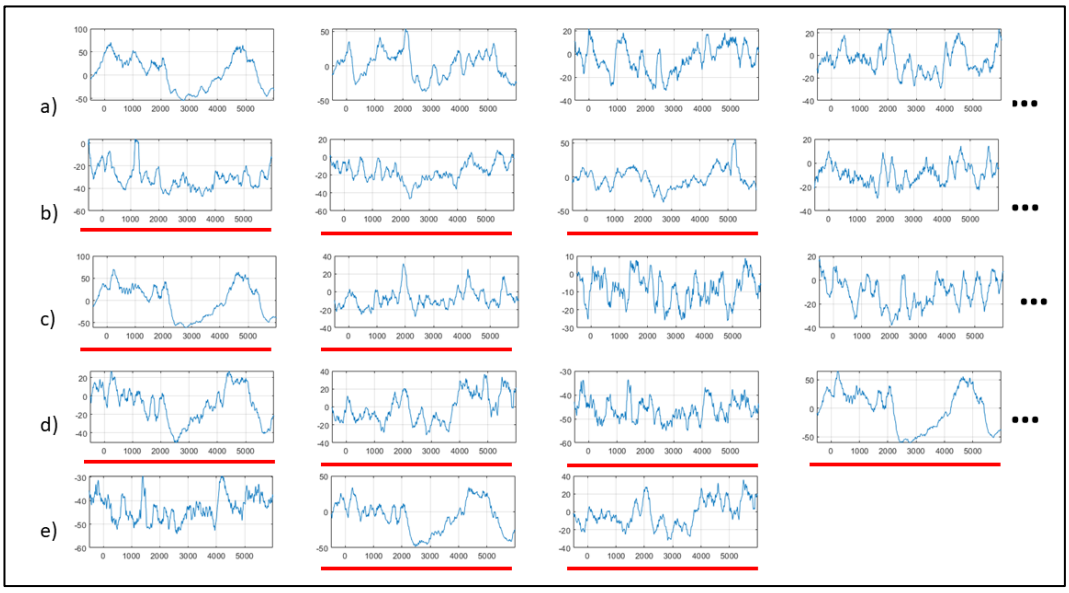


Figure 7.14: ITV plots of best-performing-ICs-reduced subject 5 LH. The ITV plots are ordered according to the IC score) 128-channels. b) 24-channels. c) 16-channels. d) 8-channels. e) 3-channels. The ITV plots which are underlined in red illustrate similar ERD/ERS characteristics

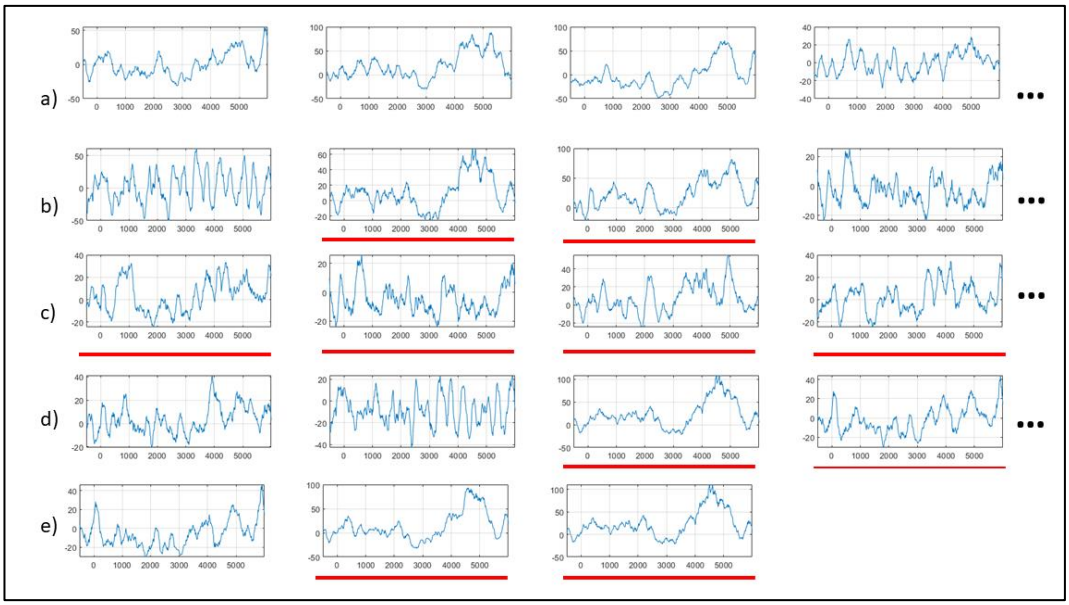


Figure 7.15: ITV plots of best-performing-ICs-reduced subject 5 RH. The ITV plots are ordered according to the IC score) 128-channels. b) 24-channels. c) 16-channels. d) 8-channels. e) 3-channels. The ITV plots which are underlined in red illustrate similar ERD/ERS characteristics

7.2.4 Variance Retained

The correlation between the variance contained in the original dataset and each reduced channel dataset is presented in Table 7.8. These results are calculated for each subject and are averaged across all subjects.

Table 7.8: The correlation between the variance contained in the 128-channel dataset and each reduced channel's dataset. These results are presented for each subject's RH and LH channel sets (when available) and are averaged across all the datasets.

	Loss in Classification Accuracy (%)								
Hand	**RH**				**LH**				
Subject	**1**	**2**	**3**	**5**	**2**	**3**	**4**	**5**	**Average**
24-channels	0.964	0.911	0.781	0.308	0.973	0.857	0.942	0.314	0.756
16-channels	0.931	0.822	0.680	0.229	0.971	0.635	0.724	0.168	0.645
8-channels	0.956	0.733	0.620	0.180	0.945	0.715	0.448	0.173	0.596
3-channels	0.619	0.554	0.401	0.123	0.927	0.364	0.169	0.196	0.419

7.3 Chapter Summary

This chapter presented the reduced-channel configurations formed by the implementation of the method (Chapter 5), as well as the results from the testing procedure, for both investigations. For each investigation, the following results were presented:

- A table of the generated reduced channel sets with their corresponding CS.
- An example of the placement of the physical electrode location from one subject for each investigation.
- The classification accuracies obtained for the 128-channel dataset and for each reduced channel's dataset, for every test subject and on average.
- The classification accuracy lost during the reduction process.
- An examination of the ICs that contributed features towards the various classifications.
- The correlation between the amount of variance contained in the baseline dataset and the reduced channel datasets.

The following chapter discusses the implication of these results in relation to answering the RQ.

Chapter 8 – Discussion

This chapter discusses the results presented in the previous chapter. Insights obtained from the results of each investigation are used to make conclusions about the effectiveness of the method and in turn help answer the RQ. In order to answer the RQ, results from the three metrics: 1) classification accuracy, 2) visual inspection of the *best-performing-ICs-baseline/reduced* and 3) variance retention are analysed. Figure 8.1 outlines how the various sub-sections of this chapter will be used to answer the RQ.

A discussion about the channel locations for the reduced configurations for both investigations are presented together. These observations may bring awareness into which brain regions should be given attention when investigating movement intention and EEG signals responsible for motor control. The significance of these findings is then presented followed by a critique of the method and then suggestions for future work is provided.

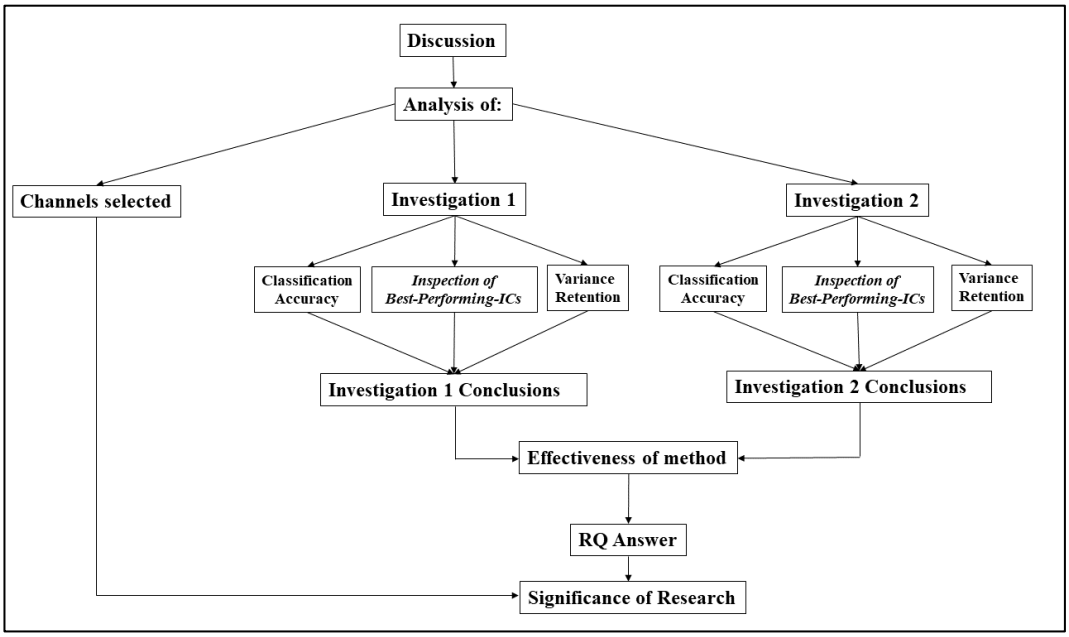


Figure 8.1: Discussion chapter overview. Conclusions from the analysis of investigation 1 and investigation 2 are used to determine the effectiveness of the method, and in turn answer the RQ.

8.1 Investigation 1 & 2 Analysis

The classification accuracies for the differentiation between RH and LH movements are summarised in Figure 7.2. The average baseline classification accuracy obtained when using the original 128-channel dataset is 80,17 %. This result lies within the range (64 % - 99 %) of classification accuracies obtained for the differentiation of RH vs LH movements in various literatures [44], [48], [55], [64], [65]. This suggests that the implementation of the techniques used in this method is acceptable for the differentiation between the desired movement types. This is an important result, as it implies that the use of ICA and ERD/ERS characteristics and the various testing methods have been implemented correctly. The classification accuracies for the differentiation between WE and WF movements are summarised in Figure 7.7. The average baseline classification accuracy obtained when using the original 128-channel dataset is 69.78 %. This result lies within a similar range to some results obtained in literature (61 % - 82 %) [20], [71], [72]. The average baseline accuracy obtained for investigation 2 (69.78 %) is significantly lower than that obtained for investigation 1 (80.17 %). This is expected since differentiating between WE and WF is significantly more difficult than the differentiation between RH and LH movements.

A graphical overview of all the results obtained is illustrated in Table 8.1. This table provides a "big picture" overview of all the results obtained for each criterion. In this table, *I1* and *I2* refers to investigation 1 and investigation 2 respectively, while *C*, *I* and *V* refer to the classification accuracy, ITV plots and variance correlation value respectively. The classification column with green shading indicates that the classification accuracy obtained is above 50 % and that the classification accuracy obtained follows an expected trend – the classification accuracies obtained decrease as the number of channels in the configuration decrease. Orange shading indicates that the classification accuracy obtained is below 50 %, however the accuracies follow the expected trend, while red shading indicates that the results obtained do not follow the expected trend, for example, when a 3-channel set obtains a higher classification accuracy than the original 128-channel set, (investigation 2, subject 5's LH). ITV plot column with a green shading indicates that many ITVs in

that channel set produced significant ERD/ERS characteristics, an orange shading indicates that minimal ERD/ERS characteristics were present, while the red shading indicates that there were no ERD/ERS characteristics present in the ITV plot. Green shading in the variance correlation column refers to a correlation values above 0.6, while an orange shading indicates that the correlation value lies between 0.4 – 0.6, while a correlation below 0.4 results in a red shading. The ideal reduced channel set across all the subjects should meet all three criteria. Hence, this graphical overview allows the reader to infer what the optimal number of channels is for each investigation, considering all three test methods.

From the classification results presented in Chapter 7 and Table 8.1, on average, a 16-channel configuration is suggested to be the ideal reduced channel configuration. This channel configuration resulted with a 12.01 % and 11.16 % loss in classification accuracy when differentiation between RH vs LH and WE vs WF movements respectively. The 8-channel and 3-channel configurations do not follow the expected trend in classification accuracies. In both these channel sets, unexpected classification accuracies were produced. This suggests that there is a flaw in those results. It is unknown what caused the unexpected results, it may be due to the limited number of trials used in the classification process or the limited number of test subjects. Repeating the study with an additional trial may result in the classification accuracy results forming different (expected) patterns. Additionally, on average, most datasets had a low correlation value (below 0.6) for the 8-channel and 3-channel configurations. This suggests that a limited amount of information was retained in these channel sets. Furthermore, the ITV plots from the 24-channel and 16-channel configurations suggest that motor control information in the form of ERD/ERS pattern was retained.

Due to the limited number of subjects in this study, definitive conclusions on the effectiveness of this method cannot be made, since several datasets obtained unexpected results. One cannot determine if the inconsistencies were due to errors in the method, inter-subject variability or to the limited number of trials in the classification process.

A detailed discussion of each investigation is provided in the next two sub-sections, Section 8.1.1 and Section 0.

Table 8.1: Graphical overview of all the results obtained for the three metrics: classification accuracy, ITV plots and a measure of variance.

	24-Channels			16-Channels			8-Channels			3-Channels		
I1	**C**	**I**	**V**	**C**	**I**	**V**	**C**	**I**	**V**	**C**	**I**	**V**
S2												
S3												
S5												
I2	**C**	**I**	**V**	**C**	**I**	**V**	**C**	**I**	**V**	**C**	**I**	**V**
S1 RH												
S2 LH												
S2 RH												
S3 LH												
S3 RH												
S4 LH												
S5 LH												
S5 RH												

8.1.1 Investigation 1 Summary

All three subjects were able to produce 16-channel configurations that can differentiate between RH and LH movements. The average classification accuracy for the 16-channel dataset is 70.51 %; this corresponds to an average loss in accuracy of 12.01 %. Through an examining of the *best-performing-ICs-reduced*,

one can infer that motor control information was retained in the 24-channel and 16-channel datasets, as majority of the ITV plots exhibit ERD/ERS characteristics. The average correlation values for these datasets (0.86 and 0.70 respectively), substantiate the assumption that motor control information was retained. Therefore, one can assume that motor control information was retained during the reduction process in the form of ERD/ERS characteristics, and that these characteristics were used for the classification.

When looking only at classification accuracy, two out of the three subjects (subject 2 and 5) were able to produce a 3-channel configuration that can differentiate between RH and LH movements. However, when examining the *best-performing-ICs-reduced* and variance from subject 2's and subject 5's results, minor ERD/ERS characteristics are visible and negligible variance is retained. Thus, it can be assumed that little motor control information was retained. This analysis shows the importance of examining the classification accuracies obtained on a deeper level, when the retention of a specific control information is the objective.

The average loss in classification accuracy for the 8-channel and 3-channel configurations are 1.04 % and 2.69 % respectively. The general trend noticeable in the average loss in classification accuracy results suggests that across all three subjects, a 16-channel configuration is ideal, and that any further channel reduction produces unexpected results. The 8-channel and 3-channel configurations do not follow the expected pattern and is not consistent across all the test subject. The classification accuracies appear far too high for such few channels (limited information). These results may be due to an error, but since the number of test subjects and trial used in the study are limited, one cannot be certain. Therefore, until the performance of the 3-channel configuration can be verified with additional testing, the 16-channel configuration is assumed to be ideal.

Therefore, it is suggested that the method can produce an optimized and reduced channel set comprising 16-channels for the investigation into RH and LH movements across all subjects used. The 16-channel configuration obtains an average classification accuracy of 70.51 %, across all the test subjects, which a

12.01 % loss in classification accuracy when comparing against the baseline accuracy. Additional testing using a larger sample size of subjects and additional trials is needed in order to make any significant conclusions about the effectiveness of this method in relation to RH and LH movements. However, these results show that using ICA to build a reduced channel set that is effective in retaining motor control information is possible for RH vs LH movements.

8.1.2 Investigation 2 Summary

There were a few inconsistencies in the results obtained for certain reduced channel's datasets. However, on average, across all datasets, it is suggested that a 24-channel and 16-channel dataset that can differentiate between WE and WF movements is achievable. The average classification accuracy for the 24-channel and 16-channel dataset is 64.01 % and 61.16 % respectively, while the average loss of accuracy is 7.02 % and 11.16 % respectively. These classification accuracies are similar to the results obtained for unilateral wrist movement studies [68]. Through an examining of the *best-ICs-reduced*, one can infer that motor control information was retained in the 24-channel and 16-channel datasets, as majority of the ITV plots exhibit ERD/ERS characteristics. The average correlation values for these datasets (0.76 and 0.65 respectively) substantiate the assumption that motor control information was retained. Therefore, one can assume that motor control information was retained during the reduction process in the form of ERD/ERS characteristics, and that these characteristics were used for the classification.

The average loss in classification accuracy for the 8-channel and 3-channel configurations is 10.39 % and 3.39 % respectively. The general trend noticeable in the average loss in classification accuracy results suggests that across all three subjects a 16-channel configuration is ideal, and that any further channel reduction produces unexpected results. The 8-channel and 3-channel configurations do not follow the expected pattern and is not consistent across all the test subject. The classification accuracies appear far too high for such few channels (limited information). These results may be due to an error, but since the number of test subjects and trial used in the study are limited, one cannot be certain. Therefore,

until the performance of the 3-channel configuration can be verified with additional testing, the 16-channel configuration is assumed to be ideal.

Therefore, it is suggested that the method can produce an optimized and reduced channel set comprising 16-channels for the investigation into WE and WF movements across all datasets used. The 16-channel configuration obtains an average classification accuracy of 61.16 %, across all the test subjects, which indicates a 11.16 % loss in classification accuracy when compared with the baseline accuracy. Additional testing using a larger sample size of subjects is needed in order to draw any significant conclusions about the effectiveness of this method in relation to WE and WF movements, since various datasets produced unreliable results. However, these results show that using ICA to build a reduced channel set that is effective in retaining motor control information is possible for WE and WF movements.

8.2 Answering the RQ

To what extent can ICA be used to find an optimized and reduced EEG channel set (from a 128-channel dataset) when discriminating between WE and WF?

The optimal number of channels varied for each subject and each investigation. On average, across all subjects and investigations, it is suggested that a 16-channel dataset, that can differentiate between LH and RH movement and WE and WF movements is feasible/achievable. This 16-channel configuration resulted in a loss of classification accuracy of 12.01 % and 11.16 % for investigation 1 and 2 respectively.

8.3 Reduced Channel Sets

The reduced channel combinations obtained through the implementation of the method are presented in Section 7.1.1 and Section 7.2.1 for investigation 1 and investigation 2, respectively. An analysis of the channels selected is combined for both investigations, since similar conclusions are reached.

The channels selected differed for each subject since the amount of cortical activity produced during movement and the way in which it spreads is unique to an individual [39] (see Section 2.3). Thus, it is difficult to predict which electrodes will measure and record the relevant motor control information. Therefore, each system must be optimized for the individual.

The distribution of the selected channels is unexpected. It is assumed that the ideal electrodes that record motor activity are the ones located above the motor cortex and its close surroundings [43], [55]. However, the channels selected by the method are spread across the surface of the head. The areas related to the motor cortex (M1, PMA and SMA) are moderately covered, but channels related to other regions of the brain were also chosen. This could be due to volume conduction (see Section 2.3) [12], [47]. The cortical activity generated by the motor cortex spreads, resulting in the neural brain signal being recorded by electrodes positioned above other regions of the brain.

These results show the importance of identifying and isolating the desired control information during a reduction process and identifying the channels related to it, since non-motor related channels were selected. This illustrates the importance of non-motor related electrodes in analysing motor activity. These results, reiterate the findings of Sepulveda et al., [73] who suggests that more consideration be given to non-motor related electrodes during movement related research. Simply choosing electrodes located over the brain region of interest as done in [43], [55], may result in vital electrodes being excluded.

While the ICs selected were in the spatial region of the motor cortices, they are constituted by channels from all over the head. This suggests that only selecting channels above the motor cortices as done for some spatial filters (such as the Laplacian) or only using C3, C4 etc. may exclude some important motor control info. This can be verified by repeating the entire study but using other spatial filters e.g. CSP [43], [44] and beamformer [94].

One must take note that the EEG signals were recorded under strict conditions. The test subjects focused entirely on the single task at hand, therefore there was minimal

noise and interference from other intentions and muscle movement. This could be the reason why strong motor activity signals were recorded from electrodes located above unexpected regions of the brain. Under less strict recording conditions (or in real-life and real-time scenarios), EEG signals from additional brain activity will be recorded by those electrodes. This may lead to an increased difficulty in isolating the motor control information from these channels, which may result in different channels being selected.

8.4 Significance of Results

This research presented a novel channel reduction method based on ICA. ICA has not been used in this capacity before. Typical applications for ICA are source localization and artifact removal. This research illustrates the potential of using ICA as the main technique in channel selection methods. By using ICA as the main technique, valuable insights are obtained into which cortical sources are providing control information. These results show that non-motor-related electrodes may have an important role in recording motor-related cortical activity. They highlight the importance of identifying and isolating the desired control information during the channel reduction process and identifying the channels related to it.

This research explores channel reduction for the classification of WE and WF movements. This research is novel, since no reliable channel selection studies for the differentiation between WE and WF movements have yet been presented (refer to Section 3.2).

8.5 Critique of the Method

This method, although suitable and advantageous for this research, has a few drawbacks that are discussed below.

8.5.1 Limitations of the Database

As mentioned previously (see Chapter 4.5), the effectiveness of the method cannot be fully evaluated, due to the limited size of the database. The database is limited

both in the number of test subjects used as well as the number of trials performed by each test subject.

The sample size (number of test subjects) is too small to determine if the unexpected results obtained are due to inter-subject variability or errors in the method. Additionally, the limited number of trials in the database may have influenced the effective training and testing of the SVM. A future recommendation would be to use transfer learning to ensure that the SVM is sufficiently trained before testing occurs [95].

A total of 20 trials were recorded per movement per test subject. This resulted in a total of 200 trials available for investigation 1 and 40 trials for investigation 2. However, the number of trials used to test the SVM was further reduced due to the removal of outliers as well as the 70% - 30% (training-testing) split. This resulted in a limited number of trials used to test the SVM. This could have affected the percentage accuracy of classification. The number of outliers removed varied per investigation, per subject, per number of features chosen. For example, in investigation 1, subject 2's dataset had 48 trials removed, resulting in a training and testing set comprising of 106 trials and a testing respectively. While in investigation 2, subject 2 LH's dataset had 15 trials removed, resulting in a training and testing set comprising of 18 trials and a testing set of 7 trials.

Due to these limitations, the number of trials used in the testing and training of the SVM may have been too small to make full use of the SVM's capabilities. As a result, the results obtained may be unreliable and thus the effectiveness of the method cannot be fully evaluated. However, it does show potential in the method for future work.

Future work with a larger database should be explored. The database should contain information from an increased number of test subjects and additional trials per subject. For example: 9-12 test subjects [20], [22], [96], [97] and approximately 100 trials per movement per test subject [22], [97]. However, fatigue per test subject during an EEG recording session is a limiting factor. Collecting data from multiple

recording sessions introduces problems in varying EEG patterns from one session to the next.

8.5.2 Limitations of Manually Selecting ICs

As mentioned in Chapter 8.3, the selected channels are distributed across the scalp and are not isolated to the scalp area in close proximity to M1. It was expected that more channels close to M1 would have been selected as optimal by the method. It may be likely that the ICs chosen manually may not have represented all the motor-control information from M1.

Additionally, the manual selection of the ICs is extremely time-consuming and user bias can heavily influence the results obtained. This may also have led to key motor control information and hidden features being discarded. Isolating specific neural signals could also have interfered with the SVM's ability to identify hidden signals and correlations that are vital to both investigations. However, this research was not aimed at identifying and using the best motor-related features. The search for the best features related to motor control is an ongoing investigation in BCI research. Features other than ERD/ERS have been investigated in recent years e.g. phase locking value, channel coherence [98]. These features may hold more discriminative abilities than ERD/ERS. Future work could involve the use of other features that may perform better, possibly from ICs that are not manually selected.

Nevertheless, the manual selection of ICs allowed for movement related cortical information to be isolated and unnecessary information discarded. This allowed one to focus on the motor cortical areas of the brain. In order to combat user bias, any ICs that showed the slightest suggestion of motor control were selected. Automating this process without bias is tough since source localisation of EEG (using ICA or any other technique) is an estimation and is not exact. The positioning of the scalp electrodes differs for each subject, and each subject's anatomy varies [39]. Modelling approaches use prior anatomical knowledge to estimate the locations of cortical areas. However, the knowledge of roles and contribution of the different brain regions involved in motor control is being updated. The experiment could be repeated using functional magnetic resonance imaging (fMRI) and EEG

simultaneously, as fMRI can better locate cortical sources of activity. This could help to remove some user bias.

8.5.3 Limitations of the Measurement Techniques

The metrics used to validate the amount of motor information which is retained during the reduction process has a few limitations which must be discussed.

The examination of the ERD/ERS pattern is a visual inspection and therefore the analysis is prone to human error and human bias. As a result, a signal comparison tool should be used in future work in order to obtain a quantitative measure of how similar the ERD/ERS pattern from an ITV plot of two ICs are. A quantitative measure such as cross correlation can be used.

The way in which the variance contained within each dataset (original and reduced) was calculated, only showed the amount of information that is contained in each dataset. It did not illustrate the actual context of the information. However, the variance measure calculated coupled with the visual inspection of the ITV plots allowed some conclusions on the validity of the method to be determined. Nevertheless, for future work a different type of information comparison tool should be used, in order to accurately quantify the amount of retained information.

Despite the limitations of the measurement techniques, they provide a first look at the verifying the worthiness of the ICA based electrode reduction method.

8.6 Future Work

In order to improve on the classification accuracies obtained, more work pertaining to this method should be explored. Future work with additional test subjects and additional trials should be investigated to fully evaluate the effectiveness of the method on a large scale, so that significant conclusions about the effectiveness of the method can be made.

This method should also be applied to other motor tasks, in order to fully evaluate its effectiveness in differentiating between different movement types. Additional research on channel reduction for WE and WF should be explored in order to obtain

comparable results. The entire study should be repeated, using other spatial filters such as CSP as well as other movement related features such as MRCP, in order to verify the designed method.

8.7 Chapter Summary

This chapter discussed the various results presented in the previous chapter. The location of the channels selected for the reduced channel set from investigation 1 and investigation 2 were discussed together. These findings were then used in order to answer the RQ. The significance of these findings in relation to expanding this research field was discussed, followed by suggestions for future work.

Chapter 9 – Conclusion

Upper-limb motor-impaired individuals struggle to communicate and perform daily tasks in conventional ways. Two hand movements that are vital for the execution of these daily tasks are WE and WF movements. Therefore, a bionic hand that can perform WE and WF movements will help in returning some motor functionality back to these individuals. A sensorimotor EEG based BCI can be used to control a bionic hand. However, numerous EEG electrodes are often required in order to record the desired brain signals. This is not ideal for the user, as it takes time to set up and is rather uncomfortable to wear. Therefore, a BCI system is required that has a minimal number of electrodes and can accurately differentiate between the neural signals responsible for WE and WF.

Existing channel reduction methods for motor task studies do not provide an understanding of the type of control information that is isolated and retained during the channel reduction process. As a result, this research focused on the design of an ICA based channel reduction method, which produces an optimized and reduced EEG channel set that retains maximal motor-control information. ICA was used in conjunction with ERD/ERS modulation patterns in order to isolate the signals responsible for motor control. Using ICA for this application is a novel approach.

This method was used for the investigation of two movement types; LH and RH movements and WE and WF movements. To the author's knowledge, no reliable channel reduction study for the differentiation between WE and WF has yet been presented. This method was tested by examining the amount of motor-control information that was retained during the reduction process. This was done by combining the analysis of three tests: 1) classification analysis of the reduced channel sets when compared to the full channel set. 2) comparison of the ITV plots of the ERD/ERS patterns pre and post reduction. 3) comparison of the amount of variance retained across all channels pre and post reduction.

The optimal number of channels varied per subject and per investigation. Overall the results suggest that a 16-channel configuration is optimal. This configuration

produced reliable results for both investigations, while results for the 8-channel and 3-channel configurations were inconsistent. In some cases, the results from these lower-channel configurations appeared too high for such a few channels. However, the small dataset may be the cause of the inconsistent results obtained from the 3-channel and 8-channel configurations. Therefore, until the performance of the 3-channel and 8-channel configurations can be verified with additional testing, the 16-channel configuration is the suggested best performing configuration.

The 16-channel configuration obtained a classification accuracy of 70.51 % and 61.61 % for investigation 1 and investigation 2 respectively. This resulted in a loss of classification accuracy of 12.01 % and 11.16 % for investigation 1 and 2 respectively. These results were analysed using ITV plots (ERD/ERS patterns) and variance retention, to ensure that motor control characteristics was retained and used for the classifications. Inconsistent results were obtained for a few datasets in both investigations.

Due to the limited number of subjects in this study, it is unknown if the inconsistencies resulted from the extremely small size of the database used, the limited number of trials used in the classification stage, subject variability or due to errors in the method. Further testing is required before any definite conclusions on the effectiveness of the method can be made. However, this research does illustrate the potential of using ICA as a primary technique for channel reduction.

The location of the selected channels is unexpected, as channels were chosen that are not in close proximity to known motor areas. These results show that non-motor-related electrodes might have an important role in recording motor-related cortical activity. This highlights the importance of identifying and isolating the desired control information during the channel reduction process and identifying the channels related to it.

References

[1] D. J. McFarland and J. R. Wolpaw, “EEG-based brain–computer interfaces,” *Current Opinion in Biomedical Engineering*, vol. 4, pp. 194–200, Dec. 2017, doi: 10.1016/j.cobme.2017.11.004.

[2] X. Mao *et al.*, “Progress in EEG-Based Brain Robot Interaction Systems,” *Comput Intell Neurosci*, vol. 2017, 2017, doi: 10.1155/2017/1742862.

[3] S. Sun, C. Zhang, and Y. Lu, “The random electrode selection ensemble for EEG signal classification,” *Pattern Recognition*, vol. 41, no. 5, pp. 1663–1675, May 2008, doi: 10.1016/j.patcog.2007.10.023.

[4] A. K. Mohamed, T. Marwala, and L. R. John, “Single-trial EEG discrimination between wrist and finger movement imagery and execution in a sensorimotor BCI,” in *2011 Annual International Conference of the IEEE Engineering in Medicine and Biology Society*, Aug. 2011, pp. 6289–6293, doi: 10.1109/IEMBS.2011.6091552.

[5] Z. Yang, P. P. H. Lim, S. H. Teo, H. Chen, H. Qiu, and Y. H. Pua, “Association of wrist and forearm range of motion measures with self-reported functional scores amongst patients with distal radius fractures: a longitudinal study,” *BMC Musculoskeletal Disorders*, vol. 19, no. 1, Dec. 2018, doi: 10.1186/s12891-018-2065-z.

[6] N. M. Bajaj, A. J. Spiers, and A. M. Dollar, “State of the art in prosthetic wrists: Commercial and research devices,” in *2015 IEEE International Conference on Rehabilitation Robotics (ICORR)*, Aug. 2015, pp. 331–338, doi: 10.1109/ICORR.2015.7281221.

[7] F. Montagnani, M. Controzzi, and C. Cipriani, “Is it Finger or Wrist Dexterity That is Missing in Current Hand Prostheses?,” *IEEE Transactions on Neural Systems and Rehabilitation Engineering*, vol. 23, no. 4, pp. 600–609, Jul. 2015, doi: 10.1109/TNSRE.2015.2398112.

[8] M. Deijs, R. M. Bongers, N. D. M. Ringeling - van Leusen, and C. K. van der Sluis, “Flexible and static wrist units in upper limb prosthesis users: functionality scores, user satisfaction and compensatory movements,” *J Neuroeng Rehabil*, vol. 13, Mar. 2016, doi: 10.1186/s12984-016-0130-0.

[9] P. K. Pattnaik and J. Sarraf, “Brain Computer Interface issues on hand movement,” *Journal of King Saud University - Computer and Information Sciences*, vol. 30, no. 1, pp. 18–24, Jan. 2018, doi: 10.1016/j.jksuci.2016.09.006.

[10] C. Guger, W. Harkam, C. Hertnaes, and G. Pfurtscheller, “Prosthetic Control by an EEG-based Brain-Computer Interface (BCI),” 2001.

[11] J. R. Wolpaw, N. Birbaumer, D. J. McFarland, G. Pfurtscheller, and T. M. Vaughan, “Brain–computer interfaces for communication and control,” *Clinical Neurophysiology*, p. 25, 2002.

[12] R. Srinivasan, “Methods to Improve the Spatial Resolution of EEG,” vol. 1, no. 1, p. 10, 1999.

[13] L. F. Nicolas-Alonso and J. Gomez-Gil, “Brain Computer Interfaces, a Review,” *Sensors (Basel)*, vol. 12, no. 2, pp. 1211–1279, Jan. 2012, doi: 10.3390/s120201211.

[14] T. Alotaiby, F. E. A. El-Samie, S. A. Alshebeili, and I. Ahmad, “A review of channel selection algorithms for EEG signal processing,” *EURASIP Journal on Advances in Signal Processing*, vol. 2015, no. 1, Dec. 2015, doi: 10.1186/s13634-015-0251-9.

[15] B. J. Edelman, B. Baxter, and B. He, “EEG Source Imaging Enhances the Decoding of Complex Right-Hand Motor Imagery Tasks,” *IEEE Transactions on Biomedical Engineering*, vol. 63, no. 1, pp. 4–14, Jan. 2016, doi: 10.1109/TBME.2015.2467312.

[16] A. Anzolin, P. Presti, F. Van de Steen, L. Astolfi, S. Haufe, and D. Marinazzo, “Effect of head volume conduction on directed connectivity estimated between reconstructed EEG sources,” Neuroscience, preprint, Jan. 2018. doi: 10.1101/251223.

[17] W. Speier, A. Deshpande, and N. Pouratian, “A method for optimizing EEG electrode number and configuration for signal acquisition in P300 speller systems,” *Clinical Neurophysiology*, vol. 126, no. 6, pp. 1171–1177, Jun. 2015, doi: 10.1016/j.clinph.2014.09.021.

[18] K. A. Colwell, D. B. Ryan, C. S. Throckmorton, E. W. Sellers, and L. M. Collins, “Channel selection methods for the P300 Speller,” *Journal of*

Neuroscience Methods, vol. 232, pp. 6–15, Jul. 2014, doi: 10.1016/j.jneumeth.2014.04.009.

[19] M. Dobiáš and J. Št'astný, "Subband optimization for EEG-based classification of movements of the same limb," in *2014 International Conference on Applied Electronics*, Sep. 2014, pp. 71–74, doi: 10.1109/AE.2014.7011671.

[20] A. Vuckovic and F. Sepulveda, "Delta band contribution in cue based single trial classification of real and imaginary wrist movements," *Medical & Biological Engineering & Computing*, vol. 46, no. 6, pp. 529–539, Jun. 2008, doi: 10.1007/s11517-008-0345-8.

[21] F. Ghani, H. Sultan, D. Anwar, O. Farooq, and Y. U. Khan, "Classification of Wrist Movements Using EEG Signals," p. 11.

[22] X. Yong and C. Menon, "EEG Classification of Different Imaginary Movements within the Same Limb," *PLOS ONE*, vol. 10, no. 4, p. e0121896, Apr. 2015, doi: 10.1371/journal.pone.0121896.

[23] J. D. Kropotov, "Chapter 2 - Alpha Rhythms," in *Quantitative EEG, Event-Related Potentials and Neurotherapy*, San Diego: Academic Press, 2009, pp. 29–58.

[24] I. Navarro, B. Hubais, and F. Sepulveda, "A Comparison of Time, Frequency and ICA Based Features and Five Classifiers for Wrist Movement Classification in EEG Signals," in *2005 IEEE Engineering in Medicine and Biology 27th Annual Conference*, Jan. 2005, pp. 2118–2121, doi: 10.1109/IEMBS.2005.1616878.

[25] B. Blankertz, R. Tomioka, S. Lemm, M. Kawanabe, and K. r Muller, "Optimizing Spatial filters for Robust EEG Single-Trial Analysis," *IEEE Signal Processing Magazine*, vol. 25, no. 1, pp. 41–56, 2008, doi: 10.1109/MSP.2008.4408441.

[26] J. Ryu, W. P. Cooney, L. J. Askew, K.-N. An, and E. Y. S. Chao, "Functional ranges of motion of the wrist joint," *The Journal of Hand Surgery*, vol. 16, no. 3, pp. 409–419, May 1991, doi: 10.1016/0363-5023(91)90006-W.

[27] H. Yuan and B. He, "Brain–Computer Interfaces Using Sensorimotor Rhythms: Current State and Future Perspectives," *IEEE Transactions on*

Biomedical Engineering, vol. 61, no. 5, pp. 1425–1435, May 2014, doi: 10.1109/TBME.2014.2312397.

[28] B. He, B. Baxter, B. J. Edelman, C. C. Cline, and W. W. Ye, "Noninvasive Brain-Computer Interfaces Based on Sensorimotor Rhythms," *Proceedings of the IEEE*, vol. 103, no. 6, pp. 907–925, Jun. 2015, doi: 10.1109/JPROC.2015.2407272.

[29] S. Bhattacharyya, A. Khasnobish, A. Konar, D. N. Tibarewala, and A. K. Nagar, "Performance analysis of left/right hand movement classification from EEG signal by intelligent algorithms," in *2011 IEEE Symposium on Computational Intelligence, Cognitive Algorithms, Mind, and Brain (CCMB)*, Apr. 2011, pp. 1–8, doi: 10.1109/CCMB.2011.5952111.

[30] J. Decety, "The neurophysiological basis of motor imagery," *Behavioural Brain Research*, vol. 77, no. 1–2, pp. 45–52, May 1996, doi: 10.1016/0166-4328(95)00225-1.

[31] Th. Mulder, "Motor imagery and action observation: cognitive tools for rehabilitation," *J Neural Transm*, vol. 114, no. 10, pp. 1265–1278, Oct. 2007, doi: 10.1007/s00702-007-0763-z.

[32] M. Hallett, O. Bai, and C. Bonin, "Predicting Movement: When, Which and Where," in *2007 IEEE/ICME International Conference on Complex Medical Engineering*, May 2007, pp. 5–7, doi: 10.1109/ICCME.2007.4381681.

[33] B. Blankertz, S. Lemm, M. Treder, S. Haufe, and K.-R. Müller, "Single-trial analysis and classification of ERP components — A tutorial," *NeuroImage*, vol. 56, no. 2, pp. 814–825, May 2011, doi: 10.1016/j.neuroimage.2010.06.048.

[34] J. Kohlmorgen and B. Blankertz, "Bayesian Classification of Single-Trial Event-Related Potentials in EEG ∗," *International Journal of Bifurcation and Chaos*, vol. 14, pp. 719 – 726, 2004.

[35] L. Parra *et al.*, "Single-trial detection in EEG and MEG: Keeping it linear," *Neurocomputing*, vol. 52–54, pp. 177–183, Jun. 2003, doi: 10.1016/S0925-2312(02)00821-4.

[36] J. D. Kropotov, “Chapter 1 - Slow, Infra-Slow Potentials, and Delta Rhythms,” in *Quantitative EEG, Event-Related Potentials and Neurotherapy*, San Diego: Academic Press, 2009, pp. 11–28.

[37] R. Srinivasan, P. L. Nunez, and R. B. Silberstein, “Spatial filtering and neocortical dynamics: estimates of EEG coherence,” *IEEE Transactions on Biomedical Engineering*, vol. 45, no. 7, pp. 814–826, Jul. 1998, doi: 10.1109/10.686789.

[38] M. Villafañe-Delgado and S. Aviyente, “A time-frequency based bivariate synchrony measure for reducing volume conduction effects in EEG,” in *2015 IEEE Global Conference on Signal and Information Processing (GlobalSIP)*, Dec. 2015, pp. 825–828, doi: 10.1109/GlobalSIP.2015.7418312.

[39] V. Morash, O. Bai, S. Furlani, P. Lin, and M. Hallett, “Classifying EEG Signals Preceding Right Hand, Left Hand, Tongue, and Right Foot Movements and Motor Imageries,” *Clin Neurophysiol*, vol. 119, no. 11, pp. 2570–2578, Nov. 2008, doi: 10.1016/j.clinph.2008.08.013.

[40] X. Jiang, G.-B. Bian, and Z. Tian, “Removal of Artifacts from EEG Signals: A Review,” *Sensors*, vol. 19, no. 5, pp. 1–18, Jan. 2019, doi: 10.3390/s19050987.

[41] M. Fatourechi, A. Bashashati, R. K. Ward, and G. E. Birch, “EMG and EOG artifacts in brain computer interface systems:A survey,” *Clinical neurophysiology : official journal of the International Federation of Clinical Neurophysiology*, vol. 118, pp. 480–49, 2007, doi: 10.1016/j.clinph.2006.10.019.

[42] C. Brunner, M. Naeem, R. Leeb, B. Graimann, and G. Pfurtscheller, “Spatial filtering and selection of optimized components in four class motor imagery EEG data using independent components analysis,” *Pattern Recognition Letters*, vol. 28, no. 8, pp. 957–964, Jun. 2007, doi: 10.1016/j.patrec.2007.01.002.

[43] L. W. Ko, S. C. Lin, M. S. Song, and O. Komarov, “Developing a few-channel hybrid BCI system by using motor imagery with SSVEP assist,” in *2014 International Joint Conference on Neural Networks (IJCNN)*, Jul. 2014, pp. 4114–4120, doi: 10.1109/IJCNN.2014.6889901.

[44] J. S. Kirar and R. K. Agrawal, “Composite kernel support vector machine based performance enhancement of brain computer interface in conjunction with spatial filter,” *Biomedical Signal Processing and Control*, vol. 33, pp. 151–160, Mar. 2017, doi: 10.1016/j.bspc.2016.09.014.

[45] D. Wu, J. T. King, C. H. Chuang, C. T. Lin, and T. P. Jung, “Spatial Filtering for EEG-Based Regression Problems in Brain #x2013;Computer Interface (BCI),” *IEEE Transactions on Fuzzy Systems*, vol. 26, no. 2, pp. 771–781, Apr. 2018, doi: 10.1109/TFUZZ.2017.2688423.

[46] R. Lahiri, P. Rakshit, A. Konar, and A. K. Nagar, “Evolutionary approach for selection of optimal EEG electrode positions and features for classification of cognitive tasks,” in *2016 IEEE Congress on Evolutionary Computation (CEC)*, Jul. 2016, pp. 4846–4853, doi: 10.1109/CEC.2016.7744411.

[47] R. Lahiri, P. Rakshit, and A. Konar, “Evolutionary perspective for optimal selection of EEG electrodes and features,” *Biomedical Signal Processing and Control*, vol. 36, pp. 113–137, 2017, doi: http://dx.doi.org/10.1016/j.bspc.2017.03.022.

[48] A. Dey, S. Bhattacharjee, and D. Samanta, “Recognition of motor imagery left and right hand movement using EEG,” in *2016 IEEE International Conference on Recent Trends in Electronics, Information Communication Technology (RTEICT)*, May 2016, pp. 426–430, doi: 10.1109/RTEICT.2016.7807856.

[49] B. Edelman, B. Baxter, and B. He, “Discriminating hand gesture motor imagery tasks using cortical current density estimation,” in *2014 36th Annual International Conference of the IEEE Engineering in Medicine and Biology Society*, Aug. 2014, pp. 1314–1317, doi: 10.1109/EMBC.2014.6943840.

[50] N. Jiang, L. Gizzi, N. Mrachacz-Kersting, K. Dremstrup, and D. Farina, “A brain–computer interface for single-trial detection of gait initiation from movement related cortical potentials,” *Clinical Neurophysiology*, vol. 126, no. 1, pp. 154–159, Jan. 2015, doi: 10.1016/j.clinph.2014.05.003.

[51] T. Lan, D. Erdogmus, A. Adami, M. Pavel, and S. Mathan, “Salient EEG Channel Selection in Brain Computer Interfaces by Mutual Information Maximization,” in *2005 IEEE Engineering in Medicine and Biology 27th*

Annual Conference, Jan. 2005, pp. 7064–7067, doi: 10.1109/IEMBS.2005.1616133.

[52] S. Datta, P. Rakshit, A. Konar, and A. K. Nagar, "Selecting the optimal EEG electrode positions for a cognitive task using an Artificial Bee Colony with Adaptive Scale Factor optimization algorithm," in *2014 IEEE Congress on Evolutionary Computation (CEC)*, Jul. 2014, pp. 2748–2755, doi: 10.1109/CEC.2014.6900550.

[53] C. J. James and C. W. Hesse, "Independent component analysis for biomedical signals," *Physiologial Measurement*, vol. 26, no. 1, pp. 15–39, 2005, doi: https://doi.org/10.1088/0967-3334/26/1/R02.

[54] J. Onton and S. Makeig, "Information-based modeling of event-related brain dynamics," in *Progress in Brain Research*, vol. 159, Elsevier, 2006, pp. 99–120.

[55] J. Sleight, P. Pillai, and S. Mohan, "Classification of Executed and Imagined Motor Movement EEG Signals," pp. 1–10, 2009.

[56] B. Zhou, X. Wu, J. Ruan, Z. Lv, and L. Zhang, "How many channels are suitable for independent component analysis in motor imagery brain-computer interface," *Biomedical Signal Processing and Control*, vol. 50, pp. 103–120, Apr. 2019, doi: 10.1016/j.bspc.2019.01.017.

[57] S. Wang and C. J. James, "Enhancing Evoked Responses for BCI Through Advanced ICA Techniques," in *2006 IET 3rd International Conference On Advances in Medical, Signal and Information Processing - MEDSIP 2006*, Jul. 2006, pp. 1–4.

[58] A. Guyton and J. Hall, *Textbook of Medical Physiology*, 11th ed. Elsevier Inc., 2006.

[59] S. Hu, H. Wang, J. Zhang, W. Kong, and Y. Cao, "Causality from Cz to C3/C4 or between C3 and C4 revealed by granger causality and new causality during motor imagery," in *2014 International Joint Conference on Neural Networks (IJCNN)*, Jul. 2014, pp. 3178–3185, doi: 10.1109/IJCNN.2014.6889769.

[60] S. Vaid, P. Singh, and C. Kaur, "EEG Signal Analysis for BCI Interface: A Review," in *2015 Fifth International Conference on Advanced Computing*

Communication Technologies, Feb. 2015, pp. 143–147, doi: 10.1109/ACCT.2015.72.

[61] D. Choi, Y. Ryu, Y. Lee, and M. Lee, "Performance evaluation of a motor-imagery based EEG-Brain computer interface using a combined cue with heterogeneous training data in BCI-Naive subjects," *BioMedical Engineering OnLine*, vol. 10, no. 91, pp. 1–12, 2011.

[62] J. Kalcher and G. Pfurtscheller, "Discrimination between phase-locked and non-phase-locked event-related EEG activity," *Electroencephalography and clinical Neurophysiology*, vol. 94, pp. 381–384, 1995.

[63] G. Pfurtscheller and F. H. Lopes da Silva, "Event-related EEG/MEG synchronization and desynchronization: basic principles," *Clinical Neurophysiology*, vol. 110, no. 11, pp. 1842–1857, Nov. 1999, doi: 10.1016/S1388-2457(99)00141-8.

[64] H. Ramoser, J. Muller-Gerking, and G. Pfurtscheller, "Optimal spatial filtering of single trial EEG during imagined hand movement," *IEEE Transactions on Rehabilitation Engineering*, vol. 8, no. 4, pp. 441–446, Dec. 2000, doi: 10.1109/86.895946.

[65] R. C. Caracillo and M. C. F. Castro, "Classification of executed upper limb movements by means of EEG," in *2013 ISSNIP Biosignals and Biorobotics Conference: Biosignals and Robotics for Better and Safer Living (BRC)*, Feb. 2013, pp. 1–6, doi: 10.1109/BRC.2013.6487448.

[66] T. Chakraborti *et al.*, "Implementation of EEG based control of remote robotic systems," in *2011 International Conference on Recent Trends in Information Systems*, Dec. 2011, pp. 203–208, doi: 10.1109/ReTIS.2011.6146868.

[67] M. Pal, S. Bhattacharyya, A. Konar, D. N. Tibarewala, and R. Janarthanan, "Decoding of wrist and finger movement from electroencephalography signal," in *2014 IEEE International Conference on Electronics, Computing and Communication Technologies (CONECCT)*, Jan. 2014, pp. 1–6, doi: 10.1109/CONECCT.2014.6740323.

[68] A. Schwarz, P. Ofner, J. Pereira, A. I. Sburlea, and G. R. Müller-Putz, "Decoding natural reach-and-grasp actions from human EEG," *Journal of*

Neural Engineering, vol. 15, no. 1, p. 016005, Feb. 2018, doi: 10.1088/1741-2552/aa8911.

[69] K. Liao, R. Xiao, J. Gonzalez, and L. Ding, "Decoding Individual Finger Movements from One Hand Using Human EEG Signals," *PLoS One*, vol. 9, no. 1, Jan. 2014, doi: 10.1371/journal.pone.0085192.

[70] M. A. Gull, H. Elahi, M. Marwat, and S. Waqar, "A new approach to classification of upper limb and wrist movements using EEG signals," in *2017 13th IASTED International Conference on Biomedical Engineering (BioMed)*, Feb. 2017, pp. 181–194, doi: 10.2316/P.2017.852-049.

[71] A. Vučković and F. Sepulveda, "A two-stage four-class BCI based on imaginary movements of the left and the right wrist," *Medical Engineering & Physics*, vol. 34, no. 7, pp. 964–971, Sep. 2012, doi: 10.1016/j.medengphy.2011.11.001.

[72] B. Edelman, B. Baxter, and B. He, "Decoding and mapping of right hand motor imagery tasks using EEG source imaging," in *2015 7th International IEEE/EMBS Conference on Neural Engineering (NER)*, Apr. 2015, pp. 194–197, doi: 10.1109/NER.2015.7146593.

[73] F. Sepulveda, M. Meckes, and B. A. Conway, "Cluster separation index suggests usefulness of non-motor EEG channels in detecting wrist movement direction intention," in *IEEE Conference on Cybernetics and Intelligent Systems, 2004.*, Dec. 2004, vol. 2, pp. 943–947, doi: 10.1109/ICCIS.2004.1460715.

[74] A. Vuckovic, "Non-invasive BCI: How far can we get with motor imagination?," *Clinical Neurophysiology*, vol. 120, no. 8, pp. 1422–1423, Aug. 2009, doi: 10.1016/j.clinph.2009.06.007.

[75] H. Cecotti *et al.*, "A robust sensor-selection method for P300 brain–computer interfaces," *Journal of Neural Engineering*, vol. 8, no. 1, p. 016001, Feb. 2011, doi: 10.1088/1741-2560/8/1/016001.

[76] L. Meng, J. Jin, and X. Wang, "A comparison of three electrode channels selection methods applied to SSVEP BCI," in *2011 4th International Conference on Biomedical Engineering and Informatics (BMEI)*, Oct. 2011, vol. 1, pp. 584–587, doi: 10.1109/BMEI.2011.6098285.

[77] A. Majkowski, Ł. Oskwarek, M. Kołodziej, and R. J. Rak, “An attempt to localize brain electrical activity sources using EEG with limited number of electrodes,” *Biocybernetics and Biomedical Engineering*, vol. 36, no. 4, pp. 686–696, 2016, doi: 10.1016/j.bbe.2016.07.002.

[78] P. Ofner, A. Schwarz, J. Pereira, and G. R. Müller-Putz, “Upper limb movements can be decoded from the time-domain of low-frequency EEG,” *PLoS One*, vol. 12, no. 8, Aug. 2017, doi: 10.1371/journal.pone.0182578.

[79] L.-W. Ko, S. S. K. Ranga, O. Komarov, and C.-C. Chen, “Development of Single-Channel Hybrid BCI System Using Motor Imagery and SSVEP,” *Journal of Healthcare Engineering*, vol. 2017, pp. 1–7, doi: 10.1155/2017/3789386.

[80] A. Shakeel, M. S. Navid, M. N. Anwar, S. Mazhar, M. Jochumsen, and I. K. Niazi, “A Review of Techniques for Detection of Movement Intention Using Movement-Related Cortical Potentials,” *Comput Math Methods Med*, vol. 2015, 2015, doi: 10.1155/2015/346217.

[81] J. Ibáñez *et al.*, “Detection of the onset of upper-limb movements based on the combined analysis of changes in the sensorimotor rhythms and slow cortical potentials,” *Journal of Neural Engineering*, vol. 11, no. 5, p. 056009, Oct. 2014, doi: 10.1088/1741-2560/11/5/056009.

[82] A. K. Mohamed, T. Marwala, les John, and L. R. John, “Towards Improved EEG Interpretation for the Control of a Prosthetic/Orthotic Hand using a BCI: Single-trial right and left hand discrimination,” presented at the Proceedings of the Twenty-Second Annual Symposium of the Pattern Recognition Association of South Africa, Vanderbijlpark, South Africa, 2011.

[83] Y. Gu, K. Dremstrup, and D. Farina, “Single-trial discrimination of type and speed of wrist movements from EEG recordings,” *Clinical Neurophysiology*, vol. 120, no. 8, pp. 1596–1600, Aug. 2009, doi: 10.1016/j.clinph.2009.05.006.

[84] A. Bashashati, M. Fatourechi, R. K. Ward, and G. E. Birch, “A survey of signal processing algorithms in brain–computer interfaces based on electrical brain signals,” *Journal of Neural Engineering*, vol. 4, no. 2, pp. R32–R57, Jun. 2007, doi: 10.1088/1741-2560/4/2/R03.

[85] P. Luu and T. Ferree, “Determination of the Geodesic Sensor Net’s Average Electrode Positions and Their 10 – 10 International Equivalents,” *Electrical Geodesics Inc*, Oct. 2005.

[86] A. Delorme and S. Makeig, “EEGLAB: an open source toolbox for analysis of single-trial EEG dynamics including independent component analysis,” *Journal of Neuroscience Methods*, vol. 134, no. 1, pp. 9–21, Mar. 2004, doi: 10.1016/j.jneumeth.2003.10.009.

[87] Y. U. Khan and F. Sepulveda, “Brain-computer interface for single-trial eeg classification for wrist movement imagery using spatial filtering in the gamma band,” *IET Signal Processing*, vol. 4, no. 5, pp. 510–517, Oct. 2010, doi: 10.1049/iet-spr.2008.0235.

[88] G. Gomez-Herrero, “Automatic Artifact Removal (AAR) toolbox v1.3 (Release 09.12.2007) for MATLAB,” p. 23.

[89] O. Bai, P. Lin, S. Vorbach, J. Li, S. Furlani, and M. Hallett, “Exploration of computational methods for classification of movement intention during human voluntary movement from single trial EEG,” *Clinical Neurophysiology*, vol. 118, no. 12, pp. 2637–2655, Dec. 2007, doi: 10.1016/j.clinph.2007.08.025.

[90] F. Nielsen, S. Boltz, and O. Schwander, “Bhattacharyya Clustering with Applications to Mixture Simplifications,” in *2010 20th International Conference on Pattern Recognition*, Aug. 2010, pp. 1437–1440, doi: 10.1109/ICPR.2010.355.

[91] F. Lotte *et al.*, “A review of classification algorithms for EEG-based brain–computer interfaces: a 10 year update,” *Journal of Neural Engineering*, vol. 15, no. 3, p. 031005, Jun. 2018, doi: 10.1088/1741-2552/aab2f2.

[92] MathWorks, “Detect and remove outliers in data - MATLAB rmoutliers,” *MathsWork Documentation*. https://www.mathworks.com/help/matlab/ref/rmoutliers.html?s_tid=doc_ta (accessed Dec. 26, 2019).

[93] MathWorks, “Correlation coefficients - MATLAB corrcoef,” *MathsWork Documentation*.

https://www.mathworks.com/help/matlab/ref/corrcoef.html#f80-999628-P (accessed Feb. 15, 2020).

[94] P. Georgieva, N. Bouaynaya, F. Silva, L. Mihaylova, and L. C. Jain, "A Beamformer-Particle Filter Framework for Localization of Correlated EEG Sources," *IEEE Journal of Biomedical and Health Informatics*, vol. 20, no. 3, pp. 880–892, May 2016, doi: 10.1109/JBHI.2015.2413752.

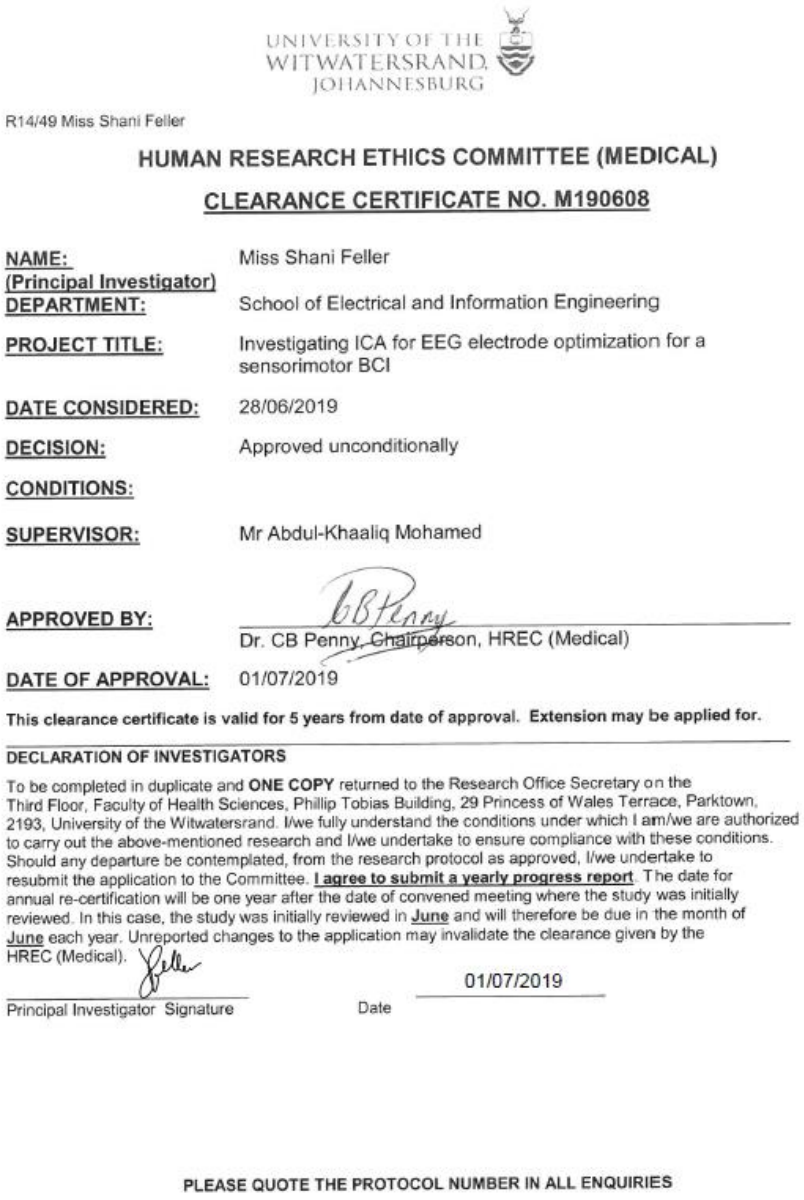
[95] A. Uran, C. van Gemeren, R. van Diepen, R. Chavarriaga, and J. del R. Millán, "Applying Transfer Learning To Deep Learned Models For EEG Analysis," *arXiv:1907.01332 [cs, eess, stat]*, Jul. 2019, Accessed: Sep. 01, 2020. [Online]. Available: http://arxiv.org/abs/1907.01332.

[96] B. Chakraborty, L. Ghosh, and A. Konar, "Optimal Selection of EEG Electrodes Using Interval Type-2 Fuzzy-Logic-Based Semiseparating Signaling Game," *IEEE Transactions on Cybernetics*, pp. 1–13, 2020, doi: 10.1109/TCYB.2020.2968625.

[97] C. Brunner, R. Leeb, G. R. Muller-Putz, and A. Schlogl, "BCI Competition 2008 – Graz data set A," p. 6.

[98] M. Hamedi, S.-H. Salleh, and A. M. Noor, "Electroencephalographic Motor Imagery Brain Connectivity Analysis for BCI: A Review," *Neural Comput*, vol. 28, no. 6, pp. 999–1041, 2016, doi: 10.1162/NECO_a_00838.

Appendix A – Ethical Clearance Certificate



UNIVERSITY OF THE WITWATERSRAND, JOHANNESBURG

R14/49 Miss Shani Feller

HUMAN RESEARCH ETHICS COMMITTEE (MEDICAL)

CLEARANCE CERTIFICATE NO. M190608

NAME: (Principal Investigator)	Miss Shani Feller
DEPARTMENT:	School of Electrical and Information Engineering
PROJECT TITLE:	Investigating ICA for EEG electrode optimization for a sensorimotor BCI
DATE CONSIDERED:	28/06/2019
DECISION:	Approved unconditionally
CONDITIONS:	
SUPERVISOR:	Mr Abdul-Khaaliq Mohamed
APPROVED BY:	Dr. CB Penny, Chairperson, HREC (Medical)
DATE OF APPROVAL:	01/07/2019

This clearance certificate is valid for 5 years from date of approval. Extension may be applied for.

DECLARATION OF INVESTIGATORS

To be completed in duplicate and **ONE COPY** returned to the Research Office Secretary on the Third Floor, Faculty of Health Sciences, Phillip Tobias Building, 29 Princess of Wales Terrace, Parktown, 2193, University of the Witwatersrand. I/we fully understand the conditions under which I am/we are authorized to carry out the above-mentioned research and I/we undertake to ensure compliance with these conditions. Should any departure be contemplated, from the research protocol as approved, I/we undertake to resubmit the application to the Committee. **I agree to submit a yearly progress report**. The date for annual re-certification will be one year after the date of convened meeting where the study was initially reviewed. In this case, the study was initially reviewed in **June** and will therefore be due in the month of **June** each year. Unreported changes to the application may invalidate the clearance given by the HREC (Medical).

Principal Investigator Signature

Date 01/07/2019

PLEASE QUOTE THE PROTOCOL NUMBER IN ALL ENQUIRIES

Figure A.1: Ethical clearance certificate.

Appendix B – Scalp Plots and ITV Plots of Best-Performing-ICs-Baseline

B.1 Investigation 1

B.1.1. Scalp Plots

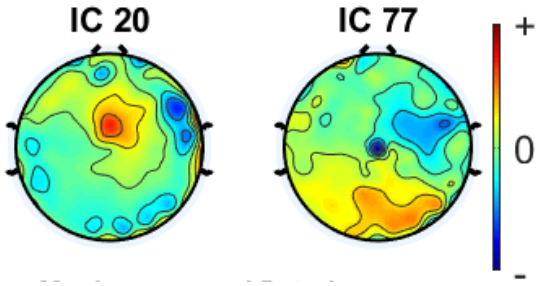


Figure B.2: Scalp plots of all best-performing-ICs-baseline for subject 2's dataset.

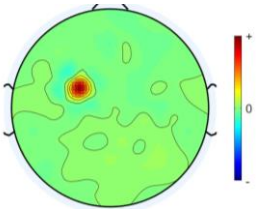


Figure B.3: Scalp plots of all best-performing-ICs-baseline for subject 3's dataset.

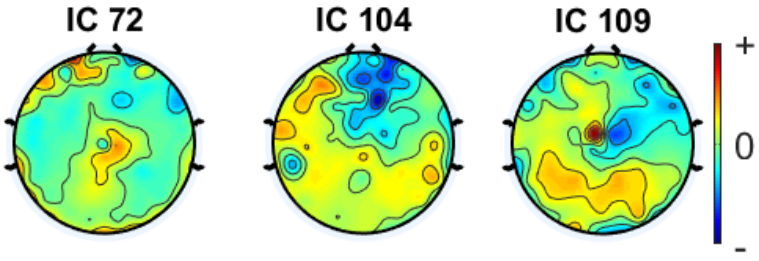


Figure B.4: Scalp plots of all best-performing-ICs-baseline for subject 5's dataset.

B.1.2. ITV Plots

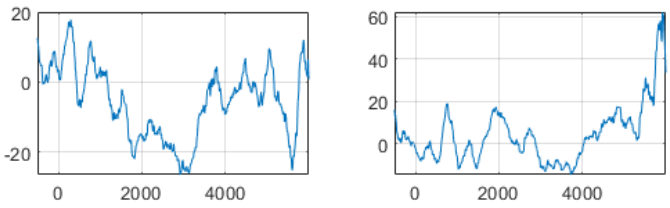


Figure B.5: ITV ERD/ERS patterns (averaged over all trials) of best-performing-ICs-baseline for subject 2.

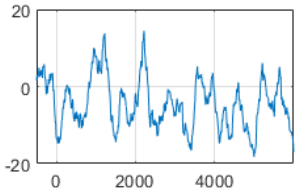


Figure B.6: ITV ERD/ERS patterns (averaged over all trials) of best-performing-ICs-baseline for subject 3.

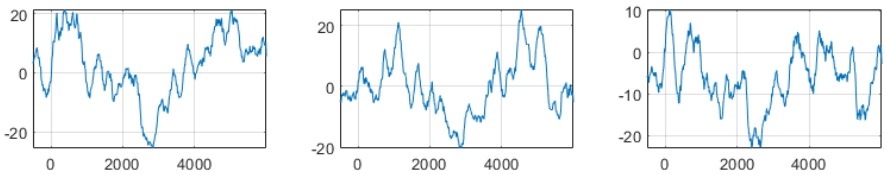


Figure B.7: ITV ERD/ERS patterns (averaged over all trials) of best-performing-ICs-baseline for subject 5.

B.2 Investigation 2

B.2.1. Scalp Plots

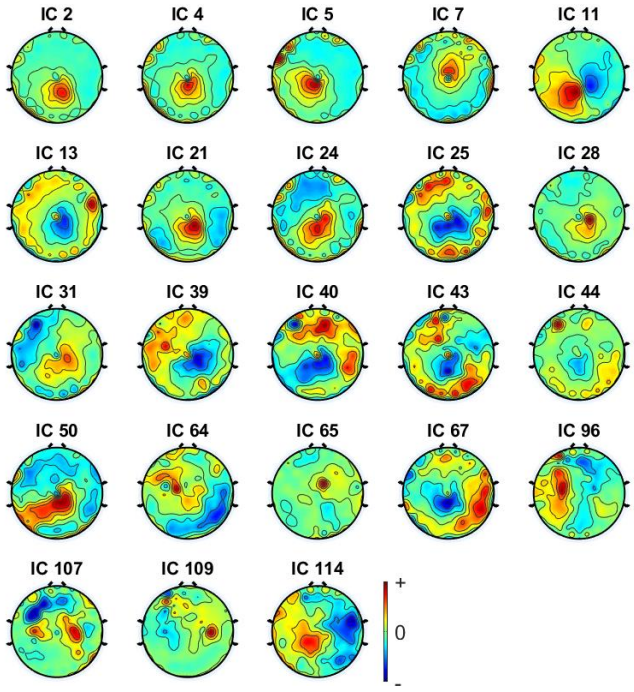


Figure B.8: Scalp plots of all best-performing-ICs-baseline for subject 1 RH's dataset.

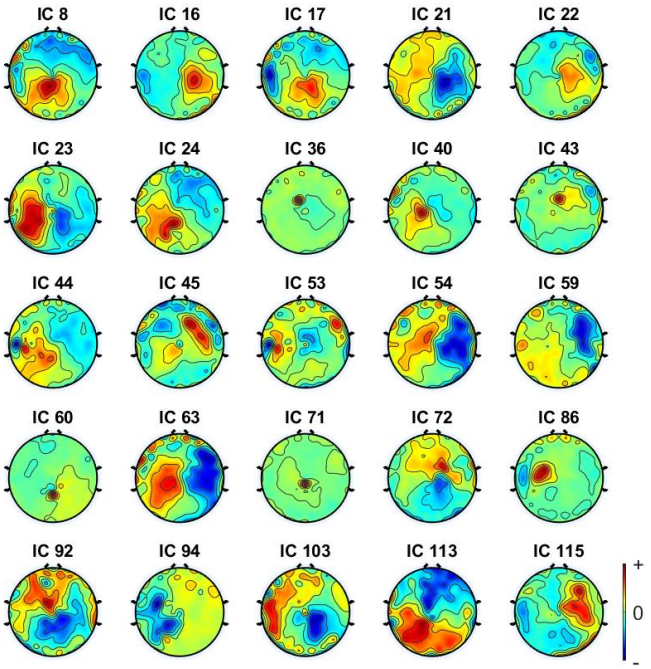


Figure B.9: Scalp plots of all best-performing-ICs-baseline for subject 2 LH's dataset.

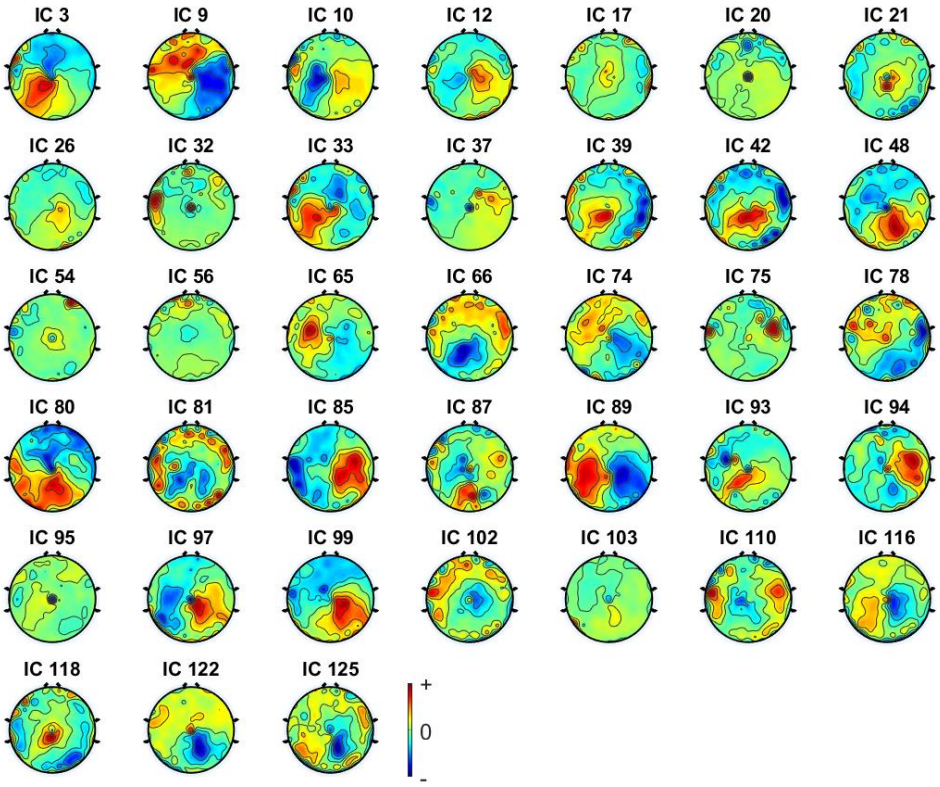


Figure B.10: Scalp plots of all best-performing-ICs-baseline for subject 2 RH's dataset.

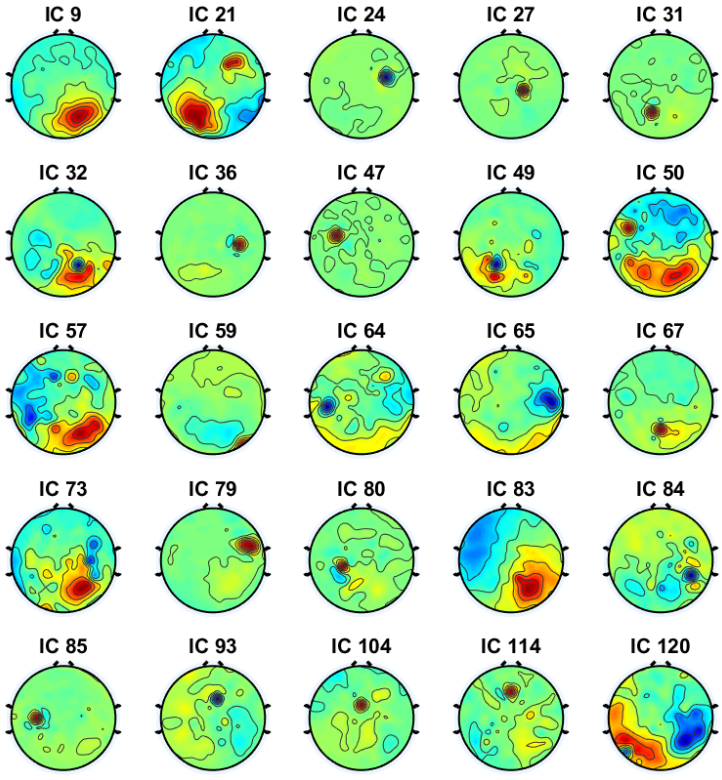


Figure B.11: Scalp plots of all best-performing-ICs-baseline for subject 3 LH's dataset.

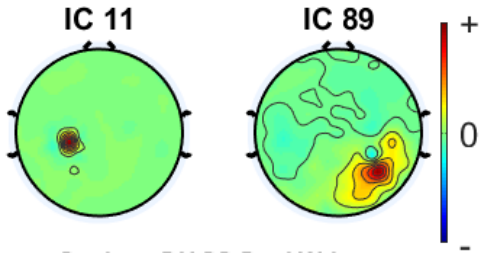


Figure B.12: Scalp plots of all best-performing-ICs-baseline for subject 3 RH's dataset.

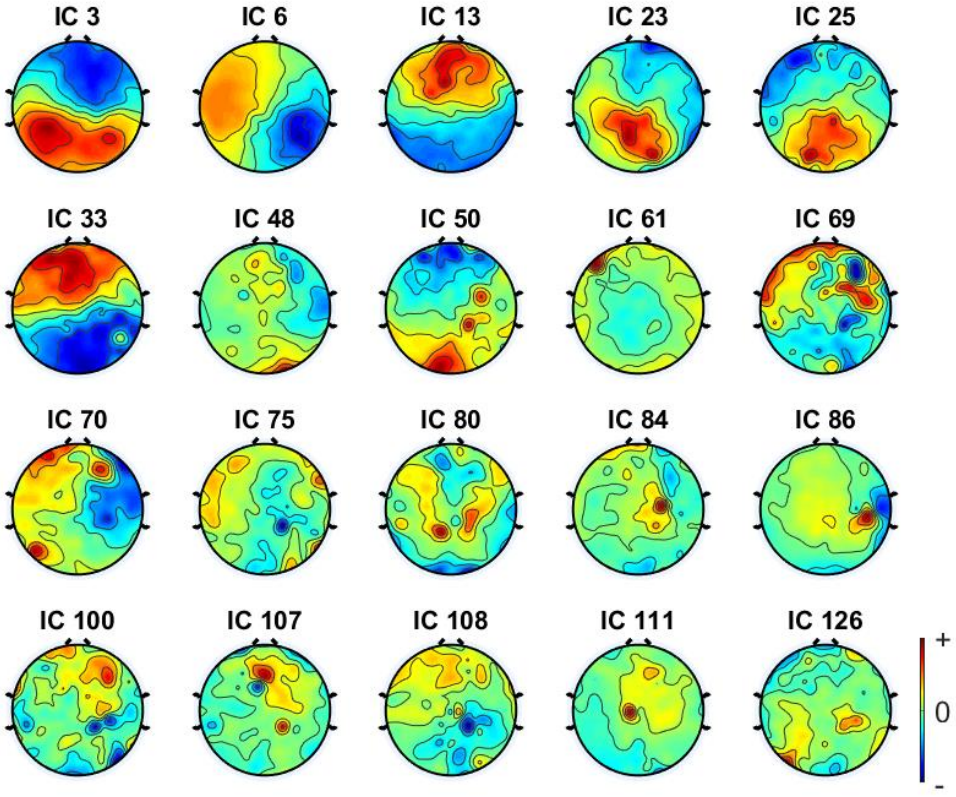


Figure B.13: Scalp plots of all best-performing-ICs-baseline for subject 4 LH's dataset.

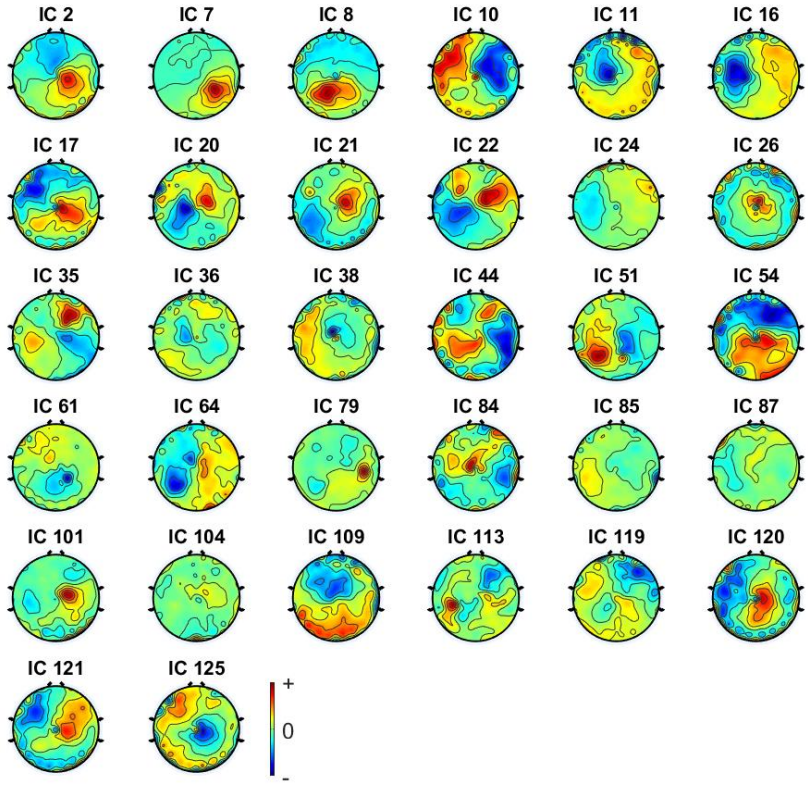


Figure B.14: Scalp plots of all best-performing-ICs-baseline for subject 5 LH's dataset.

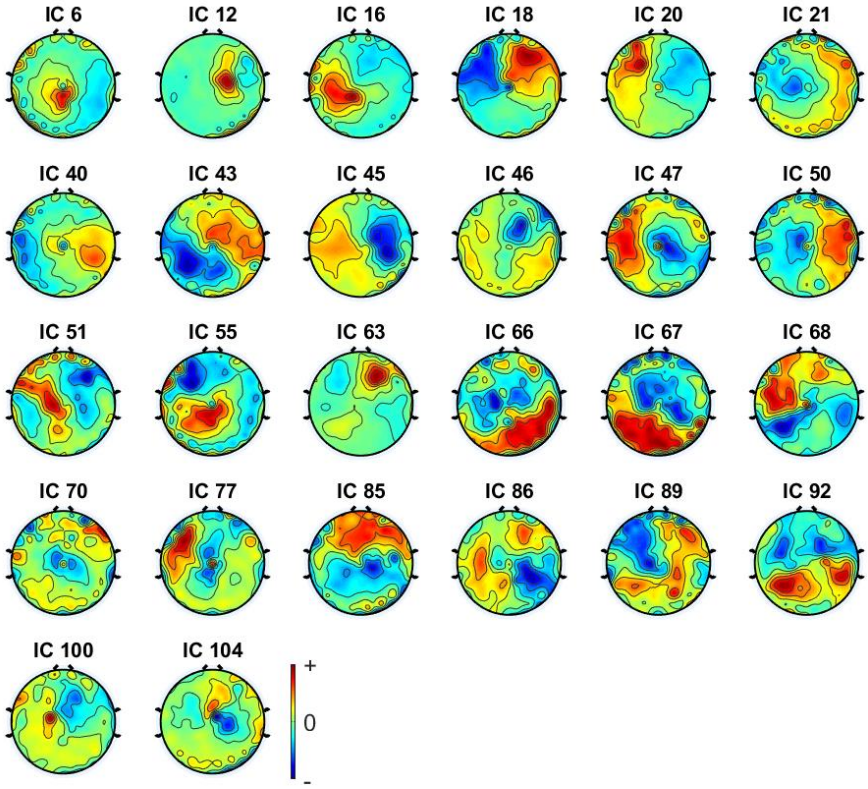


Figure B.15: Scalp plots of all best-performing-ICs-baseline for subject 5 RH's dataset.

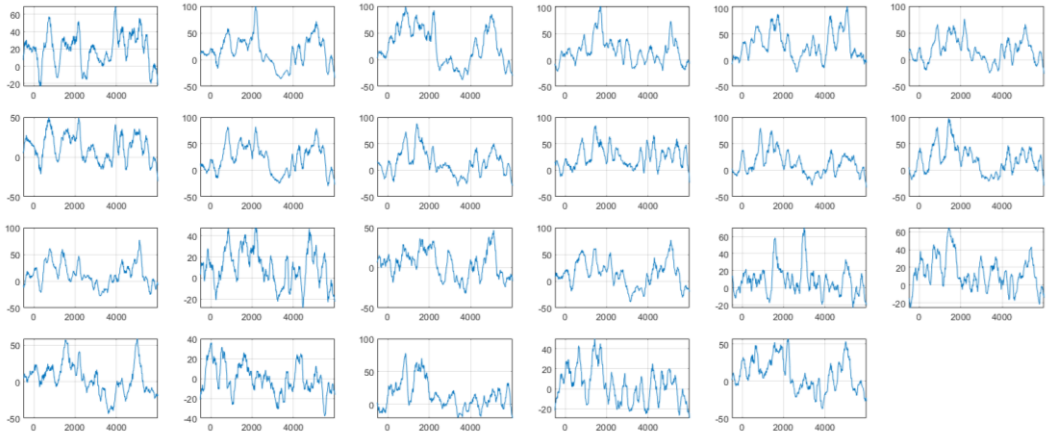


Figure B.16: ITV ERD/ERS patterns (averaged over all trials) of best-performing-ICs-baseline for subject 1 RH.

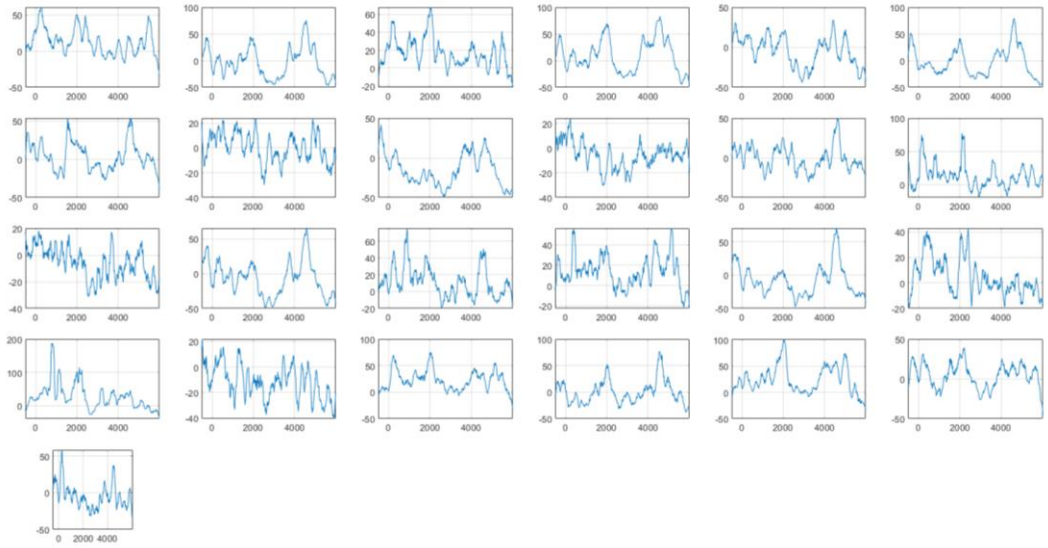


Figure B.17: ITV ERD/ERS patterns (averaged over all trials) of best-performing-ICs-baseline for subject 2 LH.

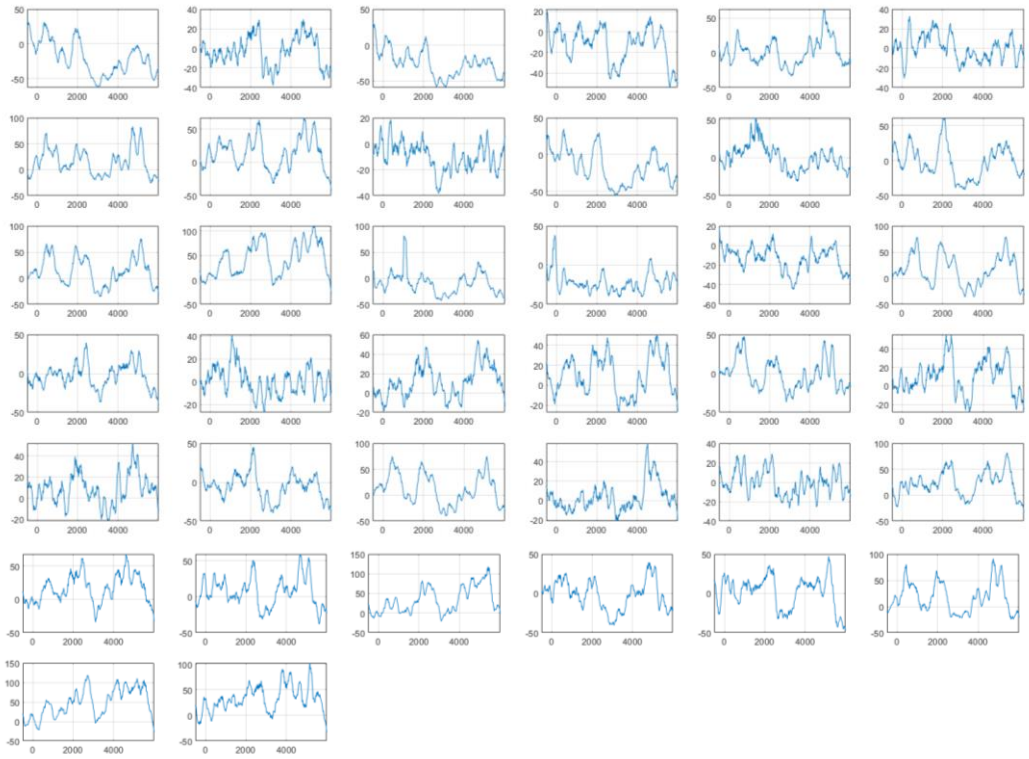


Figure B.18: ITV ERD/ERS patterns (averaged over all trials) of best-performing-ICs-baseline for subject 2 RH.

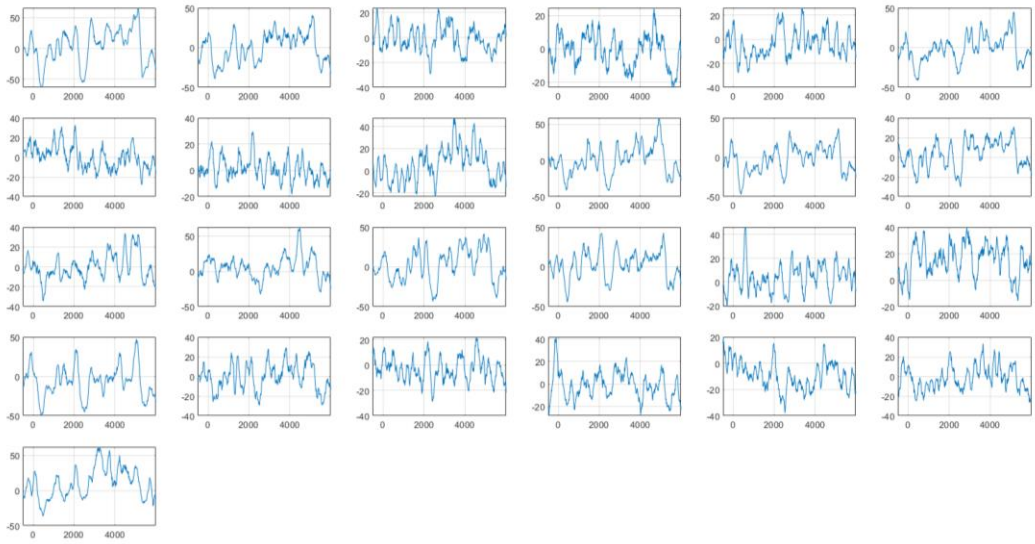


Figure B.19: ITV ERD/ERS patterns (averaged over all trials) of best-performing-ICs-baseline for subject 3 LH.

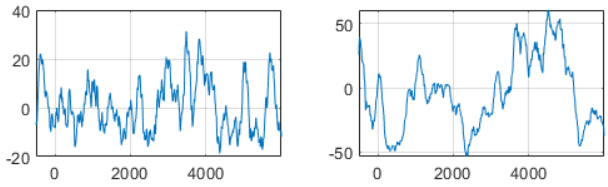


Figure B.20: ITV ERD/ERS patterns (averaged over all trials) of best-performing-ICs-baseline for subject 3 RH.

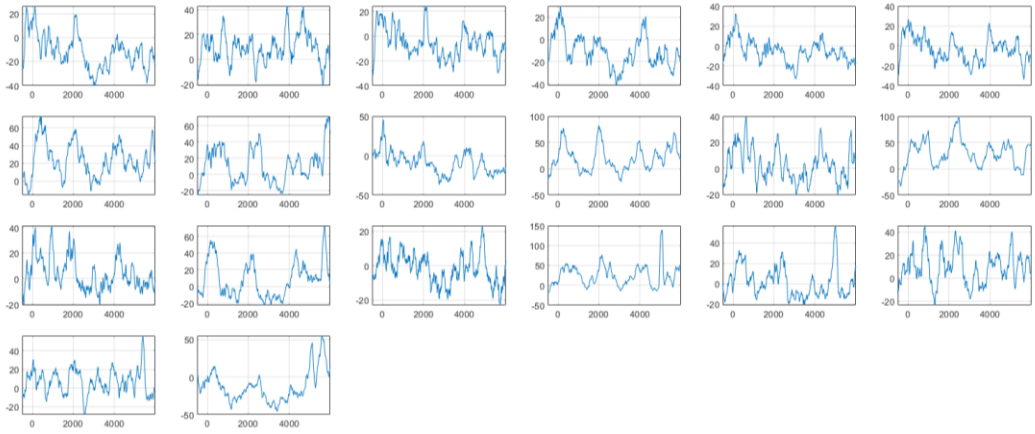


Figure B.21: ITV ERD/ERS patterns (averaged over all trials) of best-performing-ICs-baseline for subject 4 LH.

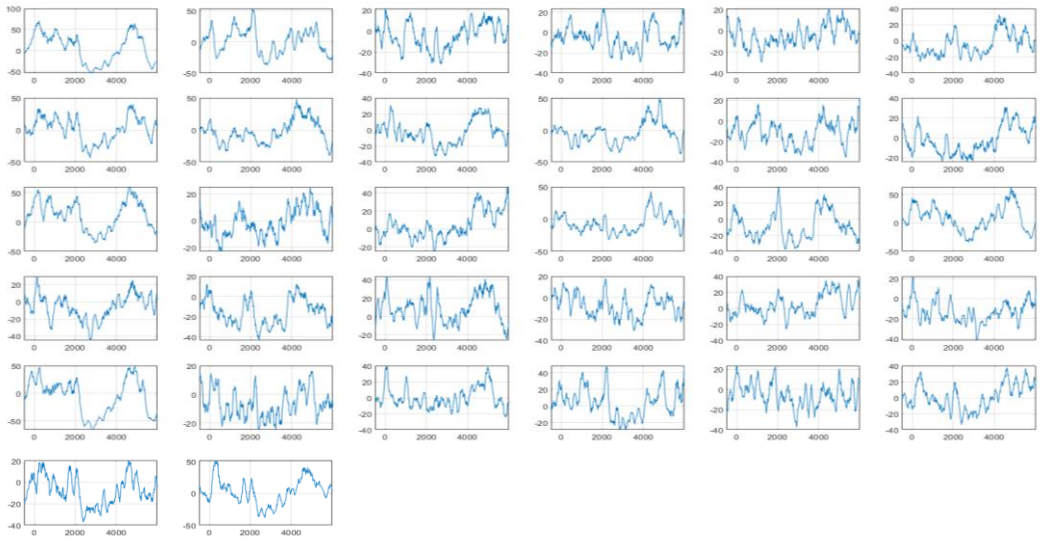


Figure B.22: ITV ERD/ERS patterns (averaged over all trials) of best-performing-ICs-baseline for subject 5 LH.

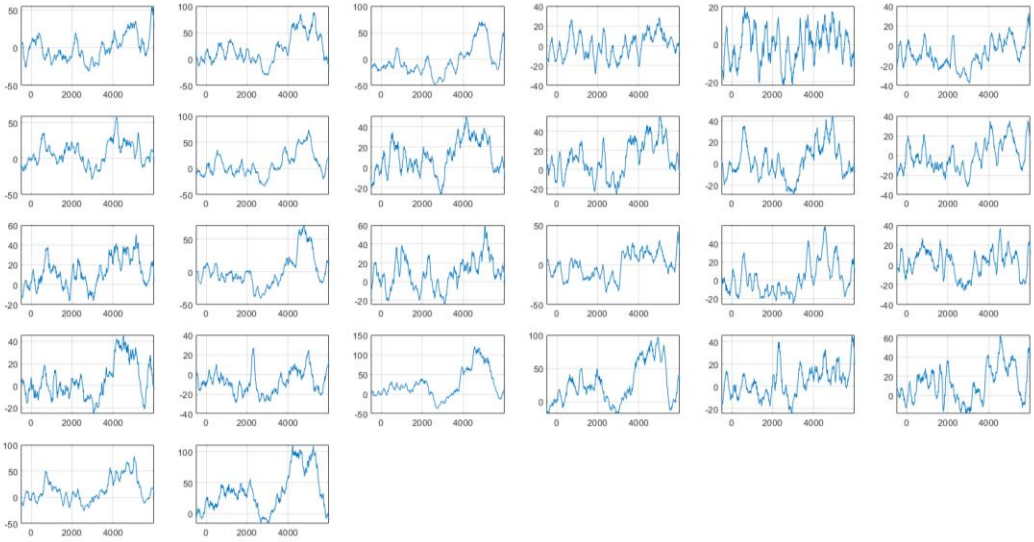


Figure B.23: ITV ERD/ERS patterns (averaged over all trials) of best-performing-ICs-baseline for subject 5 RH.

Appendix C – Electrode Location of Reduced Channel Sets

The placement of the electrodes corresponding to each selected channel for all the subjects are presented in this appendix.

C.1 Investigation 1

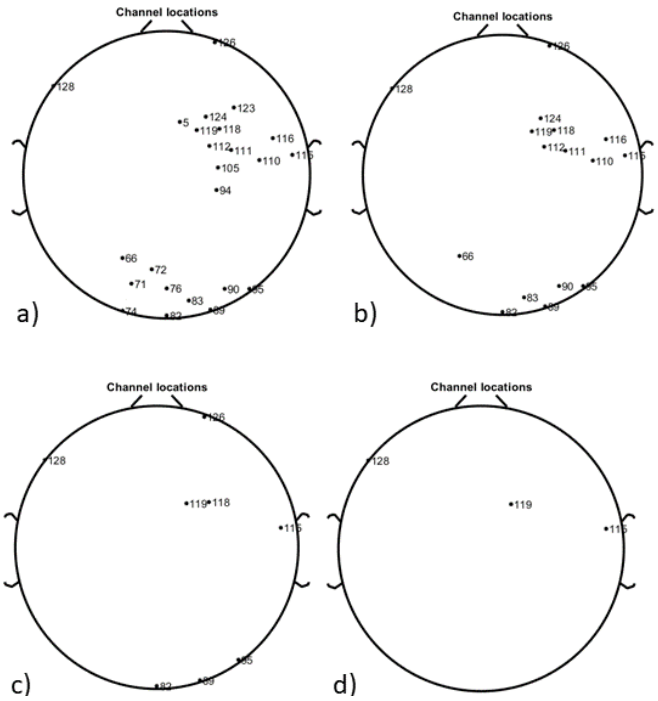


Figure C.24: Subject 2's reduced channel configurations obtained for investigation 1. The location of the electrodes corresponding to the selected channels is presented. a) 24-channel configuration, b) 16-channel configuration, c) 8-channel configuration, d) 3-channel configuration.

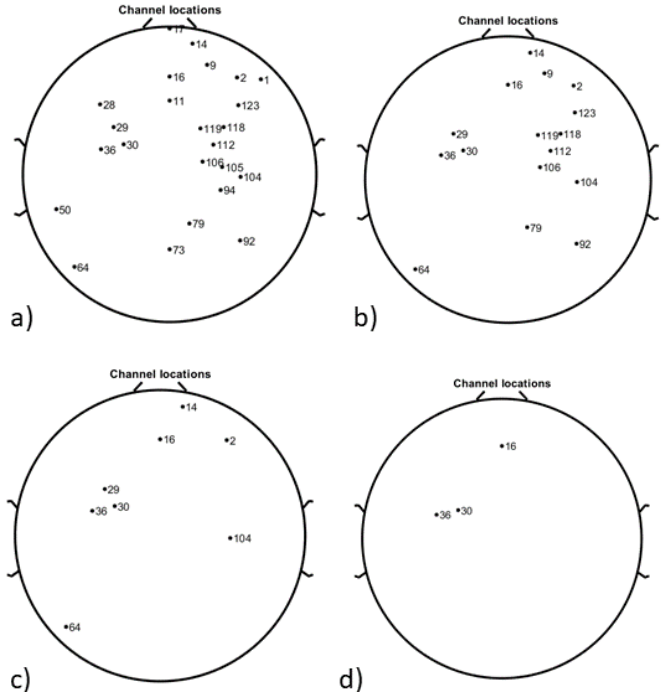


Figure C.25: Subject 3's reduced channel configurations obtained for investigation 1. The location of the electrodes corresponding to the selected channels is presented – a) 24-channel configuration, b) 16-channel configuration, c) 8-channel configuration, d) 3-channel configuration

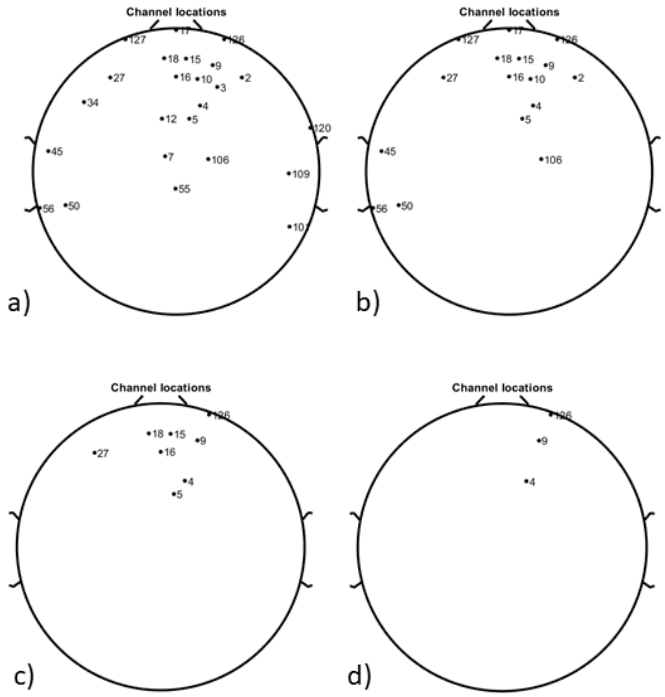


Figure C.26: Subject 5's reduced channel configurations obtained for investigation 1. The location of the electrodes corresponding to the selected channels is presented – a) 24-channel configuration, b) 16-channel configuration, c) 8-channel configuration, d) 3-channel configuration

C.2 Investigation 2

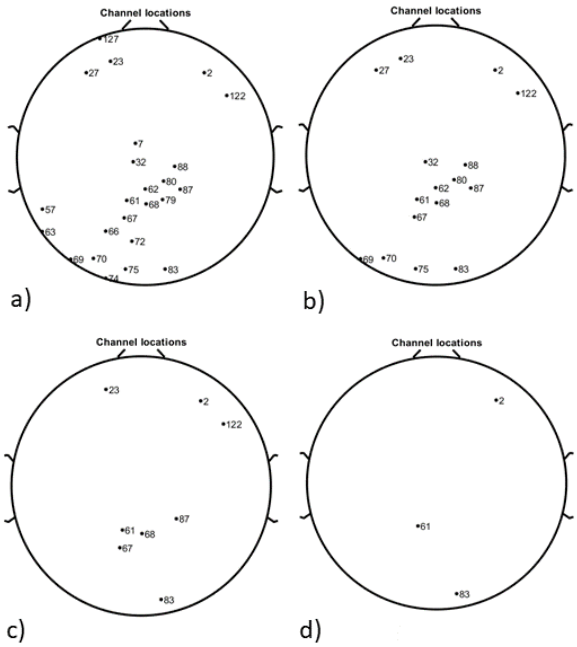


Figure C.27: Subject 1's RH reduced channel configurations obtained for investigation 2. The location of the electrodes corresponding to the selected channels is presented. a) 24-channel configuration, b) 16-channel configuration, c) 8-channel configuration, d) 3-channel configuration.

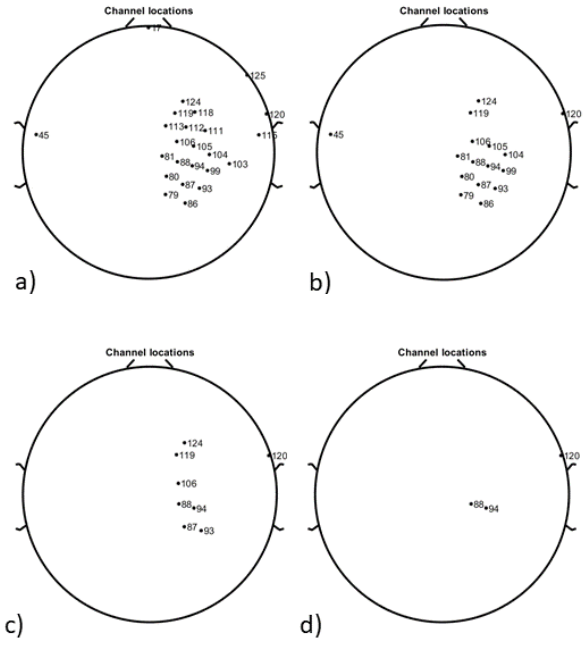


Figure C.28: Subject 2's LH reduced channel configurations obtained for investigation 2. The location of the electrodes corresponding to the selected channels is presented. a) 24-channel configuration, b) 16-channel configuration, c) 8-channel configuration, d) 3-channel configuration.

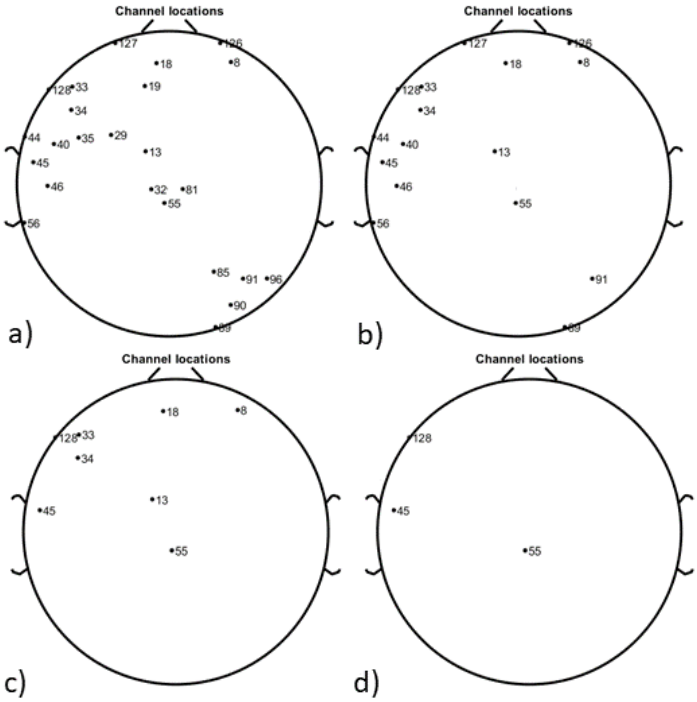


Figure C.29: Subject 2's RH reduced channel configurations obtained for investigation 2. The location of the electrodes corresponding to the selected channels is presented. a) 24-channel configuration, b) 16-channel configuration, c) 8-channel configuration, d) 3-channel configuration.

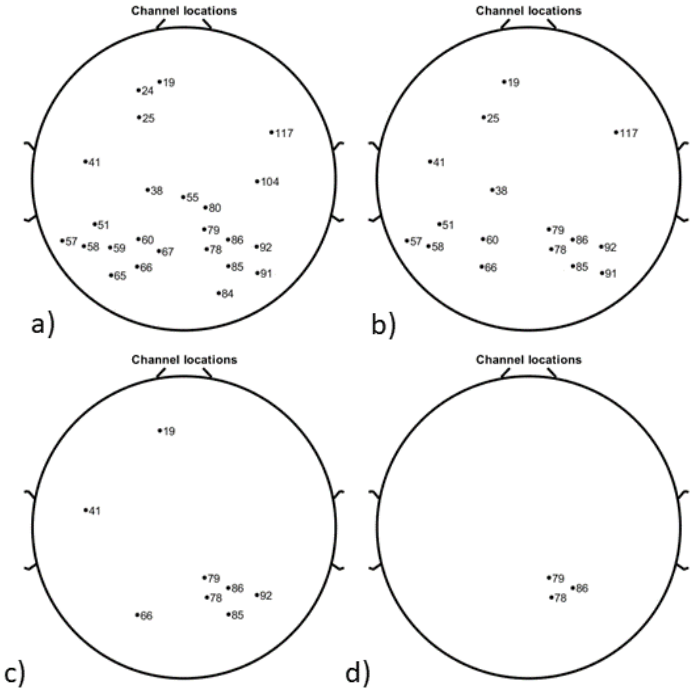


Figure C.30: Subject 3's LH reduced channel configurations obtained for investigation 2. The location of the electrodes corresponding to the selected channels is presented. a) 24-channel configuration, b) 16-channel configuration, c) 8-channel configuration, d) 3-channel configuration.

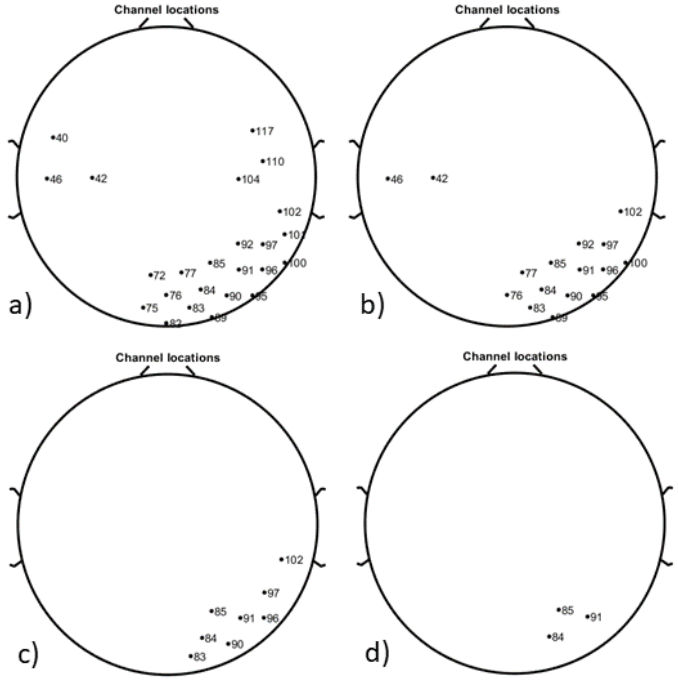


Figure C.31: Subject 3's RH reduced channel configurations obtained for investigation 2. The location of the electrodes corresponding to the selected channels is presented. a) 24-channel configuration, b) 16-channel configuration, c) 8-channel configuration, d) 3-channel configuration.

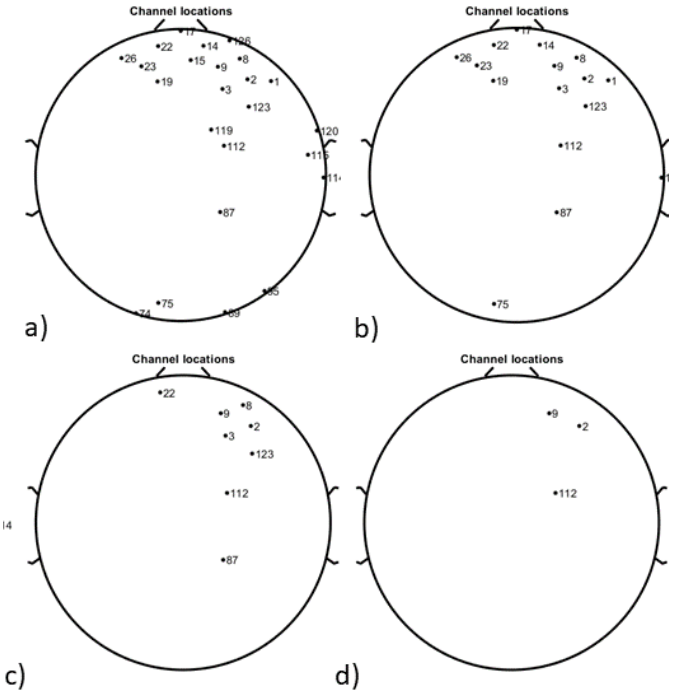


Figure C.32: Subject 4's LH reduced channel configurations obtained for investigation 2. The location of the electrodes corresponding to the selected channels is presented. a) 24-channel configuration, b) 16-channel configuration, c) 8-channel configuration, d) 3-channel configuration.

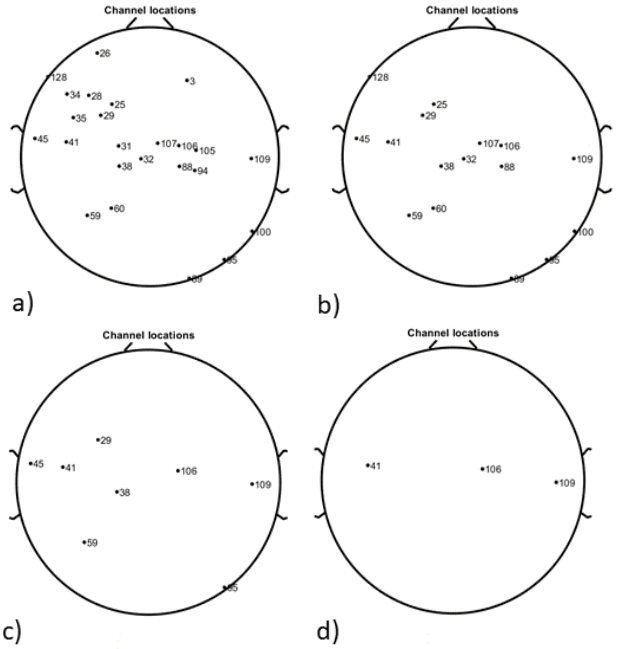


Figure C.33: Subject 5's LH reduced channel configurations obtained for investigation 2. The location of the electrodes corresponding to the selected channels is presented. a) 24-channel configuration, b) 16-channel configuration, c) 8-channel configuration, d) 3-channel configuration.

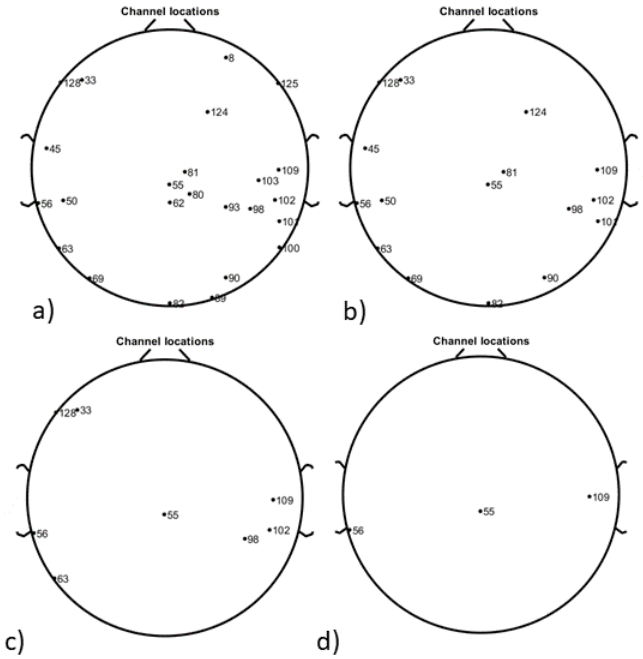


Figure C.34: Subject 5's RH reduced channel configurations obtained for investigation 2. The location of the electrodes corresponding to the selected channels is presented. a) 24-channel configuration, b) 16-channel configuration, c) 8-channel configuration, d) 3-channel configuration.

Appendix D – ITV Plots of Best-Performing-ICs-Reduced

Complete set of all the ITV plots of the *best-performing-ICs-reduced* for all the subjects for both investigations. The ITV plots of the *best-performing-ICs-reduced* are ordered according to their IC score.

D.1 Investigation 1



Figure D.35: ITV ERD/ERS patterns (averaged over all trials) of best-performing-ICs-reduced for subject 2's dataset. a) 24-channel configuration. b) 16-channel configuration. c) 8-channel configuration. d) 3-channel configuration.

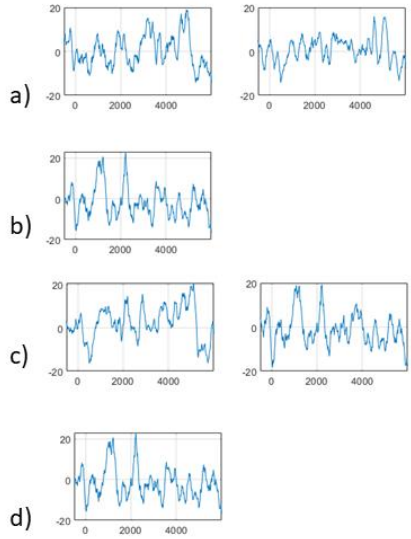


Figure D.36: ITV ERD/ERS patterns (averaged over all trials) of best-performing-ICs-reduced for subject 3's dataset. a) 24-channel configuration. b) 16-channel configuration. c) 8-channel configuration. d) 3-channel configuration.

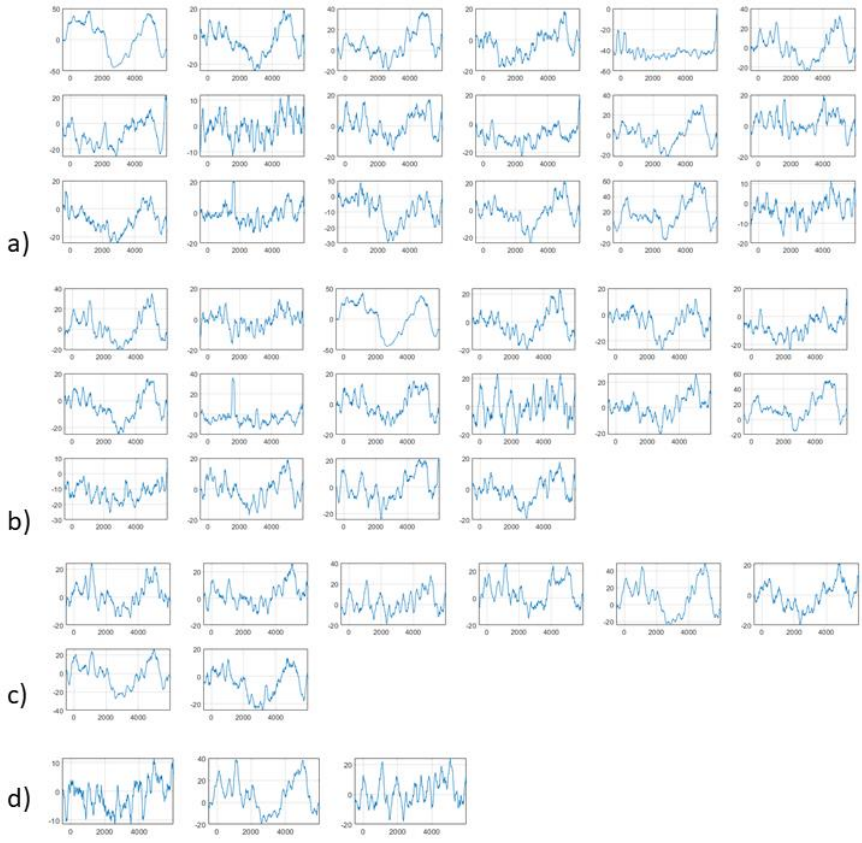


Figure D.37: ITV ERD/ERS patterns (averaged over all trials) of best-performing-ICs-reduced for subject 5's dataset. a) 24-channel configuration. b) 16-channel configuration. c) 8-channel configuration. d) 3-channel configuration.

D.2 Investigation 2

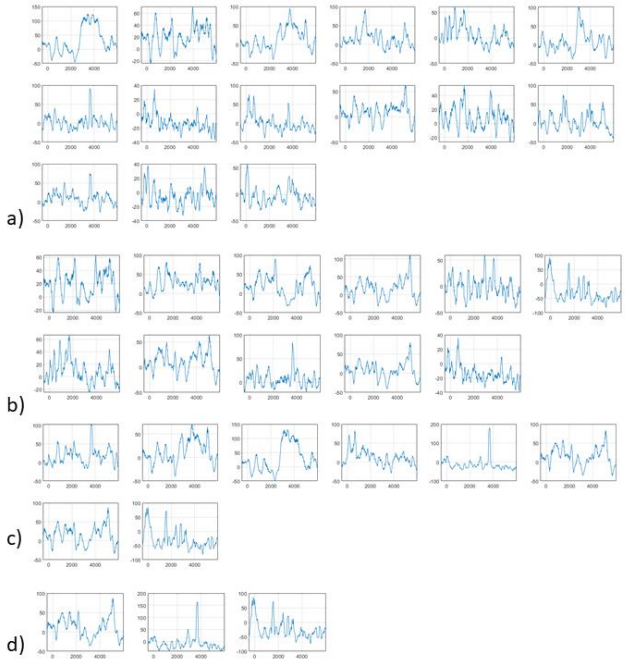


Figure D.38: ITV ERD/ERS patterns (averaged over all trials) of best-performing-ICs-reduced for subject 1 RH's dataset. a) 24-channel configuration. b) 16-channel configuration. c) 8-channel configuration. d) 3-channel configuration.

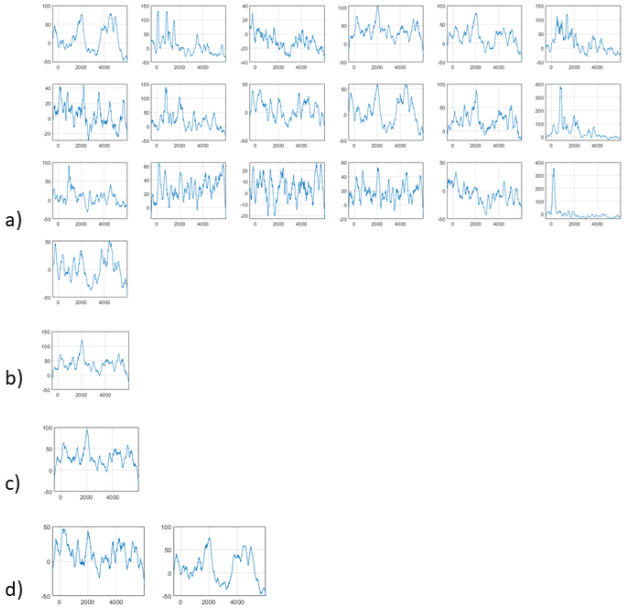


Figure D.39: ITV ERD/ERS patterns (averaged over all trials) of best-performing-ICs-reduced for subject 2 LH's dataset. a) 24-channel configuration. b) 16-channel configuration. c) 8-channel configuration. d) 3-channel configuration.

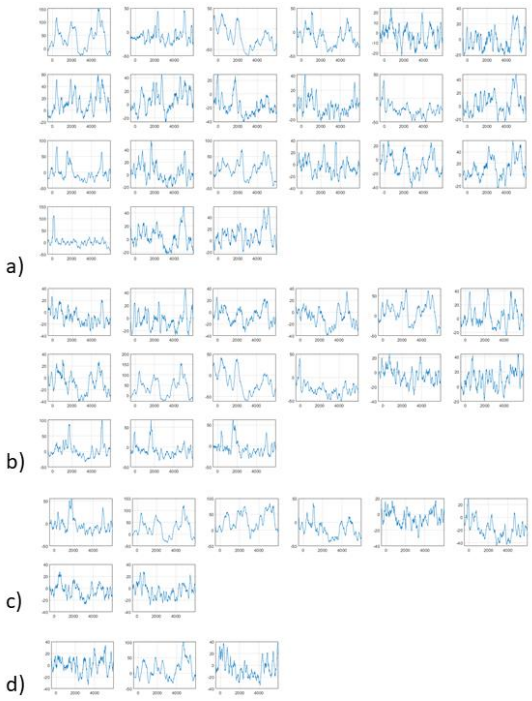


Figure D.40: ITV ERD/ERS patterns (averaged over all trials) of best-performing-ICs-reduced for subject 2 RH's dataset. a) 24-channel configuration. b) 16-channel configuration. c) 8-channel configuration. d) 3-channel configuration.

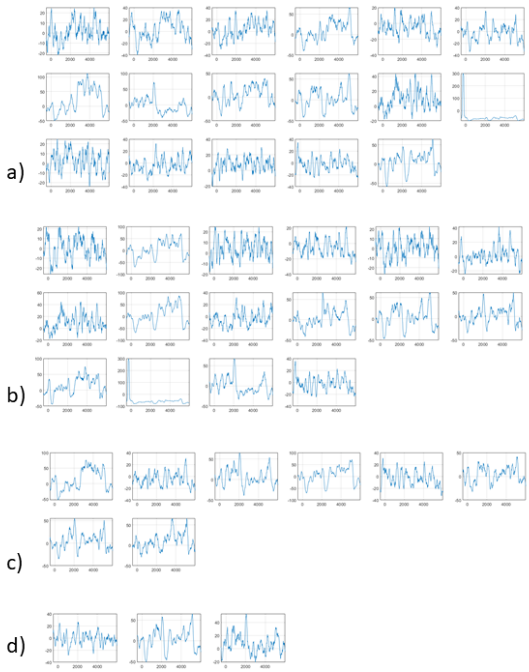


Figure D.41: ITV ERD/ERS patterns (averaged over all trials) of best-performing-ICs-reduced for subject 3 LH's dataset. a) 24-channel configuration. b) 16-channel configuration. c) 8-channel configuration. d) 3-channel configuration.

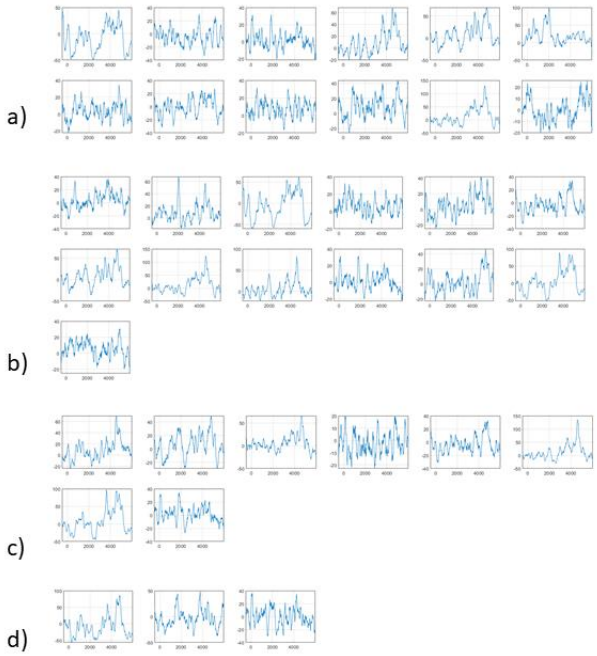


Figure D.42: ITV ERD/ERS patterns (averaged over all trials) of best-performing-ICs-reduced for subject 3 RH's dataset. a) 24-channel configuration. b) 16-channel configuration. c) 8-channel configuration. d) 3-channel configuration.

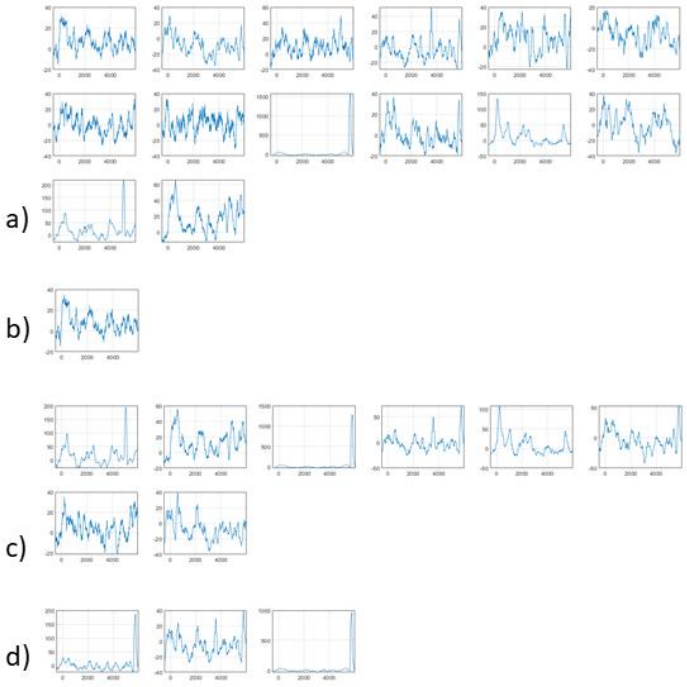


Figure D.43: ITV ERD/ERS patterns (averaged over all trials) of best-performing-ICs-reduced for subject 4 LH's dataset. a) 24-channel configuration. b) 16-channel configuration. c) 8-channel configuration. d) 3-channel configuration.

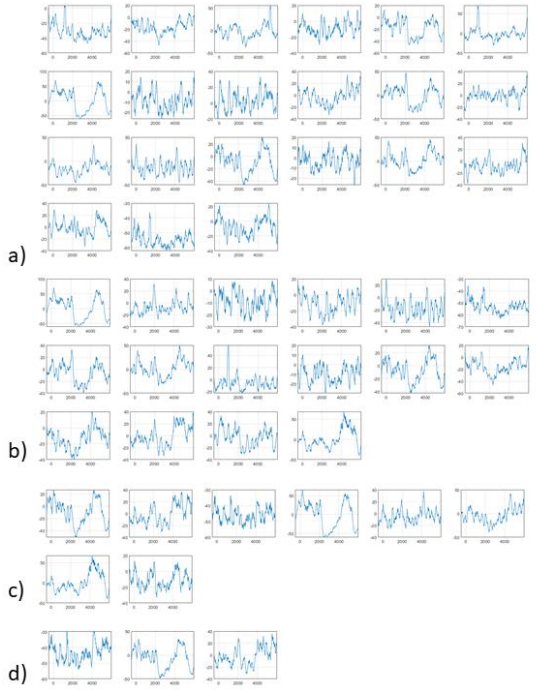


Figure D.44: ITV ERD/ERS patterns (averaged over all trials) of best-performing-ICs-reduced for subject 5 LH's dataset. a) 24-channel configuration. b) 16-channel configuration. c) 8-channel configuration. d) 3-channel configuration.

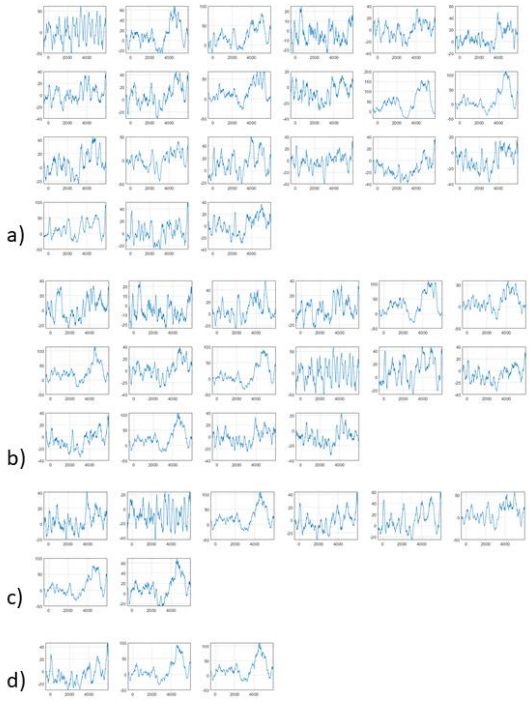


Figure D.45: ITV ERD/ERS patterns (averaged over all trials) of best-performing-ICs-reduced for subject 5 RH's dataset. a) 24-channel configuration. b) 16-channel configuration. c) 8-channel configuration. d) 3-channel configuration.